CHARACTERIZATION OF A ROBUST FLOW-THROUGH MICROFLUIDIC DEVICE FOR SINGLE-CELL ELECTROPORATION

by

Irmydel P. Lugo-Velázquez

A thesis submitted in partial fulfillment of the requirements for the degree of

MASTER OF SCIENCE

in

MECHANICAL ENGINEERING

UNIVERSITY OF PUERTO RICO

MAYAGÜEZ CAMPUS

2012

Approved by:

_____	_____
Ricky Valentín, Ph.D. Member, Graduate Committee	Date
_____	_____
Héctor J. Carlo, Ph.D. Member, Graduate Committee	Date
_____	_____
Rubén E. Díaz-Rivera, Ph.D. President, Graduate Committee	Date
_____	_____
Juan Eduardo Ramírez, Ph.D. Representative of Graduate Studies	Date
_____	_____
Gustavo Gutiérrez, Ph.D. Chairperson of the Department	Date

ABSTRACT

Electroporation, or electropermeabilization, is a physical phenomenon that occurs when a biological cell is subjected to an external electric field. This technique is typically used in laboratory or medical settings when there is a need to deliver molecules that otherwise cannot cross cell's lipid membrane. A microfluidic device with geometric constriction is proposed to enhance the electric field that the cell experiences when it flows through this section and so provide effective permeabilization in a flow through manner. Electroanalytical experiments were carried out with HeLa cells and stem cells to study the current response of the system and fluorescence experiments were carried out in order to get optical feedback of the process.

Voltage pulses of constant magnitude and in the range of tens of seconds were applied with a potentiostat and electrochemical software (chronoamperometry) was used to detect the state of permeabilization of the membrane. Drops in electrical current provided a means of detecting the flow of cells through the channel in real time. It was observed that this current drop is proportional to the size of the cell. It was observed that the profile of the current drop was different when cells reached permeabilization.

The release of the fluorescent Calcein from inside the cell confirmed that the membrane was permeabilized. The acquired electrical parameters may be useful data for the functional electroporation of other cell types. In addition, the device could be used for future clinical trials in cell-based medical treatments.

RESUMEN

La electroporación, o electropermeabilización, es un fenómeno físico que se produce cuando una célula biológica se somete a un campo eléctrico externo. Esta técnica es típicamente utilizada para aplicaciones de laboratorio o médicas en la cuales se necesita introducir moléculas que de otra forma no pueden atravesar la membrana celular. Un dispositivo microfluídico con constricción geométrica se propone para mejorar el campo eléctrico que la célula experimenta cuando fluye a través de esta sección y así proporcionar permeabilización eficaz en un flujo. Experimentos electroanalíticos se realizaron con células HeLa y células madre para estudiar la respuesta de corriente del sistema y experimentos de fluorescencia se llevaron a cabo con el fin de obtener retroalimentación óptica del proceso.

Pulsos de voltaje de magnitud constante y en el rango de decenas de segundos se aplicaron con un potenciostato y un programa de electroquímica (cronoamperometría) se utilizó para detectar el estado de permeabilización de la membrana. Las caídas de corriente eléctrica proveen un medio para detectar el flujo de las células a través del canal en tiempo real. Se observó que esta caída de corriente es proporcional al tamaño de la célula. Se observó que el perfil de la caída de corriente era diferente cuando las células alcanzaron la permeabilización.

La liberación de calceína fluorescente del interior de la célula confirmó que ocurrió permeabilización de la membrana. Los parámetros eléctricos adquiridos podrían proveer data útil para la electroporación funcional de otros tipos de células. Además, el dispositivo podría ser utilizado para futuros ensayos clínicos de tratamientos médicos celulares.

This thesis is dedicated to anyone
that may get benefit from it to improve their quality of life…

ACKNOWLEDGEMENTS

Many people contributed directly and indirectly in a positive way during my graduate studies journey. Without their help it would have been impossible to complete this process. This section is intended to recognize those individuals and thank them for all their support.

I sincerely thank my advisor, Dr. Rubén Díaz, for giving me the opportunity to carry out research under his guidance and supervision. I am deeply grateful to Idaris De Jesús, from the UPRM Department of Biology, and Luis Padilla for being kindly available whenever the HeLa cells died. Also thanks to Claudia Acevedo for providing the stem cells and sharing all her knowledge in Biology. I owe my deepest gratitude to Dr. Héctor Carlo, Dr. Paul Sundaram and Dr. Ricky Valentín for trusting me and giving me the honor of being part of my committee. Their good will, ethics and professionalism are traits that I will always remember and emulate.

I am heartily thankful for my colleagues of the ME Department and the friends I made during this process; for they made this a rich and fun experience. My sincere thanks to Dr. Vázquez, who pushed me into pursuing higher education and always believed that I could accomplish anything I propose myself to. I offer my regards and blessings to those who supported me in any respect during the completion of this project.

Lastly and most importantly I thank my family for their unconditional love which was the fuel that, combined with coffee, gave me the momentum to keep going. I dedicate my deepest gratitude to my mother, my sweet aunts and my awesome brother.

TABLE OF CONTENTS

LIST OF TABLES

LIST OF FIGURES

CHAPTER 1

INTRODUCTION

Electroporation (EP) is a phenomenon that increases the permeability of biological cells when they are subjected to an external electric field. The interior organelles of cells are protected by a surrounding bilayer lipid membrane, which has a natural resting potential due to the gradient in ionic concentrations across this membrane. The applied electrical field acts as a force on all polar components of the membrane [1]. The permeability of the cell increases due to a rearrangement of the membrane components. If the induced electric field is of sufficient magnitude, this resting potential changes and it results in a rearrangement of the membrane components that allows access to large molecules that normally cannot cross the membrane (i.e., DNA, proteins, drugs). This increased permeability is believed to be due to nanoscale transient hydrophilic “pores” that form in the membrane [2], [3], thus the name electroporation. These nanopores can close up shortly after treatment (through a process called “resealing”), allowing the cell to survive. As expected, the size and resealing properties of these nanopores would have a dependence on the amplitude and duration of the applied voltage. If the applied voltage is too high or applied for a long time, the membrane cannot recover and the cell contents from the cytoplasm spill, resulting in cell death. This is called irreversible electroporation and has also been taken advantage of for medical applications. Irreversible electroporation uses electrical pulses that are slightly longer and stronger than those used in reversible electroporation. With this technique, the holes in the cell membrane do not reseal, causing the cell to lose its ability to maintain homeostasis (regulation of a stable microenvironment) and die [4]. The most significant application that has demonstrated successful results is tumor ablation [5].

Reversible electroporation also has potential for many medical applications. It is currently used as a physical technique for drug insertion (e.g., electrochemotherapy) and gene therapy (gene transfection) [6], [7]. It presents advantages when compared to traditional chemical methods used to modify cells. In gene therapy, for example, the most used technique employs modified viruses as vectors to carry DNA across the lipid barrier and into the cell nucleus. However, it has been showed that viral vectors can induce oncogenic effects and

adverse immune response in the patient [8]. On the other hand, EP eliminates this by targeting the interested cells selectively. However, it also has some drawbacks. For example, for a cell sample in suspension, at a specified applied voltage some cells might never reach permeabilization while others might get irreversibly damaged. This size dependence might result in low efficiency transfection protocols.

Single-cell electroporation gets rid of these inconveniences and allows for treatment on the microscale. Microfluidic devices can be manufactured with microsized features that allow the treatment of single-cells. They also show great potential in microelectroporation (MEP) technology because of its reduced reagent consumption. Despite all of the promising features, clinical applications of MEP are limited. Much of the attention in the laboratory research setting is being devoted to elucidate the molecular mechanism behind electroporation [9] and to optimize devices for effective single-cell targeting.

The purpose of this work is to experimentally characterize a device that uses microfluidic technology to serve as an alternative to treat individual cells *in vitro*. Previous experiments have shown that handling adherent cells such as HeLa cells inside microfluidic systems can be cumbersome. Cell adhesion experiments have been performed and various sample loading methods have been tested to assess this technique. Cell agglomeration was fixed with surface modification of the microchannels and a passive pumping method was implemented to introduce the cells into the device. Mainly, this document focuses on the characterization of the device for real time detection of cell membrane permeabilization and some improvements for cell sample handling that may be of benefit for future applications in the microfluidic research community.

1.1 Literature Review

Bio-microfluidics is a relatively new field in bioengineering, so it is necessary to have a continuous literature review process in order to keep up with the latest developments. First, it is necessary to understand the concept of electropermeabilization and how it has been taken advantage of in medicine. After this, the miniaturization advances of this technique are briefly explained, with emphasis in the concept of microfluidics, which uses fluid flows at the microscale that are suitable when working with biological material.

Electropermeabilization of human cells was discovered when it was found that applying electric pulses to vesicles resulted in the release of the vesicle's contents, demonstrating a *temporary* increase in the conductance and permeabilization of the membrane [10], i.e. the membrane reseals after some time. A vesicle is a structure that forms naturally when a lipid is in contact with water; such that the hydrophobic tails arrange with all of their tails pointing toward the center leaving the hydrophobic tails outside. Vesicles serve as "bubbles" to enclose material, they don't have complex organelles inside, as can be observed in Figure 1-1.

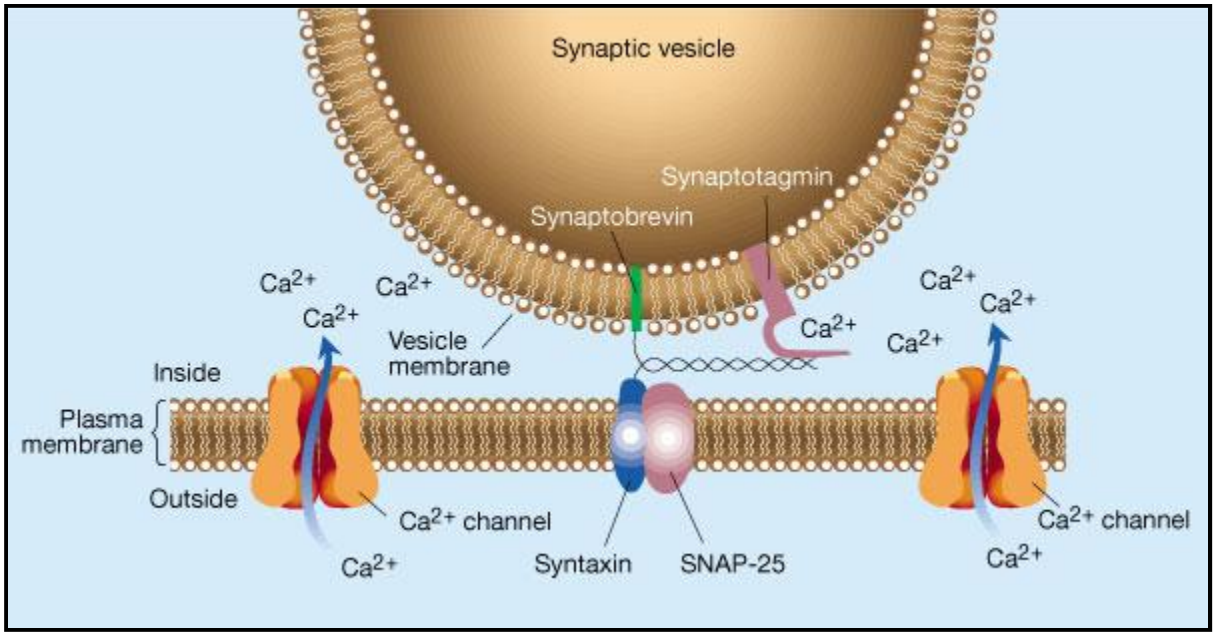

Figure 1-1. Schematic of a vesicle and a cell's plasma membrane. The image shows a vesicle on top and at the bottom a cell's plasma membrane with its protein channels and other complex components. Both structures are made of lipid molecules arrangement. [11]

It is easier to study membrane permeabilization with vesicles since they are simpler and also they can be prepared artificially to bigger sizes by adding phospholipids' molecules into aqueous buffers. Many studies are still performed on vesicles due to the inherent similarity in its membrane to the cell's plasma membrane.

Neumann et al. [12] later developed the first device for electroporation of a batch of cells which is the model that actual commercial electroporators follow. Many advances have been made in order to electroporate cells individually to eliminate the risk of damaging other cells, and so increase the efficiency. Here is where engineers enter with the application of micro-

technology, which obviously offers many advantages when working at the microscale. Some of these novel devices are discussed below. Micromanipulators such as patch clamp and the micro-pore chip concept are discussed first, which target individual cells with focused high intensity electric fields. Though successful results are recorded from these devices, they are rather complicated to use. Following this, microfluidic devices are discussed, which provide a tool for manipulating cells in a flow of microscopic dimensions. This technology brings to the table the ability of trapping cells with pressure differentials and treating many cells in a shorter time (high throughput). Improvements in this field such as real time monitoring of the electroporation state and cell handling are discussed at the end of the section.

1.1.1 Conventional Electroporation

The first publication found on functional electroporation was authored by Neumann [12] in the 1980's. Transformation (genetic alteration of the cell) of mutant mouse lyoma cells was achieved by applying 5μs electrical pulses of 5kV/cm. At this time, the mechanism that governs the permeabilization of the lipid membrane was not fully understood, but it was observed that short, high strength electrical pulses resulted in transient membrane permeabilization without cell damage. Transformation resulted from the cells uptake of DNA molecules that were added to the cell suspension. This showed that it was possible not only to achieve transient permeabilization of the cell membrane, but also to insert DNA molecules to alter cells genetically and keep them viable afterwards in culture. The setup consisted of a chamber that contained the cell suspension and the genetic material to be introduced, with two large electrodes (See Figure 1-2). This is the idea behind commercialized electroporators [13], which have been widely used mostly for genetic transformation but have the disadvantage of large reagent and sample consumption and low efficiency.

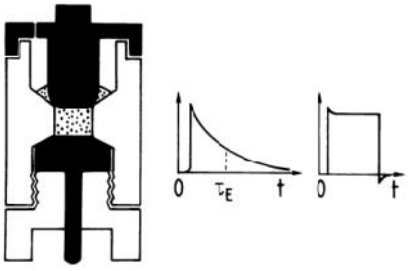

Figure 1-2. Electroporation setup by Neumann et al. The chamber for the electric impulse experiments has a filling volume of 0.35mL. Graphs show time courses of the electric field for capacitor discharge (left) and for rectangular pulses from the cable discharge (right). [12]

Also, since the electrodes create a homogeneous electric field to treat the whole cell population, some cells never reach permeabilization while others get irreversibly damaged. When dealing with expensive biomolecules such as DNA and cell lines with limited availability such as stem cells, this method is not appropriate.

1.1.1 Micromanipulators

Electroporation at the single-cell level (treating cells individually) results in a higher efficiency process (compared to treating a batch of cells). Advances in micro-manufacturing have allowed researchers to develop novel devices with microsized features to treat cells individually. Also, microsized electrodes can be manufactured to generate intense localized fields using less power. Single-cell electroporation has been achieved by focused electric fields with the use of micromanipulators that position microelectrodes to target cells individually (see Figure 1-3). This is obviously a task that requires dexterity and constant observation.

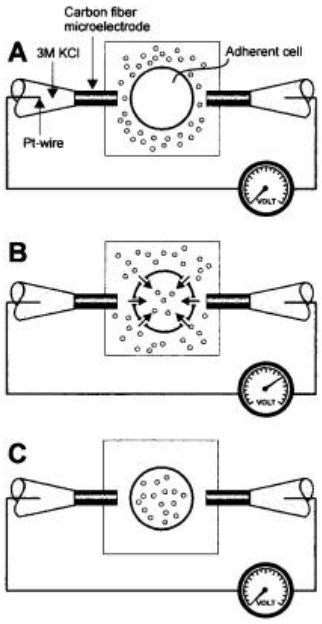

Figure 1-3. Single cell EP by the use of micromanipulators. Two carbon fiber microelectrodes with an outer diameter of 5μm were positioned close to each side of the cell by high-graduation micromanipulators. The two carbon fiber electrode tips (anode and cathode) were positioned at 2-5μm from the boundaries of a cell at an angle with respect to the object plane. [14]

Electroporation at the single cell level has also been achieved by the use of micropipettes that suction individual cells to apply highly localized pulses to the small portion of the cell that is

deformed inside the pipette [15], [16]. This is called the patch-clamp technique (See Figure 1-4). The typical setup includes a micropipette filled with a solution of DNA or other molecules to be delivered, a pipette holder, a micromanipulator, a microscope, a voltage stimulator and wire connections. Even though it treats cells individually, the patch-clamp technique requires constant observation and it results in a very low throughput process.

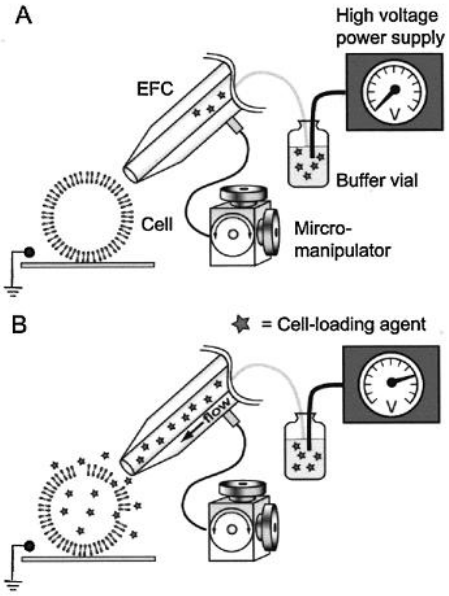

Figure 1-4. Micropipette patch clamp technique schematic. [15]

Other researchers have used micromachining technology, typically used to manufacture computer chips, to fabricate devices that allow for cells to be trapped and electrically treated in a similar way to patch clamping [17], [18], [19]. These are called planar patch clamping devices and Wood et al did a review comparing them. (Figure 1-5).

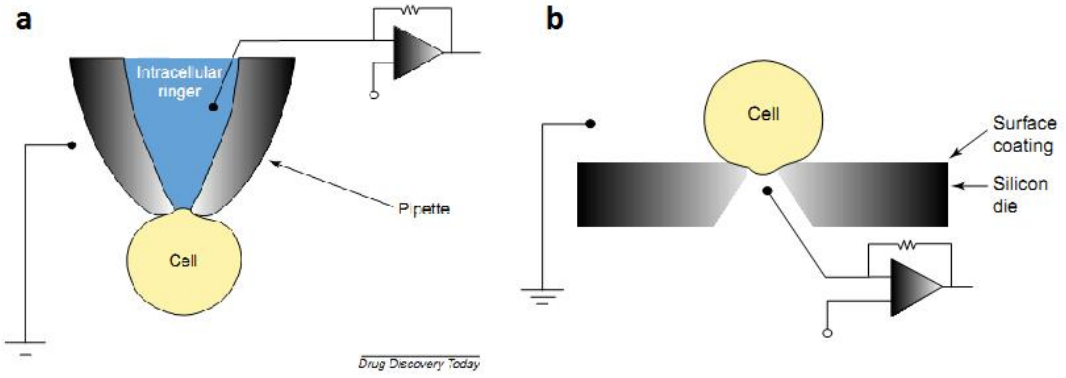

Figure 1-5. Schematic of (a) patch-clamp technique and (b) micro-hole (or "micro-pore") based EP chip. [20]

Microsized features can be machined in a substrate such as a silicon wafer. A “micro-pore” as small as 2μm in diameter has been machined in a silicon substrate and located between two small chambers filled with a saline solution phosphate buffered saline (PBS) [19]. A cell is trapped in the micro-pore by negative pressure from the bottom chamber and the membrane is in close to the surface of the machined hole, leaving a nanometric “seal” of the buffer solution between them. This results in a localized electric field that is higher in the area that the cell is trapped while the current response can be measured simultaneously. Electropermeabilization is detected by observing an increase in the measured ionic current passing through the chip. This feature of the device presents a means of real-time control of the electroporation process without the need for optical corroboration of the permeabilization state of the cell. However, immobilizing the cell in the microchip requires skillful manipulation and optical monitoring to make sure the cell is trapped in the hole. It is also a low throughput protocol because it treats one cell at a time.

1.1.2 Microfluidics

Microfluidic technology has enjoyed great popularity amongst scientists because of the ease in device fabrication and the prospective of developing innovative biomedical applications. These devices manage volumes of fluids in the sub-milliliter scale. The main advantage of microfluidics is the ability to manipulate and position biological material flowing within microchannels. Microvalves, micropumps and microchannels can be built in this scale which presents many advantages for working with biological material. They are usually fabricated with transparent materials such as glass or polydimethylsiloxane (PDMS) that facilitate microscope observation. Khine et al. [21] developed a device with multiple restrictions to immobilize cells using PDMS microchannels. Figure 1-6 shows the configuration of the device.

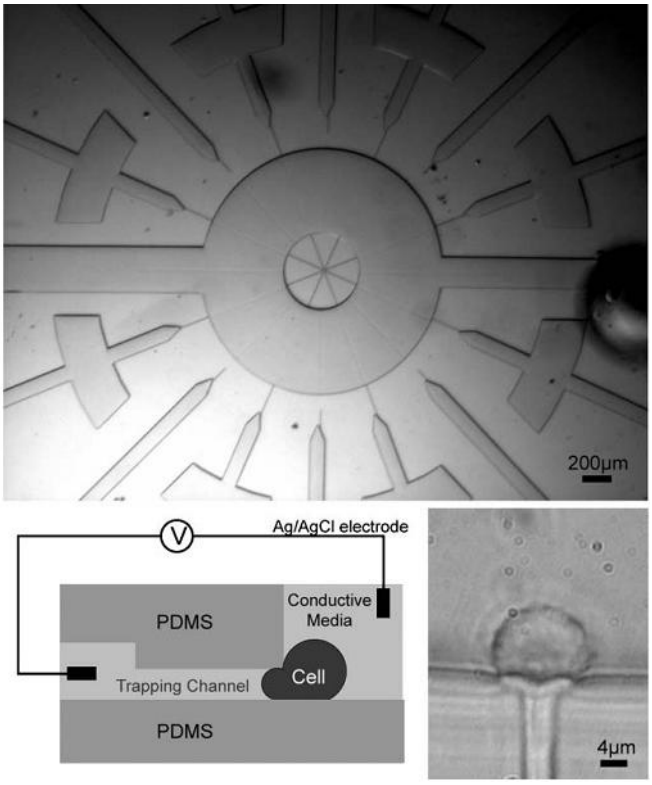

Figure 1-6. Microfluidic device for electroporation of an array of single-cells. (a) The two wide inlet channels on the left and right are used for cell input and output. An electrode is connected to one of these main channels. The other electrode is connected to the small channel where the cell is trapped. (b) A schematic of the cross-section of the chip. When trapped, a cell is pulled laterally into the small trapping channel by applying a negative pressure. The trapped cell acts as a high resistance component in the circuit. (c) An image showing the cell trapped in the channel. The cell extends into the channel leaving a tail-like structure in the channel. Because of its viscoelastic nature, the cell retains its deformed shape after the negative pressure is removed. [21]

Recent novel devices have been designed to overcome all the principal limitations such as managing cell flow for higher throughput devices (i.e. treating more cells in less time). Microfluidic devices that have microchannel structures are ideal for a flow-through approach. Flow-through implies more cells being treated in an autonomous way, thus increasing efficiency. Ramsey et al. [22] used a microchannel device for integrated cell handling, rapid cell lysis, and electrophoretic separation and detection of fluorescent cytosolic dyes. Cell analysis rates of 7-12 cells per minute were demonstrated and were >100 times faster than those reported using standard methods.

An important improvement for electroporation detection is real time feedback of electroporation which is a great tool for automation; this means greater potential for clinical

applications. It was proven that the flow through technology could perform single-cell electroporation with current feedback. Khine [23] developed a model that allows treating more cells by having multiple parallel traps as shown in Figure 1-7. But more importantly, it gives real time control of the EP state of the cell by monitoring the current feedback of the cell when the pulse is applied.

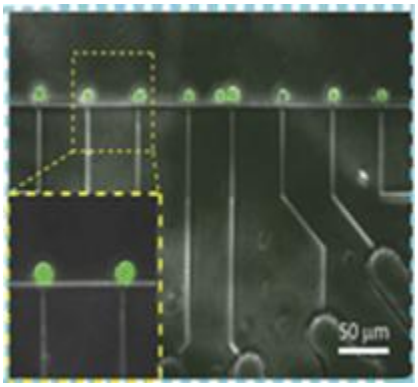

Figure 1-7. Microfluidic device with multiple traps in parallel to electroporate cells. Viewing window (within one of the wells) shows an array of HeLa cells trapped. [23]

Another issue found with most microfluidic devices is cell agglomeration, especially when dealing with adherent cells in small restricted dimensions like microchannels. Our group found that using a passive pumping mechanism to introduce the cells into the microchannel eliminates this problem. Beebe [24] was the first one to develop this pumping method by taking advantage of surface tension in the liquid drops at the inlets of the microchannels.

Figure 1-8 shows a schematic of the concept for passive pumping of a fluid.

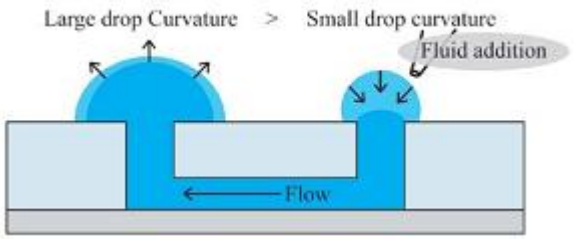

Figure 1-8. Passive pumping schematic. [25]

This method has the potential of being incorporated to flow-through microchannel electroporation devices.

Geometry variation

It was recently found that Wang et al. have used a narrow section approach in order to achieve a high intensity electric field using a constant pulse [26]. The basic concept of this method stems from the fact that the same voltage will induce a higher electric field in a section of smaller distance as shown in Equation 1-1. This follows from the definition of the electric field:

$$E = \frac{V_1}{d_1} = \frac{V_2}{d_2}$$ **Equation 1-1**

Figure 1-9 shows the experimental setup used by Wang's group. Cells are injected in one port and flow through a restricted section of 58µm where the electric field is higher. This way electroporation will occur in this zone without damaging the rest of the cells that have not reached this section. They are traveling through the wider channel and so experience an electric field of lower intensity.

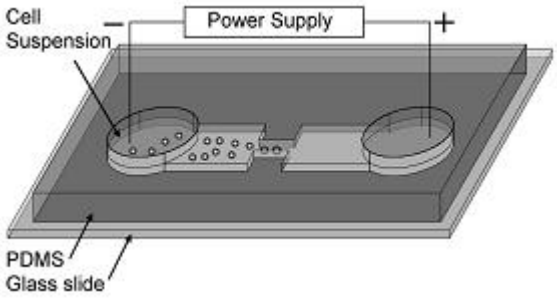

Figure 1-9. Schematic of experimental setup based on narrows section electric field focusing concept used by Wang et al. [27]

After treatment, cells are cultured after the addition of a fluorophore. The intake of the fluorescent molecules is evaluated later on cells in culture and so efficiency is evaluated. This is still an expensive and time-consuming method, besides it does not give any real time information about the process.

It is taken from literature that microfluidic technology is relatively easy to implement and has many features to be taken advantage of for *in vitro* electroporation. A flow-through microchannel device is proposed to treat cells individually and monitor current feedback in real time. This should result in a high-throughput device that can reach clinical application.

1.2 Motivation

Microfluidic devices show great potential in microelectroporation (MEP) technology because of miniaturized dimensions and reduced reagent and biological sample consumption. However, optical detection systems must often be incorporated to run the device [23], making them time-consuming and difficult to use. Therefore, the drive of this research is to provide a high-throughput device to treat individual cells continuously without the need for optical corroboration. A flow-through microfluidic device able to provide permeabilization information in real-time is proposed to achieve this objective.

The electrical characterization of the device will be useful for fundamental biological research or biomedical applications. Since the design of the device is intended to work regardless of cell size, the acquired electrical parameters may be useful data for the functional electroporation of other cell types. In addition, the device could be used for future clinical trials in cell-based medical treatments.

1.3 Summary of the following chapters

Chapter 1 presented an introduction to the concept of electroporation and explains a review of previous research on microfluidic devices for biomedical applications and devices specifically devoted to cell electroporation. The basic necessary background theory on electroporation phenomenon and techniques is found in Chapter 2. Chapter 3 presents the methodology used for this research, including manufacturing details and experimental setup description. The results of the electrical characterization of the device are presented and discussed in Chapter 4. Chapter 5 presents the results of the electrical detection of cell permeabilization, while Chapter 6 presents the results for the optical corroboration of this permeabilization. Chapter 7 summarizes the conclusions and includes recommendations for device improvement and possible future research.

CHAPTER 2

THEORETICAL BACKGROUND

2.1 Electroporation mechanism theory

Many models have been developed to explain what occurs at the membrane when an electric field is applied. The consensus is that the rearrangement of the membrane occurs due to a change in the natural transmembrane potential.

Cells are composed of water, inorganic ions, and carbon-containing (organic) molecules [28]. The inside of the cell (the cytoplasm) can be modeled as an electrolyte surrounded by an electrically insulating shell (the plasma membrane). When a cell is exposed to an external electric field, the electric field in its very vicinity concentrates within the membrane, which thus shields the cytoplasm from the exposure. The concentration of the electric field inside the membrane results in an electric potential difference across it, termed the *induced* transmembrane voltage, which superimposes onto the natural transmembrane voltage typically present under physiological conditions. As the electric field vanishes, so does the induced component of transmembrane voltage. This voltage affects the functioning of voltage-gated membrane channels, initiates the action potentials, stimulates cardiac cells, and when sufficiently large, it can also lead to cell membrane electroporation [29].

From a geometrical point of view, the cell in suspension is usually modeled as a sphere or an ellipsoid and the transmembrane potential can be determined analytically. This comes from the solution of the Laplace equation which describes the spatial and temporal distribution of the electric potential.

$$\nabla \cdot (\nabla ¤) = 0 \qquad \textbf{Equation 2-1}$$

where the voltage ¤ is a function of distance; in polar coordinates r and θ. Solving this equation gives the induced voltage, which for a spherical cell placed into a homogeneous electric field is:

$$¤_m = -\frac{3}{2} E r_{cell} \cos^{-} \qquad \textbf{Equation 2-2}$$

This is known as Schwan's equation and shows that the transmembrane voltage is higher in larger cells and at points in the membrane that are in the direction of the electric field. With irregular geometries or cells that are close to each other, the transmembrane voltage cannot be determined with analytical methods and numerical methods are used. Computational models have been developed based on this equation and proved to be consistent with experimental results [30], [31]. Figure 2-1 shows the model used for the computational method by Krassowska et al.

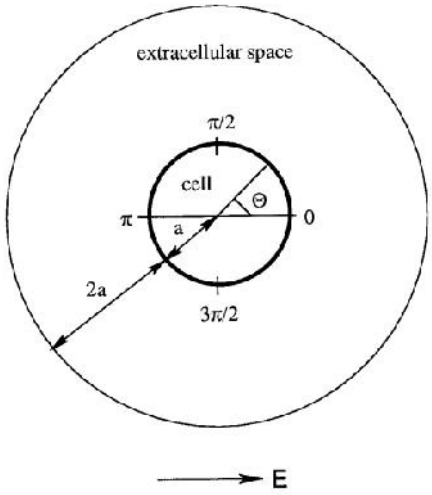

Figure 2-1. Schematic of spherical cell model used for mathematical calculations by Krassowska et al. [30]. The cell with radius "a" (r_{cell}) is immersed in a spherical shell of extracellular space with thickness 2a.

The previous mathematical model considers cells in suspension. Due to complications in cell heterogeneity in suspensions and different cell shapes when not in suspension, experimental approaches have been used to detect the change in the transmembrane voltage. For applications, however, the permeabilization of cells is not evaluated by the actual change in transmembrane potential, but is measured empirically, either by fluorescence molecules uptake or by changes in electrical resistance. The following sections will explain some of the parameters considered in the experimental approach.

2.2 Electroporation setups

In rough terms, the electroporation technique is based on the application of electrical pulses to a group of cells. This can be done either *in vivo* or *in vitro*. *In vivo* treatments are primarily used to kill cells (cell lysis, tumor ablation) but also have been recently used successfully for gene therapy *in vivo* in mouse retina [32]. In this case, a pair of electrodes is soaked in an ionic solution to maximize conduction and put in contact with the area to be treated to apply the pulse directly. *In vitro* treatments are more common and are widely studied. In medical applications, cells are removed from the patient, treated subsequently *in vitro*, and then are reinserted in the patient's body. When the process is performed *in vitro*, the cells are suspended in an ionic medium (buffer) to facilitate the passage of current. Microchannels can be used for this type of treatment. Figure 2-2 depicts how an electric field is distributed in a biological cell located between electrodes. As mentioned earlier, when the pulse is applied, permeable pores form on the cell membrane which allows the passage of the desired molecules (drugs in the case of electrochemotherapy, DNA for gene therapy).

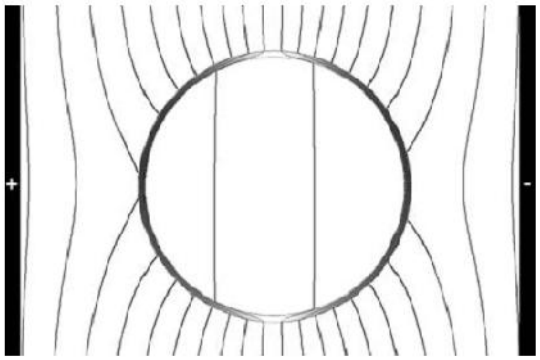

Figure 2-2. Schematic representation of a cell in an electric field. Black depicts high electric field strengths; white depicts low electric field strengths. The lines are equipotential lines. [33]

The basic concept of the setup consists primarily of the microchannel, which is filled with the buffer (e.g. PBS), the biological material to be inserted into cells, a pair of electrodes to transmit the pulse and the interconnections for the cell suspension to enter the microchannel to be treated and to exit after treatment.

2.3 Equivalent electric circuit

In the microchannel approach, biological cells are located between electrodes in an ionic solution that allows the passage of current. This can be modeled as an electric circuit with a voltage source (applied pulse), resistors and capacitors. There is an electrical resistance inherent to the ionic solution (buffer) inside the channel. This resistance (R) is defined by the properties of the fluid and the volume it occupies, as seen in Equation 2-3.

$$R = \frac{\rho L}{A} \qquad \textbf{Equation 2-3}$$

where ρ is the resistivity of the buffer ($\Omega \cdot m$), L is the length of the volume occupied by the fluid (μm), and A is the cross-sectional area of the channel (μm^2). The biological cell also imposes an additional resistance for the current to pass. Several researchers [34], [35] have identified capacitances in the EP system, in the electrode/buffer interface and some also in the cell membrane (See Figure 2-3). However, when a cell is in a constricted location, such as in a micro-hole device, the electrical resistance imposed is so high that it contributes the most to the total impedance.

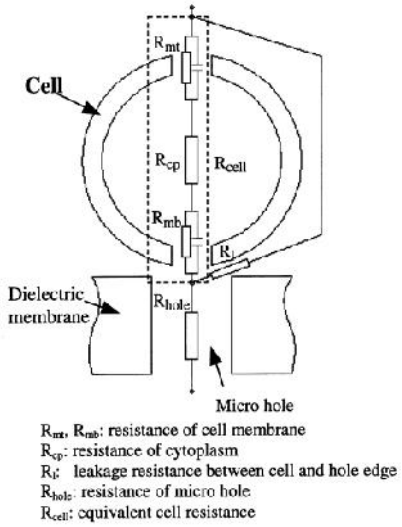

Figure 2-3. Circuit model for a cell trapped in a micro-hole. The hole resistance (R_{hole}) is the resistance of the electrolyte, equivalent to the resistance of the electrolyte (buffer) filling the microchannels. [34]

Electrode resistance is usually negligible if the electrodes are well conditioned. This means that there is negligible accumulation of material on the surface of the electrodes. The measured resistance between two Ag/AgCl electrodes for a micro-hole based EP device in the

laboratory was found to be around 5kΩ, and some studies with similar devices report it to be around 35kΩ [36]. On the other hand, a trapped cell in this type of device has a resistance in the range of MΩ. This was demonstrated for Khine et al microfluidic device [23] which has a network of microchannels of varying width, allowing the immobilization of cells in a manner similar to the micro-hole device (See Figure 1-6). Because electrical resistance is inversely proportional to cross-sectional area (Equation 2-3), the small portion of the cell inside the immobilizing channel has a much higher resistance (~80X) than the portion outside the channel. The greatest potential drop therefore occurs across the portion of the cell membrane inside the channel [35]. The membrane behaves as a capacitor due to the migration of ions from the surrounding ionic solution. However, if the applied pulse is long enough, capacitive effects can be neglected. Thus, neglecting these small resistances and capacitances leaves us with a circuit modeled with only some resistive components.

Microchannels filled with ionic solution (without cells) have been proven to behave according to Ohm's law [37]. If an electric circuit is purely resistive, the current signal received will be proportional to the voltage applied. This follows from Ohm's law as presented in Equation 2-4.

$$i = \frac{V}{R}$$ **Equation 2-4**

A microchannel with a biological cell embedded in a narrow section behaves as a purely resistive circuit, composed of a series of resistances (Figure 2-4). So, when a voltage is applied across the narrow section we should monitor a current inversely proportional to the resistance. The current will find opposition, first, along the wide channel sections filled with ionic solution. Then it will find a much higher resistance due to the cell that is blocking the narrow section and the volume surrounding the cell, which is also filled with the ionic solution. This volume surrounding the cell is very small (ideally in the nanometer range), so that its cross sectional area is so small that the resistance is very high. This resistance will be called the "seal resistance".

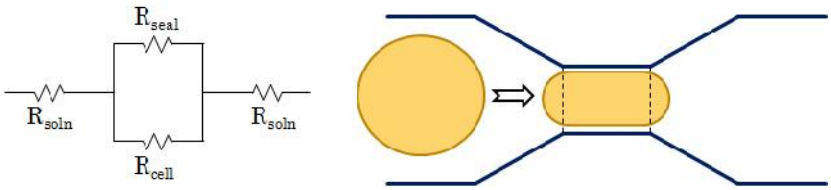

Figure 2-4. Simplified equivalent electric circuit for a microchannel with a cell embedded in a narrow section.

If membrane permeabilization occurs, the total measured resistance is lowered by the formation of passages in the cell membrane, so a higher electrical current will pass. This serves as a direct real time indication of the permeabilization state of the cell.

2.4 Pulse parameters

Pulse properties such as magnitude, duration, and wave shape have been varied by many researchers in order to study the optimal combination to achieve functional electropermeabilization. For example, when modifying cells for gene therapy, electroporation should be reversible. This means that the pores formed in the membrane need to reseal after some time or the contents of the cell spill and the cell dies. There is an optimal combination of electrical parameters to achieve resealing. Some of these parameters are discussed below.

2.4.1 Power supply

Direct current (DC) voltage sources are widely used for the electroporation process [36]. Alternating current (AC) voltage signals have been studied for EP protocols to eliminate gas bubble formation in microchannels due to electrolysis and proved to be efficient [38]. Analyzing the behavior of AC gets complicated as it involves complex terms. On the other hand, the behavior of DC pulse electroporation is well characterized and has proven to be effective.

2.4.2 Duration

Another important parameter is the pulse duration for the electroporation of cells. Most studies use short pulses, from microseconds to milliseconds, to achieve electroporation. If the electric pulse is applied for a long period of time, the cell will get irreversibly damaged.

Many groups have found that a sequence of pulses with short inter-stimulus interval (time between pulses) was much more effective than a single long pulse [16].

2.4.3 Magnitude

One of the principal advantages of microscale electroporation devices is that high intensity electric fields can be obtained with low voltages due to the small dimensions of the

channel. This follows from the equation that describes the electric field, which is proportional to the distance of the voltage drop (Equation 2-5).

$$E = \frac{V}{d}$$ **Equation 2-5**

where E is the electric field (V/m), V is the voltage applied (V) and d is the distance between the electrodes that apply the pulse (μm). Electric field is the parameter that causes electroporation, not the voltage itself.

2.5 Device design

The concept of the device is based on the geometry of the microchannel, where flowing cells are pushed by hydrodynamic flow through a narrow section forcing them to pass one at a time. Previous mathematical analysis of the micro-pore chip (like the one shown in Figure 1-5b) has shown that in micro-electroporation a nano-scale channel exists between the cell membrane and the micro-aperture wall. Using a new mathematical model, which incorporates the nano-scale channel concept, it was found that the electrical parameters required to induce electropermeabilization in MEP are independent of the physical dimensions of the cell and depend only on the relationship between the cell radius and the micro-aperture radius, which is related to the nano-channel characteristics. This finding was confirmed with micro-electroporation experiments of cells from a population with variable dimensions [39]. The finding suggests that it should be possible to perform micro-electroporation simultaneously on an unlimited number of individual cells, with real time control of the process in each cell through the control of the nano-scale channel dimensions. The results are better explained in the captions of Figure 2-5 and Figure 2-6.

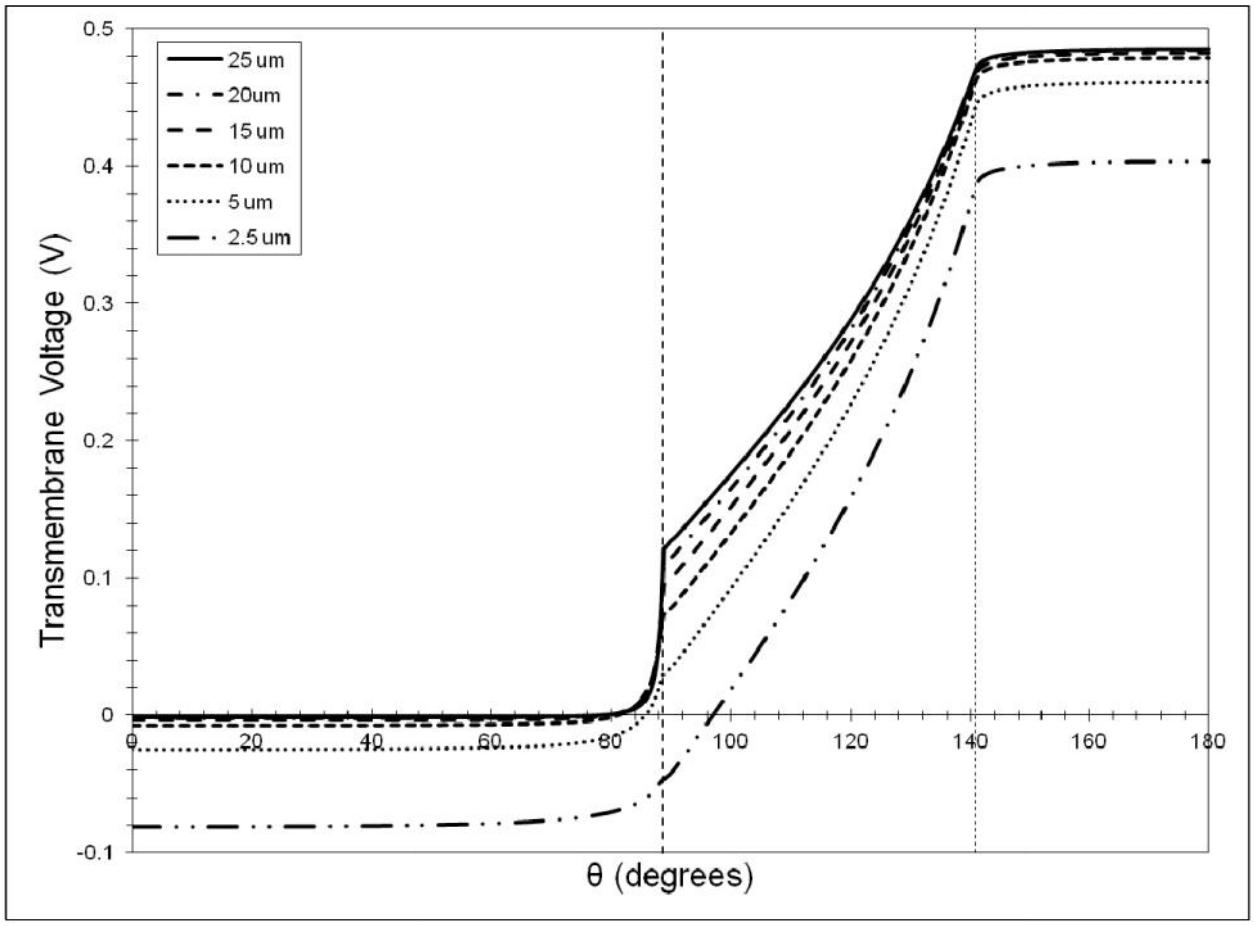

Figure 2-5. Graphical results of the finite element model of transmembrane voltage. The cell is modeled as a circular shape in two dimensions, with a nano-scale channel of ionic fluid between the pore wall and the cell. The angle θ refers to the position at the membrane (θ=0° being a point at the north pole of the cell and θ=180° being a point at the south pole, in the micro-aperture). The resulting transmembrane voltage is higher at the part of the cell that is embedded in the micro-aperture. At the sites of higher transmembrane voltage is where electropermeabilization will occur first. Modeled transmembrane voltage in a 1.25 μm radius pore for different cell radii (2.5-25 μm) shows the same behavior, regardless of cell size.

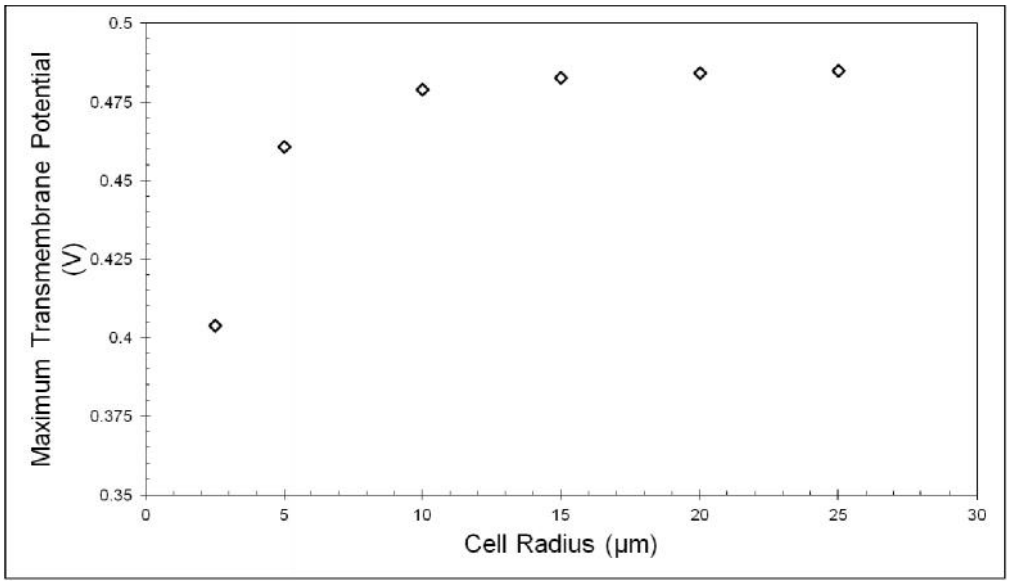

Figure 2-6. Modeled maximum transmembrane potential, at the angle of 180î, as a function of cell radius for a 1.25µm radius pore. The value for the maximum transmembrane voltage (where electroporation is supposed to occur first) is approximately the same for cell size greater than 10µm.

The design of the channel includes a narrow section, where the cell deforms and there is increased contact of the membrane with the channel wall. This geometric restriction should allow ionic current feedback when cells are flowing through this section.

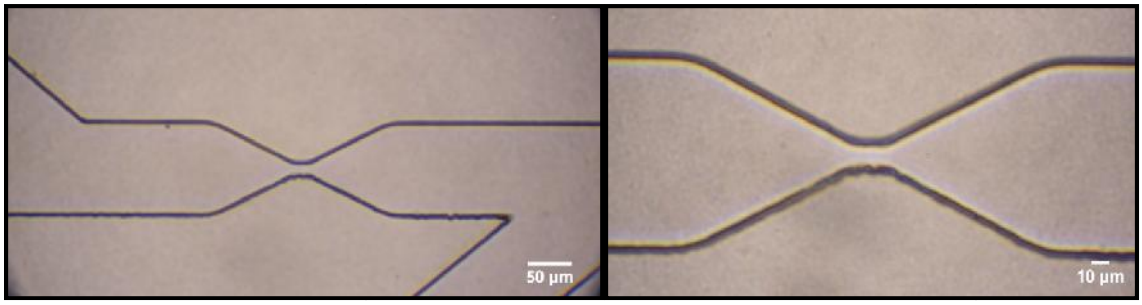

Figure 2-7. Micrograph of the main microchannel. (Left) Center area of the microchannel and (Right) magnified view to show the narrow section (~10µm wide) where the biological cell will pass and get electroporated.

The design (shown in Figure 2-7) has a narrow section of ~10µm where the cells will deform and leave a small volume of ionic solution ("seal") between the membrane and the channel walls. The resistance imposed by the biological cell is much higher than the seal resistance, so the current will tend to pass though this area, generating electric fields of high intensity. This is where electropermeabilization should occur first.

CHAPTER 3

MATERIALS AND METHODS

The project includes the design, fabrication and electrical characterization of a microfluidic electroporation device. Also, optimization of the device interface with the biological sample ("world-to-micro") is required. This section is devoted to explain in detail the manufacturing processes for the complete fabrication of the device. Also, the tools and methods used for the electrical characterization are introduced.

3.1 Microchannel manufacturing

Microchannel manufacturing is performed in the laboratory shortly before cell passage and experiments. They are not fabricated many days before experimentation because the hydrophilicity associated with the packaging technique is lost with time. This makes the filling of the channels with the ionic solution difficult. Also, the conditions of the laboratory are unsuitable for having many microdevices stored for a long period of time and make them vulnerable to contamination.

The manufacturing process starts with the fabrication of the master mold with the microchannel pattern. This is done in a clean room and the process is summarized in Figure 3-4. The fabrication of the microchannels consists of using this master to copy the pattern on the PDMS (this is called soft lithography). The final step is the packaging; bonding the PDMS to a glass substrate and incorporating the connections to the "macro" components.

3.1.1 Photolithography

To get the pattern of the microchannel, typical photolithography is used. The pattern is fabricated over a silicon wafer using a negative photoresist (PR) called SU-8. This is the master mold for the microchannels. A silicon wafer is spin-coated with a negative photoresist called SU-8. This leaves a thin film of SU-8 over the wafer. The thickness of this film will be the approximate height of the microchannels. The SU-8 is then soft baked in a hot plate at 65ºC

during 1 minute and then at 95ºC during 7 minutes. This is to eliminate the excess of solvent and harden the SU-8 thin film. Then the wafer is placed in contact with a chrome mask that has the pattern to be transferred and is exposed to ultraviolet light for ~90 seconds. The design of this mask which is done in CAD software is shown in Figure 3-1.

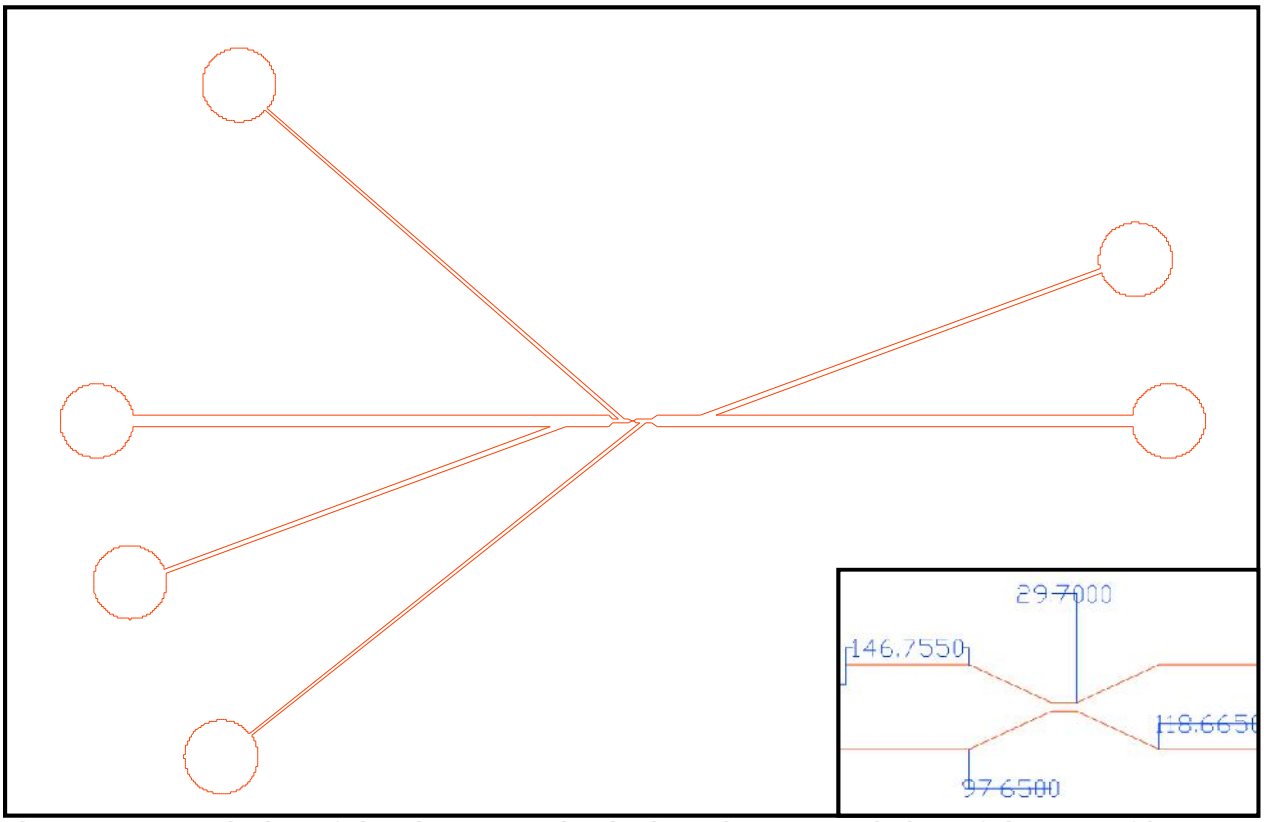

Figure 3-1. CAD design of the chrome mask. The inset is a zoomed view of the area of interest, where the cells will be restricted. The width of this area is about 10µm.

The mask has an area of glass (the microchannel part) and the rest is covered with chrome. The light goes only through the areas that do not have chrome. After exposure to UV light, a post-exposure bake is performed to harden the exposed SU-8 and reduce the effect of standing waves. Then the wafer is submerged in developer for approximately 1 minute. During the developing process the parts that were not exposed dissolve. The silicon wafer is left with an SU-8 elevated pattern of the microchannel that serves as a mold; this is called the “master”. The photolithography process is explained schematically in Figure 3-4 (steps a-d).

3.1.2 PDMS Casting

Polydimethylsiloxane (PDMS) is a silicon-based organic polymer widely used for microfluidic applications due to its many advantages. These include low cost, mechanical strength and transparency (useful for microscopy). The process to fabricate the PDMS microchannel structure is called soft lithography. A mixture of PDMS base and curing agent (10:1 ratio by weight) is poured onto the master mold and cured at 65°C for 4 hours. The cured PDMS is a flexible, transparent material with the shape of the microchannel engraved at the bottom. The holes for the inlets of the microchannel are fabricated in the PDMS with a biopsy punch and then the PDMS is joined to the glass substrate to make the sealed microchannel structures. The procedure is shown pictorially in Figure 3-2 and schematically in Figure 3-4 (steps e-g). After the PDMS is cured with the inlet and outlet holes, the connections world-to-micro will be incorporated.

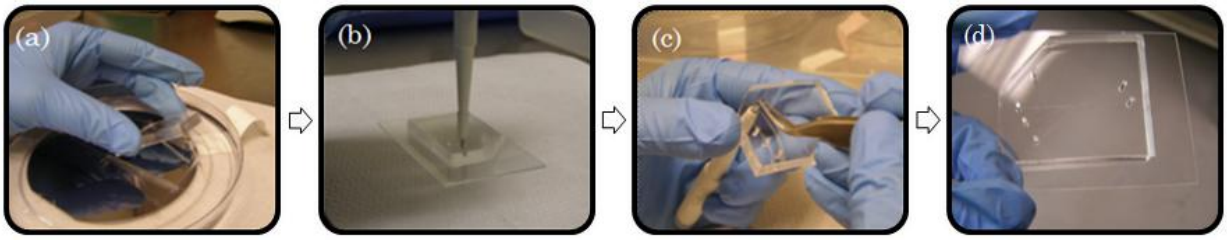

Figure 3-2. PDMS microchannel structure manufacturing. (a) PDMS with microchannel pattern is cut and removed from the master. (b) Holes of 2mm outer diameter are punched at the inlets with a biopsy punch. (c) The residual PDMS from the punch is removed leaving the holes for the ports. (d) The resulting PDMS structure is placed over a glass slide, which constitutes the final wall that encloses the channels.

3.1.3 Packaging

Packaging is the process of enclosing the microchannel to protect the inner walls from the external environment. It includes the bonding of the pattern to the substrate (glass) and the connections to the biological sample loader in an effective manner. This is usually the last step in the entire fabrication process and the most important, especially when it is not performed in a clean room. Any particle in the environment that comes in contact with the microchannel structure presents a disruption in the flow, since the channel dimensions are so small. Thus, a rigorous cleaning process is very important.

Packaging of biomedical devices confronts challenges in which bio-compatibility, bio-functionality, reversibility and macro-to-micro interfaces preclude many of the traditional packaging processes from being used in traditional microelectronics [40]. So, the packaging process includes surface modification to prevent cell adhesion.

Plasma Bonding

Plasma activation refers to the process of modifying the properties of a surface by exposing it to oxygen plasma, which is generated by applying low frequency electric field to air at vacuum pressure. It is used to bond surfaces and also to make the surfaces extremely clean. This process oxidizes the surface of both materials and activates hydroxyl groups which form strong bonds when the surfaces are placed in contact. This makes an irreversible bonding between the PDMS and the glass slide. This was initially used to bond the PDMS to the glass slide and thus make a seal for the channel, so it can withstand very high pressures. However, through experimentation, it was observed that a thicker layer of PDMS enables it to withstand high pressure without a permanent bond. The plasma chamber was used to clean and make the surface of the device hydrophilic, to make filling easier. The PDMS is placed over the glass and then inside the chamber. A vacuum closes the chamber and the RF is turned on. Figure 3-3 shows the chamber used and the pink glow that is generated inside it.

Figure 3-3. Plasma chamber (Harrick Plasma). The characteristic pink glow inside the chamber indicates that the plasma is working.

Figure 3-4 show a schematic of the whole fabrication process, from the photolithography fabrication of the master to the PDMS casting. Figure 3-5 shows a schematic of the finished device prior to the “macro” connections.

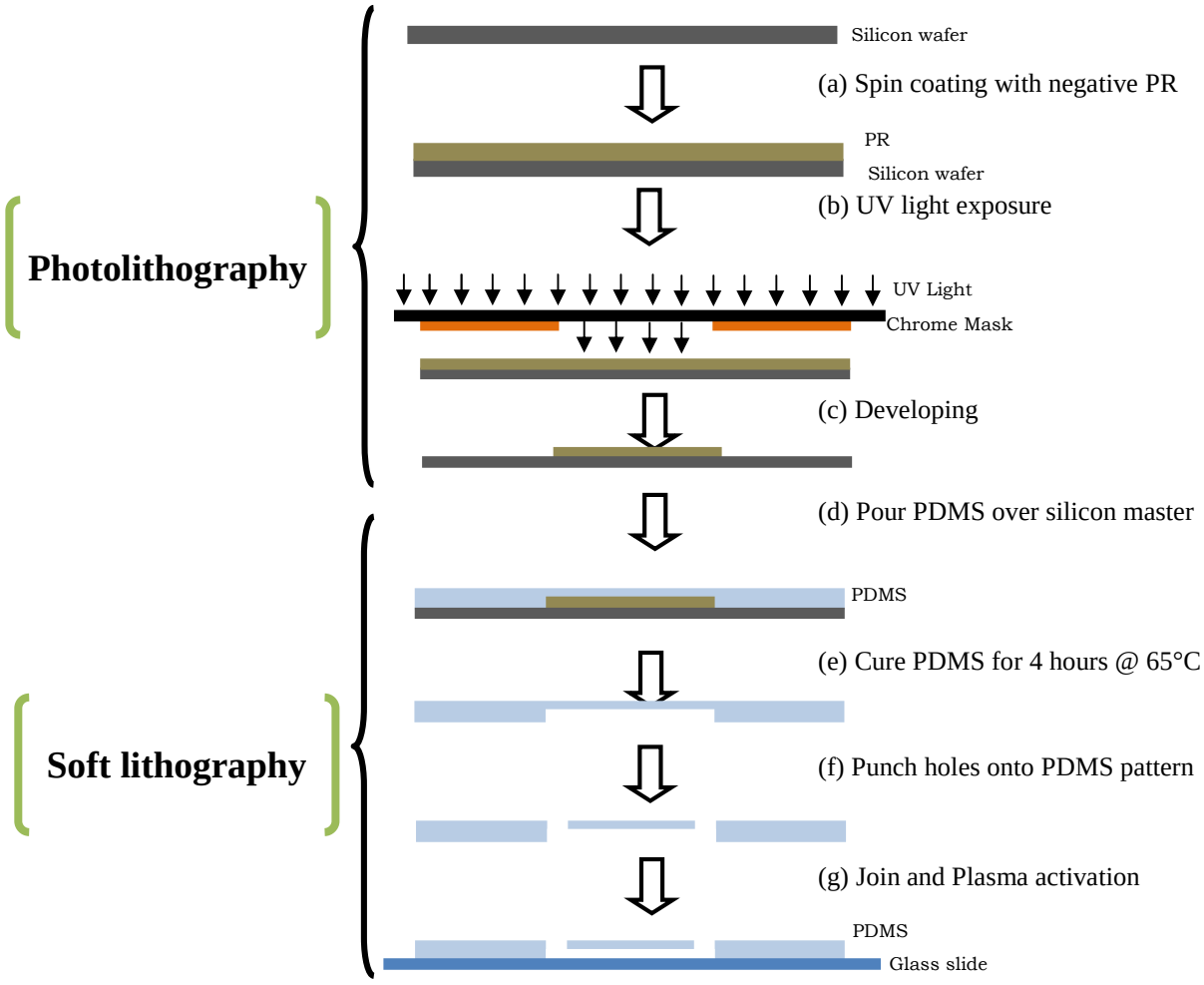

Figure 3-4. Cross-sectional view of process flow for photolithography. (a) A silicon wafer is spin-coated with SU-8. (b) The wafer is placed in contact with a chrome mask that has the pattern to be transferred and is exposed to ultraviolet light for ~20 seconds. (c) After exposure to UV light, a post-exposure bake is performed and the wafer is developed so the parts that were not exposed dissolve. The silicon wafer is left with an SU-8 elevated pattern of the microchannel that serves as a mold, called the “master”. (d) PDMS is poured over the silicon wafer and (e) it is left to stand for 4 hours in a hot plate at 65ºC so that it solidifies. (f) The holes for the inlets are fabricated in with a biopsy punch. (g) The PDMS structure is joined with the glass and is put in vacuum in a plasma chamber for 1 minute, leaving silanol groups on the surface, rendering the surface hydrophilic.

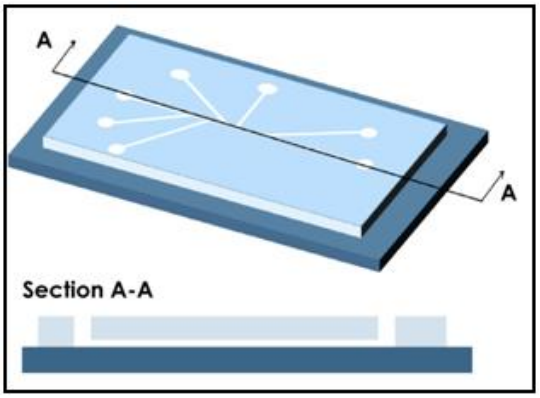

Figure 3-5. Schematic of finished PDMS microchannel device before incorporation of the port connections. (Not to scale).

Macro-to-micro interconnections

This connection is a very important feature of the device. It connects the "macro" components (syringe with biological sample, pumps, etc.) to the "micro" components (interior of the microchannel). The Ag/AgCl electrodes, used for the electrical treatment of the cells are also incorporated into these connections. The typical interconnection configuration consists of glued transparent plastic micro-tubing (Tygon) to the inlet/outlet holes of the PDMS. One of these tubes is connected to a syringe with cells, which in turn is connected to a syringe pump (New Era Pump Systems, Inc.). This was, in fact, the fabrication method used for the first experiments. However, it presented handling difficulty and cell agglomeration. Figure 3-4, shows a picture of the previous fabrication of PDMS microchannels.

Figure 3-6. Picture of previous microchannel fabrication. Finished microchannel has Tygon tubing at the inlet/outlet ports.

Figure 3-7. NE-100 programmable syringe pump.

The connections used consisted of polypropylene luer lock fitting of 1/16” (1.57mm) ID to Tygon tubing of 0.09”(2.29mm) OD and 0.05”(1.27mm) ID. This tube is connected to a smaller tube of 0.07” (1.78mm) OD and 0.04” (1.02mm) ID. This is useful in controlling the depth that the tube reaches inside the channel, as shown in Figure 3-8. In a typical configuration, this depth cannot be controlled because the insertion is done manually. In a reusable device that is not permanently bonded, this leads to PDMS lifting from the glass and causing leakage.

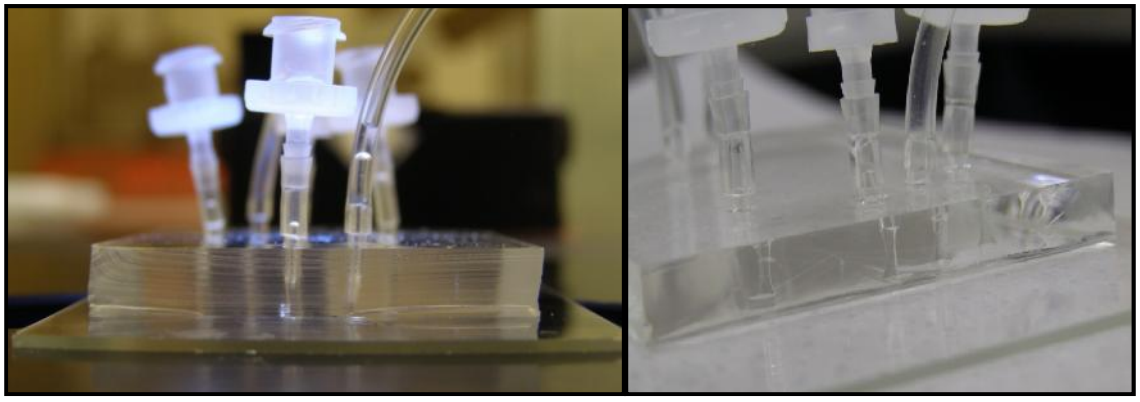

Figure 3-8. Macro-to-micro interconnections. Luer-lock fittings are connected to tubing and inserted into the PDMS inlets. The two different sized tubing allows control over the depth the tube reaches inside the channel.

Macro-to-micro interconnections were developed using polypropylene luer lock fittings shown in Figure 3-9. The main components are the T-shaped fitting which has the electrode connected and the barbed male luer which connects this to the microchannels.

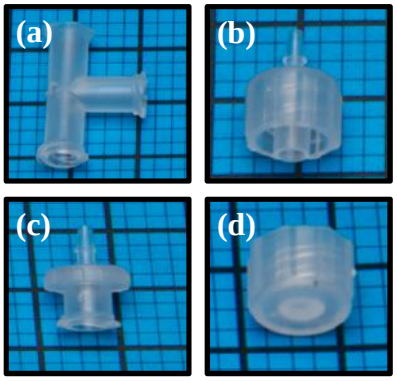

Figure 3-9. Polypropylene luer lock fittings used for the macro-to-micro interconnections. (a)Female luer tee with full threads is used to connect the electrodes at one side and inject the cell sample at the other (b) 1/16"barbed male with locking nut connects to (a) and to the device at ports A and F, (c) 1/16"barbed female with full thread connects to the device at ports B, C, D and E, (d) male luer plug with locking nut closes the fittings at ports B, C, D and E.

Further experimentation demonstrated that using only the main channel fittings results in effective cell focusing through the main channel, from port A to port F. The interconnection setup is reduced to just the inlet and outlet that consist of the T-luer that is connected to the channels at one end, the electrode which is connected at the other end and the other end is left open to atmosphere.

Surface modification

Cell adhesion is the main problem in transferring the biological sample into the microchannels. Surface modification has been used as a technique to solve this problem. A protein called bovine serum albumin (BSA) has been used to slow attachment of cells in suspension in chambers for optical trapping [41]. The solution was used in this case to coat the channel walls to inhibit cell agglomeration and adhesion. The solution seemed to make PDMS surface hydrophilic as shown in Figure 3-10.

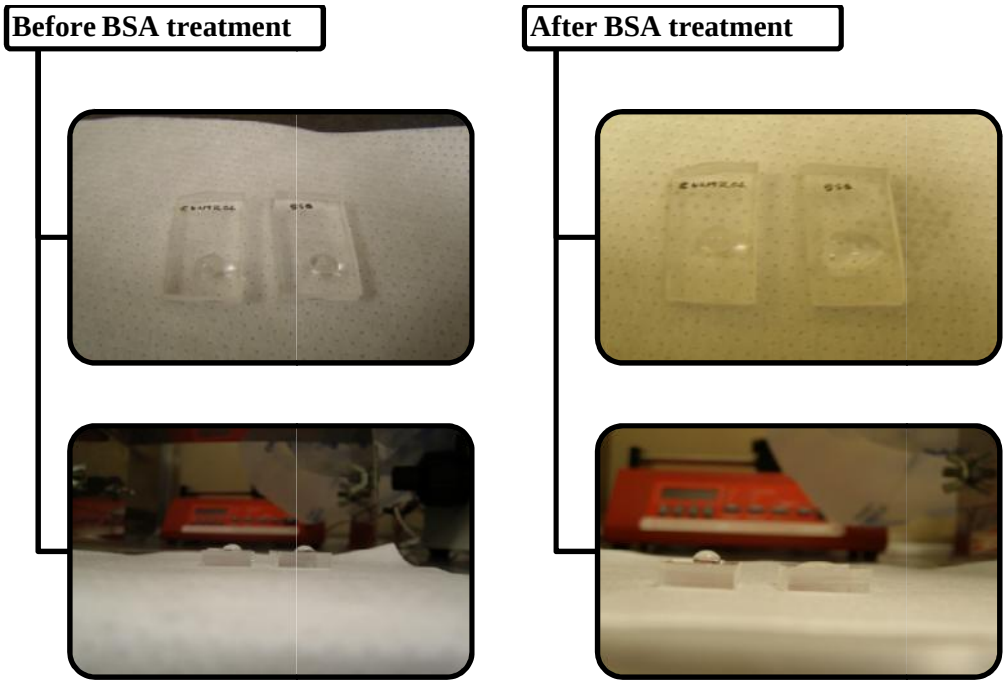

Figure 3-10. Effect of BSA functionalization on PDMS. Before the BSA treatment the polymer surface is hydrophobic, as shown by the bead-like nature of water on top of the surface. With BSA the surface becomes hydrophilic such that water spreads over the surface, as shown in figures at the right.

PDMS is hydrophobic by nature, so it tends to "repel" water molecules. When BSA was poured over a PDMS sample and incubated for 15 minutes, the surface became hydrophilic as shown by the water spreading in the previous figure. The protocol for the functionalization of the device consisted on injecting BSA into the channels with a syringe and incubating the device for 15 minutes at 37ºC. The BSA was then removed by injecting PBS into the channels using a syringe pump.

3.2 Cell line

Cervical cancer (HeLa) cells are used for the experiments with microchannels. The HeLa cell line is adherent, a classic and representative tumor cell line commonly used in research. Cells were cultured as a monolayer in 25cm^3 culture flasks (Falcon). The cells were incubated at 37ºC with 90% (v/v) Dulbecco's modified Eagle's medium (DMEM) supplemented with 10% (v/v) fetal bovine serum (FBS). For cell detachment, the cells were washed three times with PBS, followed by addition of trypsin–EDTA and incubated for ~5 minutes at 37ºC. The sample was

then centrifuged for 3 minutes leaving a pellet of cells at the bottom of the centrifuge tube. This pellet was resuspended with PBS for experiments. The size of the cells after being resuspended ranged between 13-25 µm as seen in Figure 3-11.

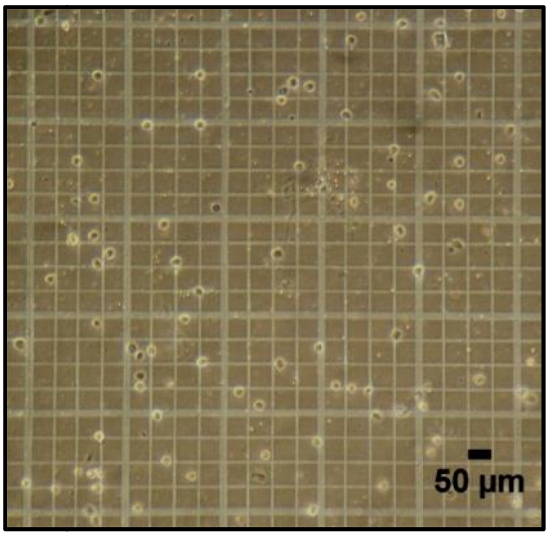

Figure 3-11. HeLa cells suspended in PBS. Cells are in a hemocytometer. Diameters range between 13-25 µm. Picture taken using a digital camera connected to inverted optical microscope (Olympus CK2).

3.3 Electrochemical tests

Electrochemical experiments are performed to obtain the current response of the system in real time when the electric pulses are applied. Since the system is composed of a pair of electrodes and an ionic solution to help the passage of current, it involves an electrochemical cell. The ionic solution used is phosphate buffered saline (PBS), a buffer salt solution that has the function of an electrolyte in an electrochemical cell. From now on, the PBS will be called the buffer. Ag/AgCl wire electrodes are used and connected to a potentiostat to apply the voltage. Three tests are performed using a Gamry Potentiostat (Gamry Instruments) under the software control of Gamry Framework.

The potentiostat is a four-probe instrument, which means that there are four relevant leads that need to be placed in any experiment [42]. Two of these leads carry the current and the other two are sense leads that measure the voltage. Figure 3-12 below shows a legend for these color-coded leads. The leads can be connected for two-, three- and four-electrode experiments.

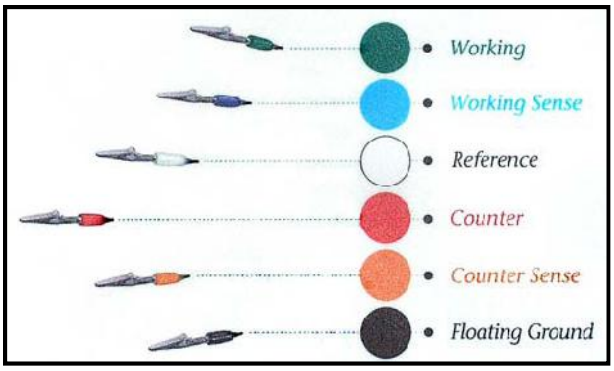

Figure 3-12. Gamry color-coded leads. The working (green) and counter (red) leads carry the current; and the working sense (blue) and reference (white) measure the voltage (potential). [42]

The system is connected as a two-electrode experiment as explained in Section 4.2. With this configuration the current and sense leads are connected together. The working and working sense leads are connected to one electrode; and the counter and reference are connected to the other electrode. As a consequence, the current carrying electrodes are also used for sense potential measurement. Figure 3-13 shows the physical setup used for the electrochemical experiments.

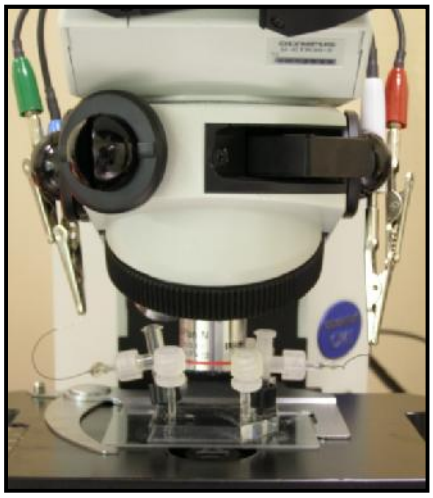

Figure 3-13. Experimental setup for the electrical experiments. The device is over the microscope stage and the electrode tips are connected to the leads of the potentiostat. Working (green) and working sense (blue) are connected to the left electrode; and the counter (red) and reference (white) are connected to the right electrode.

The two-electrode experiment has the simplest configuration but the results are more complicated to analyze. Since each electrode is both carrying the current and sensing the potential, the interface resistance (i.e. due to the voltage drop) between the electrode and the

buffer will be measured. So, the actual measured resistance is larger than the resistance of interest, which is the microchannel resistance. This is explained schematically in Figure 3-14.

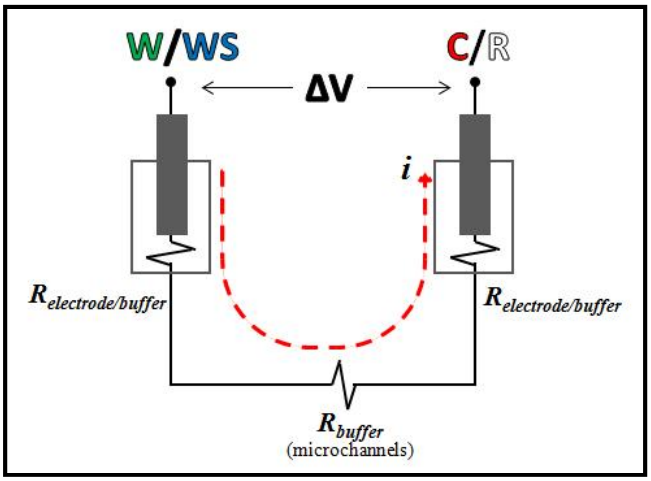

Figure 3-14. Two-electrode configuration schematic. The current passes through the electrodes resulting in a total voltage drop due to the sum of the resistances. Since the current carrying electrodes are also the sense electrodes, the measured resistance is the sum of the interface resistance and the resistance of the bulk (microchannel buffer resistance).

A four electrode experiment has the advantage of eliminating the contribution of the interface resistance. Since the sensing electrodes are connected apart from the current carrying electrodes, the current does not travel through the part of the circuit where the voltage is measured, and this eliminates a voltage drop due to the electrode interface.

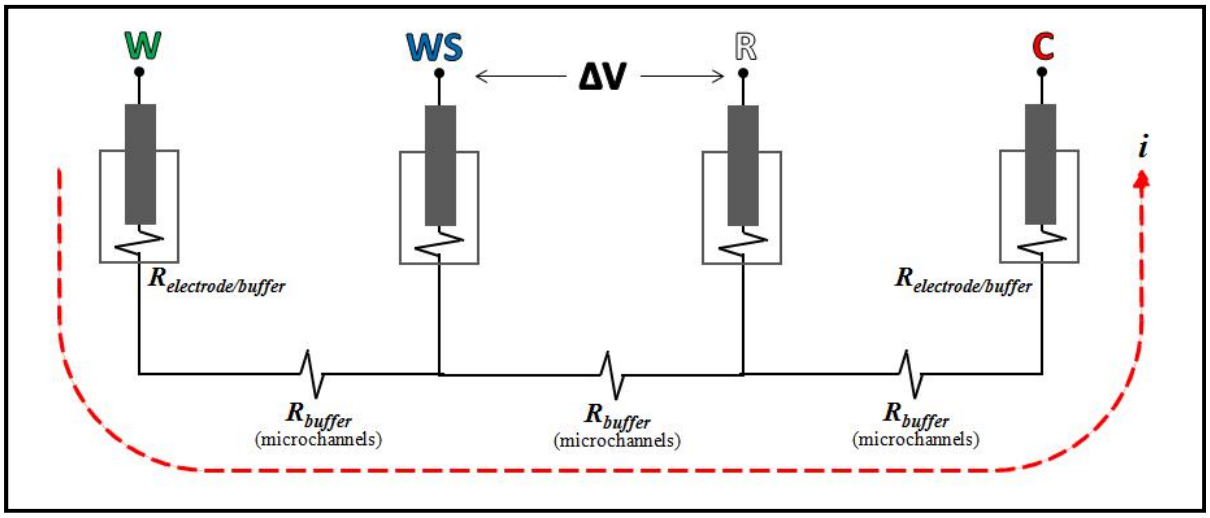

Figure 3-15. Four-electrode configuration schematic.

However, the four-electrode setup was unfit for the experiments due to the geometric nature of the microchannels. This will be explained in detail in Section 4.1. The two-electrode setup was used successfully.

3.3.1 Chronoamperometry

In this test a voltage pulse is applied and instantaneously changed from one value to another. The resulting current that flows is then measured as a function time. The main variables that can be controlled are the pulse magnitude and duration. Figure 3-16 shows a plot of the data obtained for a chronoamperometry test in the microfluidic device filled with PBS (without cells). The plot appears to start at negative values in the time axis because the first pulse is a "pre-pulse"; i.e. a low voltage pulse that is not supposed to cause electroporation. This can be fixed by eliminating this pre-pulse, setting this first value to zero in the software window.

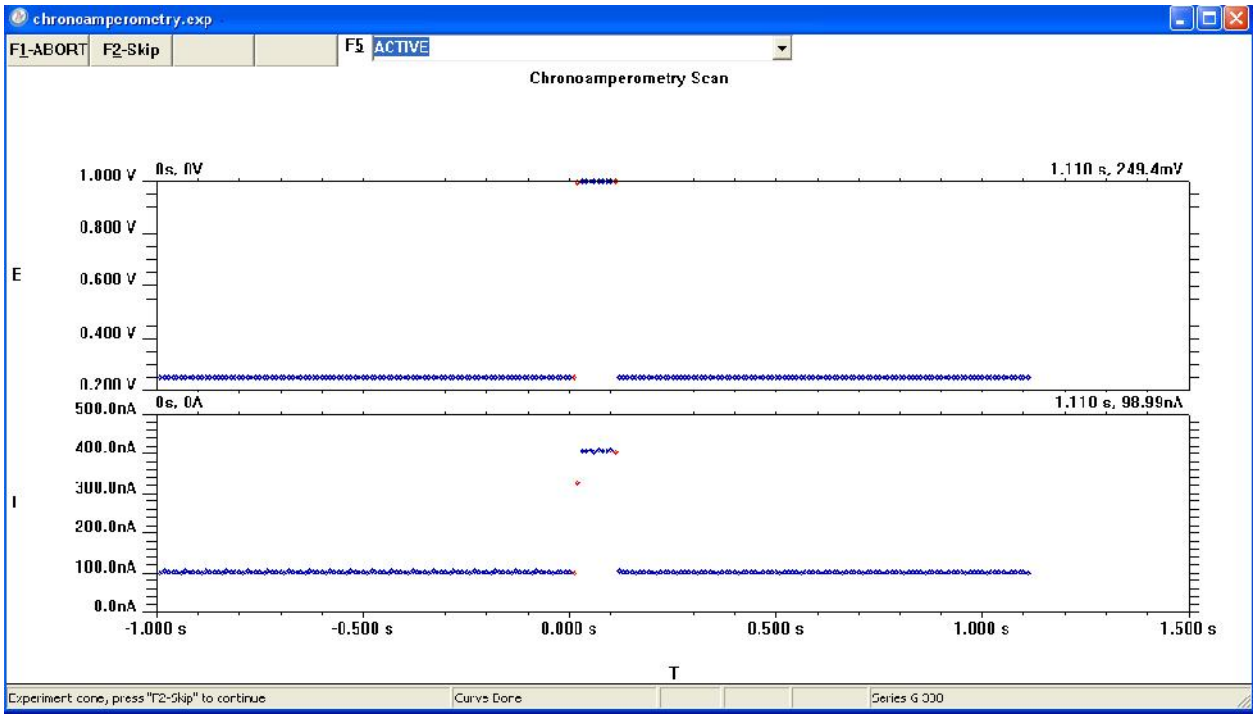

Figure 3-16. Chronoamperometry plot obtained for micro-pore EP device filled with PBS (without biological cells). Screen capture from the Gamry software active window.

The test is performed first with the device filled with PBS (without cells) to characterize the system's resistance. Running the test later with cells inside the microchannel should give a different current response.

3.3.2 Cyclic voltammetry (CV)

In cyclic voltammetry the voltage is swept between two values at a fixed rate and the current response is monitored. It is similar to linear sweep voltammetry (LSV) where the voltage is scanned from a lower limit (usually 0V) to an upper limit. However, in CV when the voltage reaches the upper limit (V_2) the scan is reversed and the voltage is swept back to the lower limit (V_1). Measurements of the current response are plotted as a function of voltage rather than time, unlike chronoamperometry. The test was run in the laboratory with the microchannel filled with saline solution, and the plot resulted linear as shown in Figure 3-17.

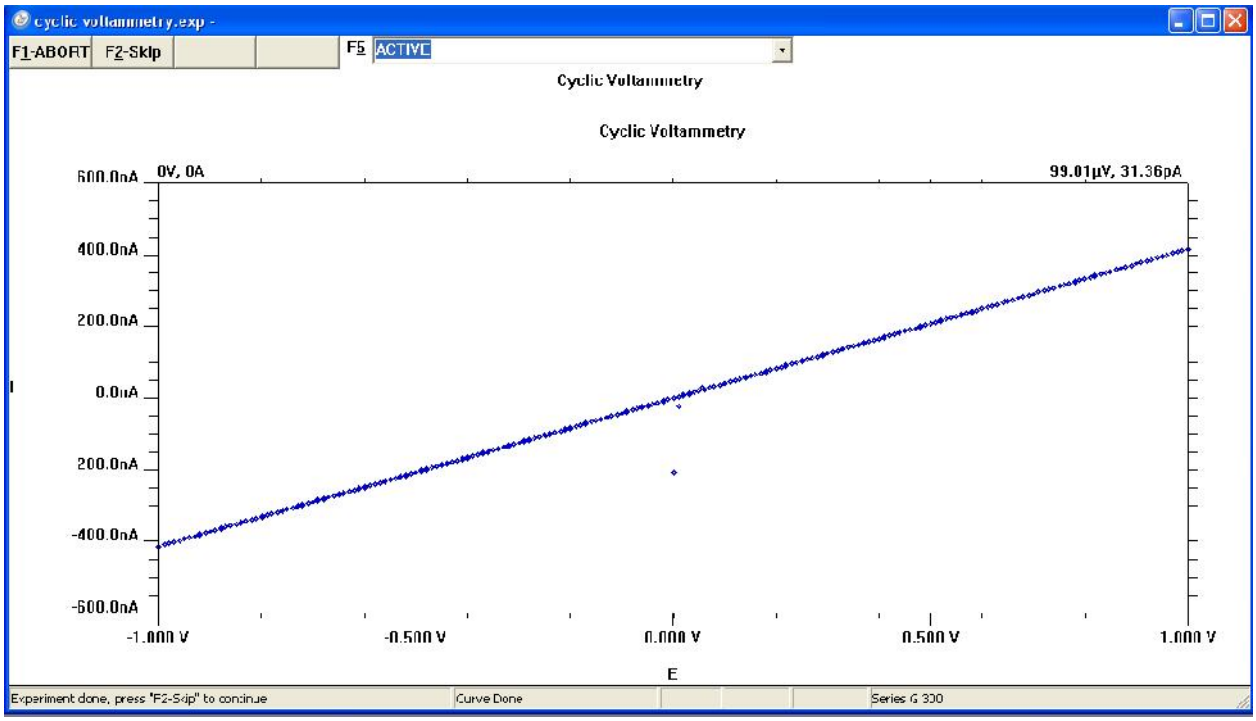

Figure 3-17. CV plot obtained for the microdevice filled with PBS, without biological cells (Gamry Framework). In this case the voltage is swept from V_1 = -1V to V_2 =1V. Screen capture from Gamry software active window.

So, if the plot is linear it is inferred that the system is purely resistive. The slope of this curve represents the inverse of the total electrical resistance of the system (Equation 2-4). The test is run without cells and with cells. In the case where cells are in the microchannel, an increase in the slope means there is more current passing, which is an indicator of permeabilization of the membrane.

3.4 Fluorescence assays

A scientific approach to corroborate if cells were actually electroporated consists of including a dye in the cell suspension that in normal conditions does not permeate the cell membrane. Cells that do not show the dye indicate that the membrane was not permeabilized. If the cell membrane was electroporated, the dye will be visible inside the cell through fluorescence. When the applied electric parameters are not optimal, the membrane is in fact permeabilized, but does not reseal as a result of which the cell content gets out and the cell dies.

Ethidium homodimer

Ethidium homodimer (EthD-1) is a fluorophore that does not permeate to the cell interior when the membrane is intact, i.e. when the cell is alive. When the cell membrane is compromised, EthD-1 enters and adheres to the DNA, emitting a bright red fluorescence (ex/em ~ 495nm/~515nm).

Calcein

Calcein is a fluorophore permeable to the cell membrane that is excited by the presence of intracellular esterase activity, which results in the enzymatic conversion of the nonfluorescent Calcein AM to the intensely fluorescent Calcein. This dye is well retained with live cells, producing an intense uniform green fluorescence (ex/em ~495 nm/~635 nm) in live cells.

EthD-1 at a concentration of 10µM and Calcein at a concentration of 20 µM are added to the cell suspension before entering the microdevice. The intensity of EthD-1 inside the microchannel will be monitored simultaneously as the pulse is applied with the potentiostat. Fluorescence tests will be able to show if electroporation was effective and a success percentage can be calculated to classify the effectiveness of the device. Also, it can be determined if the cells are in good condition. This is extremely important because in a real-life application, these cells will be reinserted into the patient’s body.

CHAPTER 4

DEVICE ELECTRICAL CHARACTERIZATION

The permeabilization state of the cells will be determined by the changes the system experiments when cells are passing through the target zone. In order to study the behavior of the system with biological cells flowing, it is important to understand the electrical behavior of the system when no cells are flowing through the channels.

The basic components of the electrical system are the Ag/AgCl electrodes and the buffer (PBS) which acts as an electrolyte. The buffer needs to be a conductive solution in order to get effective transfer of current. When a salt is diluted in a solvent, such as water, it dissociates into ions making the solution an ionic conductor (or electrolyte).

PBS can be used to provide a buffer system to maintain cell culture media in the physiological pH range (pH~7.1) or to irrigate, transport or dilute fluid while maintaining cell tonicity and viability. The PBS solution is composed of different sodium and potassium salts diluted in water, making it a strong electrolyte. The composition of the PBS used is shown in Table 4-1.

Table 4-1. PBS composition in water

Name	Formula	g/L
Sodium Chloride	NaCl	8
Sodium Phosphate, Dibasic	Na_2HPO_4	1.15
Potassium Phosphate, Monobasic	KH_2PO_4	0.2
Potassium Chloride	KCl	0.2

When a voltage (or potential difference) is applied across the electrodes, the ions in the solution will move and current will flow through the buffer. If there is current flowing, there is an inherent resistance to this fluid. This electrical resistance depends on the properties of the fluid and the volume occupied by it, as given by Equation 2-3.

The conductivity, as well as the resistivity, are properties of the fluid given by its chemical composition and depend on the temperature. The definition of conductivity is given by Equation 4-1.

$$\pm = \frac{1}{\circ} \qquad \textbf{Equation 4-1}$$

The other variables are properties given by the geometry of the channel, which has a rectangular cross-section, as shown in Figure 4-1.

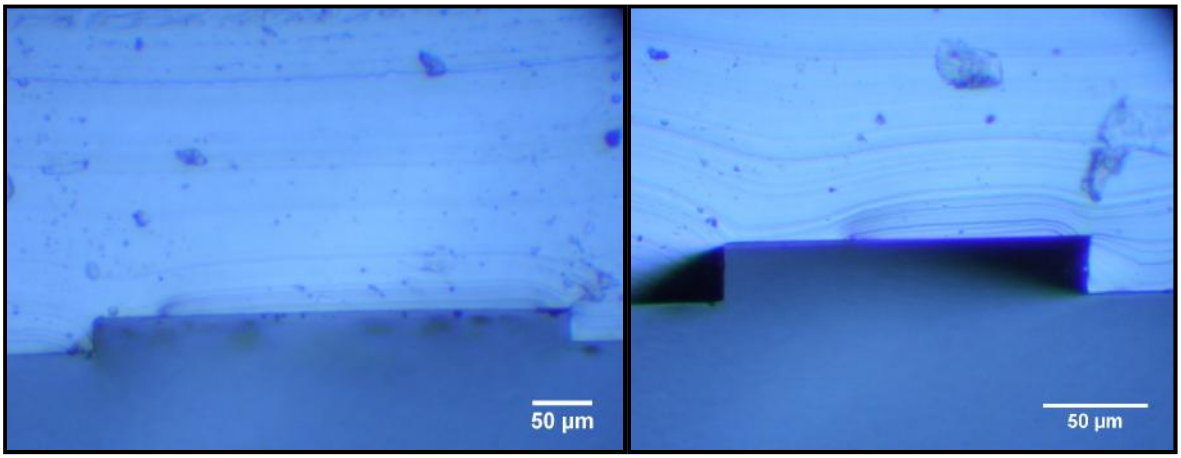

Figure 4-1. Picture of cross-sectional area of microchannels. (Left) The main channel has a width of ~400µm and (right) a subchannel has a width of ~160µm. All the channels have the same height, in this case it is ~30 µm.

From the previous equation it can be observed that a channel with a larger cross-sectional area will have less resistance. So, since the height of the entire channel is fixed, it means that wider channels have less resistance, and vice versa. The effect of this will be seen in the current response when a voltage is applied across the electrodes in the characterization experiments, as will be explained in the following sections.

4.1 Four-electrode experiments

There are three principal configurations for electrochemical experiments. Two-, three- or four-electrode setups can be developed and each has its purpose. The geometry of the microchannels was designed so that, when entering from the left side and exiting on the right side, particles would flow by the principal wider channel. Four additional sub-channels would be used to position the electrodes so that a four-electrode setup could be used. As shown in Figure 4-2, the

main channel goes from port labeled “A” to the port labeled “F”. The subchannels are connected to ports B, C, D and E.

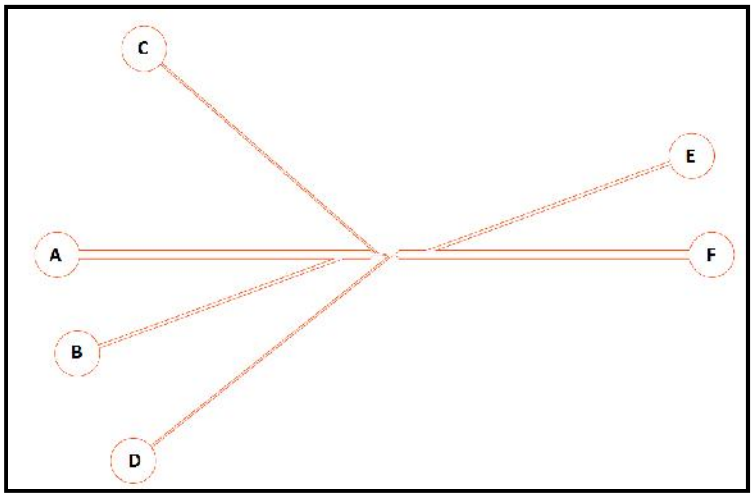

Figure 4-2. Schematic of microchannel geometry. Ports labeled A, B and C are on one side of the target zone. Ports D, E and F are on the right side of the target zone.

A four-electrode setup impedance (resistance) uses a pair of electrodes that carry the current and an additional pair of electrodes to measure the potential. This gives the advantage of eliminating the electrode polarization effects in the measured resistance. The sensing (measuring) electrodes would be connected to the channels close to the (ports C and D) and the current carrying electrodes would be positioned at the farther ports (B and E). The current passing is the same across the main channel, as shown in Figure 3-15, but the voltage drop measured is smaller. Different configurations were tested but the current response was too small to be detected with the resolution of the potentiostat software. This is due to the high resistance imposed by the subchannels, which have the smaller cross-sectional areas.

4.2 Two-electrode experiments

The presumption that the voltage drops homogeneously within the channels does not hold if there are electrical inhomogeneous layers at the electrode interfaces, which create a significant voltage drop and by this reduce the electric field in the channels. Such layers may be created by the accumulation of ions at the electrode from the electrolyte; which is known as electrode polarization. In the two-electrode setup, the current carrying electrodes are also the sensing electrodes, so the resistance imposed by the electrode/electrolyte interface needs to be taken into

consideration. However, since our interest is to detect a *change* in the resistance; the only drawback presented by this setup is that the measured resistance will be larger.

So, there is only one pair of electrodes in this configuration. The working and working sense leads are connected to one electrode and the counter and reference leads are connected to the other. Theoretically, there are 6·6 = 36 possible configurations of placing a pair of electrodes in this six ports device. However, this number of combinations is reduced to 18 because each electrode must be at one side and the other across the narrow section, in order to measure a change in the current response when cells are flowing. Table 4-2 shows the configurations that were studied.

Table 4-2. Two-electrode experiment configurations.

Setup	A	B	C	D	E	F
1	In		W/WS	C/R		Out
2	In		C/R	W/WS		Out
3	In	W/WS		C/R		Out
4	In	C/R		W/WS		Out
5	In	W/WS			C/R	Out
6	In	C/R			W/WS	Out
7	In		W/WS		C/R	Out
8	In		C/R		W/WS	Out
9	In	W/WS			Out	C/R
10	In	C/R			Out	W/WS
11	In		W/WS		Out	C/R
12	In		C/R		Out	W/WS
13	W/WS	In		C/R		Out
14	C/R	In		W/WS		Out
15	W/WS	In			Out	C/R
16	C/R	In			Out	W/WS
17	W/WS	In			C/R	Out
18	C/R	In			W/WS	Out

The inlet and exit were varied as can be seen. The cells could be entered from either port A or port B, and exited either from port E or port F. Even though all of these setups were studied, it has to be noted that there are practically 9 possible setups. For example, the only difference between setup 1 and setup 2 is that the leads are inverted. The only difference should be the sign

which was experimentally proved. The purpose of studying all the possible setups was to determine the least resistance path for the current.

4.3 Theoretical resistance

The device filled with PBS and connected to Ag/AgCl electrodes acts as an electrical circuit, with the buffer acting as an electrolyte. The electrical resistance of an electrolyte is determined by the properties of the liquid and its geometry, as in Equation 4-1. So, neglecting the resistance at the electrode/electrolyte interface, the total electrolyte resistance can be taken as the sum of the resistance of the microchannels and the interconnection fittings.

$$R_{total} = R_{channels} + R_{\text{int}erconnections} \qquad \textbf{Equation 4-2}$$

Regarding the microchannels, the length and cross sectional area will vary across the channels. So, the resistance of the microchannels is determined by adding the contribution of each segment.

$$R_{channels} = \sum_{i=1}^{n} \frac{\rho L_i}{A_i} \qquad \textbf{Equation 4-3}$$

The resistivity depends on temperature; it can be taken to be constant throughout the channels assuming there is no significant change in temperature.

$$R_{channels} = \rho \frac{\sum_{i=1}^{n} L_i}{\sum_{i=1}^{n} A_i} \qquad \textbf{Equation 4-4}$$

where n is the number of segments that are between the electrodes. The whole design was divided into 23 segments of different shapes (rectangular, circular and trapezoidal) to study the contribution of each segment to the total resistance (Figure 4-3). The resistance of each setup is approximated as the sum of the segments that are connecting one electrode with the other one.

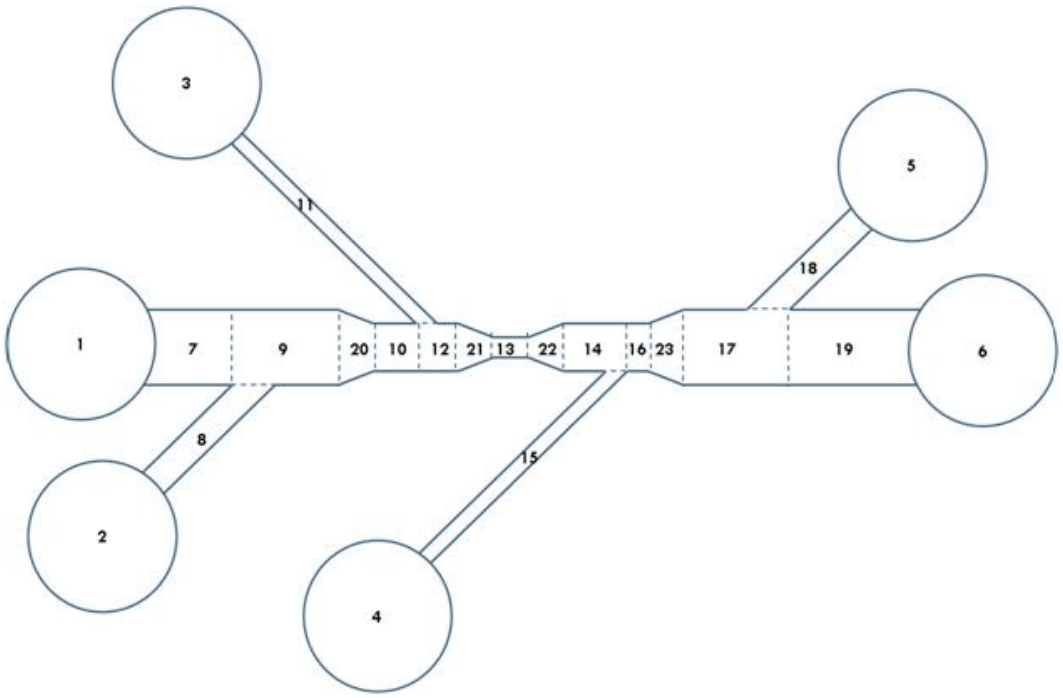

Figure 4-3. Microchannel segments considered for the theoretical electrical resistance.

For example, for setup 1 the electrodes are located into ports C and D, so the contribution of the segments between these entrances is added (i.e. i = 3, 11, 12, 21, 13, 22, 14, 15, 4). This gives a source of error since the current is not exactly flowing normal to the areas of all segments. This is true especially for the segments that connect the subchannels to the main channel.

The resistance for the rectangular areas,

$$R_{rectangular} = \frac{°L}{hw} \qquad \textbf{Equation 4-5}$$

Where h is the height of the channel, which is constant and w is the width. For the trapezoidal areas, the width changes as a function of the length, so:

$$R_{trapezoid} = \int_0^L \frac{°}{hw(x)}dx = \frac{°L}{h}\left(\frac{w_f + w_0}{2}\right) \qquad \textbf{Equation 4-6}$$

where L is the length of the trapezoidal segment, usually known as the "height" of a trapezoid; w_f is the "base" of the trapezoid (widest part) and w_o the "top" of the trapezoid. The port areas (where the fittings are connected to the channels) are circular, so the resistance is given by:

$$R_{ports} = \frac{4 \cdot t}{\pi D^2}$$ **Equation 4-7**

where D is the diameter of the punch (2mm). The interconnections that connect the path from the electrodes to the microchannels are luer lock fittings, as explained in Chapter 3. The total resistance includes the contribution of the PBS volume inside the fittings; however, this value is so small that it can be neglected. The resistance of these interconnections is calculated as follows,

$$R_{interconnections} = \frac{4 \cdot L_{fitting}}{\pi D_{fitting}^2}$$ **Equation 4-8**

Due to the fact that the resistance is inversely proportional to the cross sectional area, the resistance of the fittings will be small compared to the resistance of the microchannels since the cross sectional area is extremely large in comparison to those of the channels. Thus, it can be assumed to be negligible. The complete calculations are included in Appendix A.

The results of the calculations for the 18 setups are shown in Table 4-3. As mentioned before, for practicality, there are 9 different values.

Table 4-3. Theoretical resistance values for two-electrode setups.

Setup	Resistance (MΩ)
σ=1.533S/m (ρ=0.6523 Ω-m)	
1,2	6.615
3,4	5.400
5,6	3.993
7,8	5.208
9,10	2.972
11,12	4.188
13,14	4.380
15,16	1.953
17,18	2.973

The major contribution for the total resistance is in the smaller areas, such as the narrow section at the center and the thinner subchannels. The resistance is larger when the electrodes are connected. It can be seen that the path of least resistance is in setup 15 and 16, where the electrodes are connected across the main channel. When connecting the electrodes in the thinner

subchannels (such as in setup 1 and 2) the resistance increases considerably. In this case the reduced area dominates the total resistance.

4.4 Experimental resistance

The experimental resistance was determined by the analysis of electrochemical tests. The setup consisted of the device filled with PBS and the electrodes connected to the potentiostat. The conductivity of the PBS was measured before running the experiment in a centrifuge tube at ambient temperature using a conductivity meter (Oakton Con 6).

Running a cyclic voltammetry test resulted in a linear behavior as shown in Figure 4-4. This is a way of understanding the behavior of the system as mostly resistive. The experimental resistance was calculated by finding a linear fit to the graph. The inverse of the slope of this fit was taken as the experimental resistance.

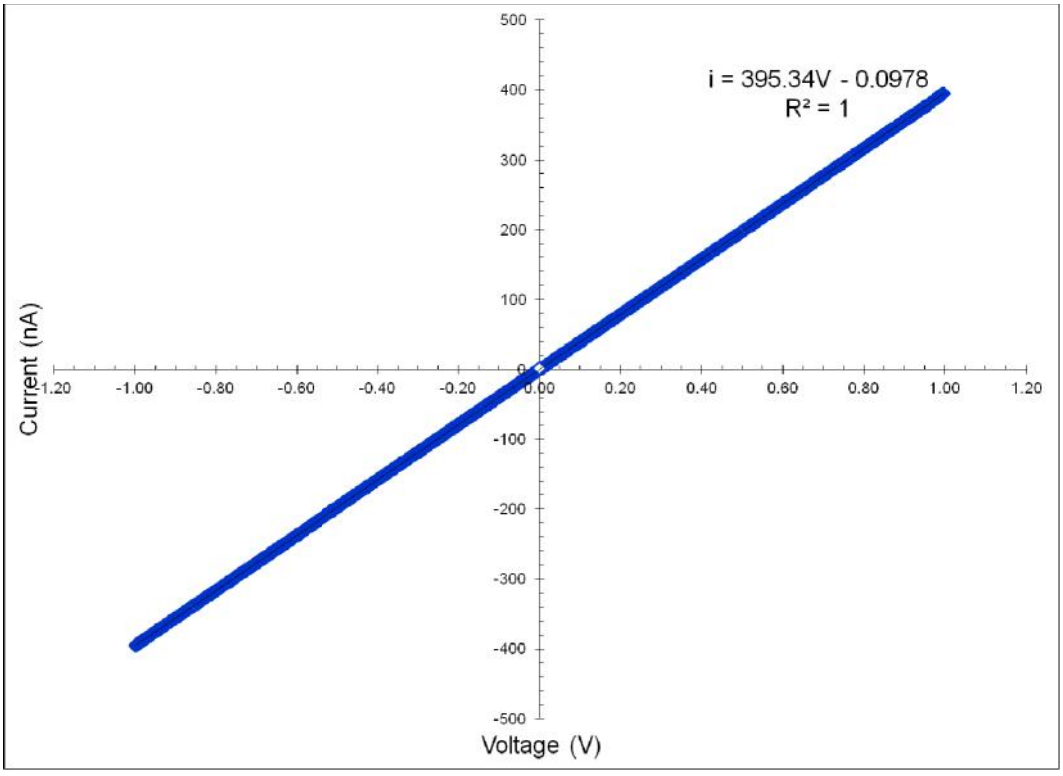

Figure 4-4. Cyclic voltammetry for device filled with PBS. In this case the electrodes were positioned at ports A and F (setup 15). The inverse of the slope gives an experimental resistance value of 2.529MΩ.

An approximation of this resistance can be made by selecting any two points from the plot and using the inverse of the slope equation:

$$R \approx \frac{V_2 - V_1}{i_2 - i_1} \qquad \textbf{Equation 4-9}$$

The experiment was repeated and was compared to the approximated theoretical resistance, as shown in Figure 4-5.

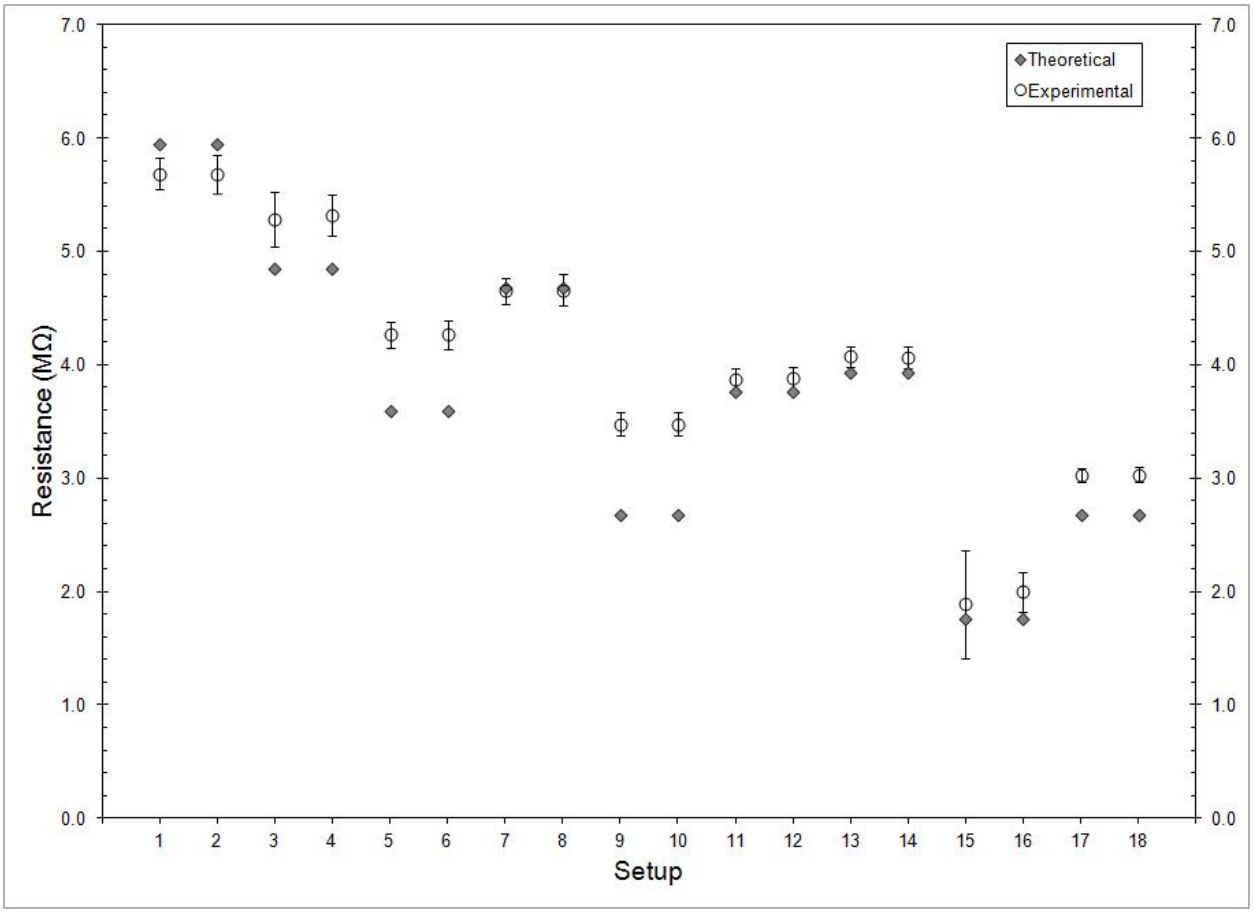

Figure 4-5. Experimental electrical resistance of the device filled with PBS compared to approximated theoretical resistance.

The effect of the approximation for the theoretical resistance can be appreciated in the setups that include complicated junction that were approximated (e.g., in setup 1&2, the junction of areas 14 and 15). The approximation on setups that include port B generate a systematic error in the calculation of the resistance. In general, the resulting behavior taken from experiments is similar to the expected behavior from the theoretical resistance. The path of least resistance was found to

be when the electrodes are positioned at ports A and F; these are the ports that connect the main (wider) channel. The importance of this finding is that the contribution of cross-sectional area is significant in the resistance for these devices. For future designs, it needs to be taken into consideration. The following experiments for cell detection and permeabilization were done with the setup of least resistance. So, when the channels are filled with PBS, using setup 15 or 16, the system has a resistance of ~2MΩ; and the flow of a particle through the narrow zone will induce an additional resistance due to the area restriction. This should give a detectable current feedback.

Chronoamperometry Results (Setup 15)

Applying different square pulses of different time duration resulted in a current square response as shown in Figure 4-6.

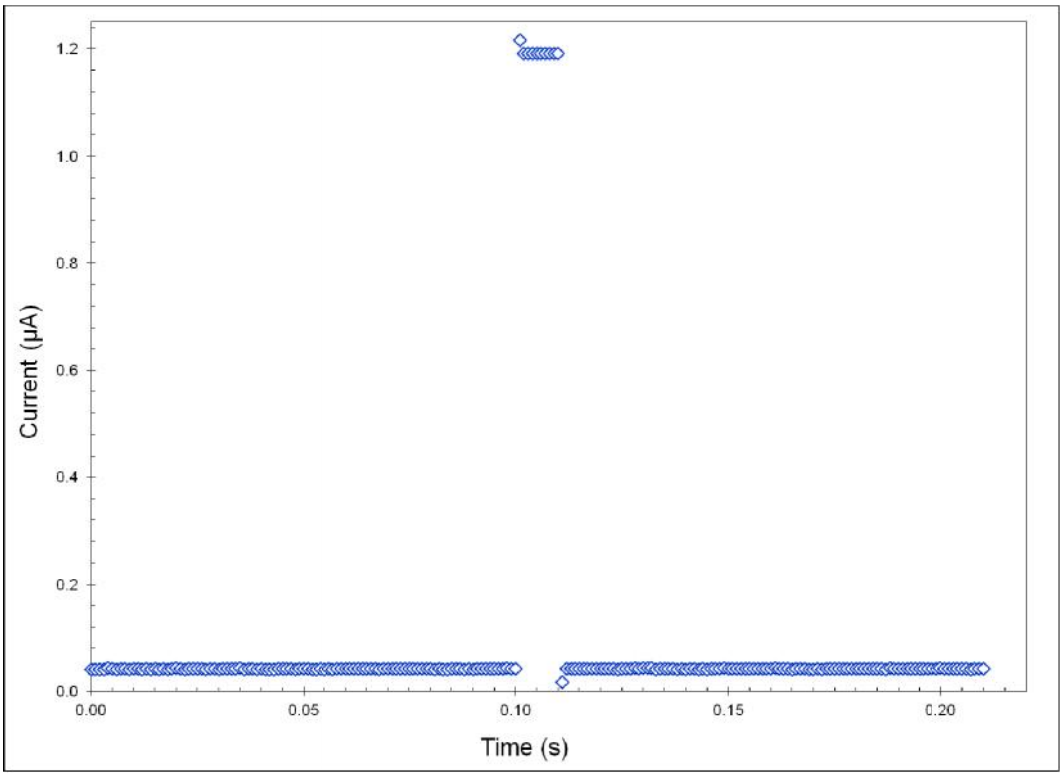

Figure 4-6. Chronoamperometry for device filled with PBS. Constant pulses of 100mV, 3V, 100mV were applied.

Dividing the magnitude of the applied pulse by the resulting current gives the resistance of the device, as given by Ohm's law. The results for the resistance calculated for all the pulses studied

are shown in Figure 4-7. The average is 2.408MΩ, which roughly can be taken as a reference resistance for the device without cells.

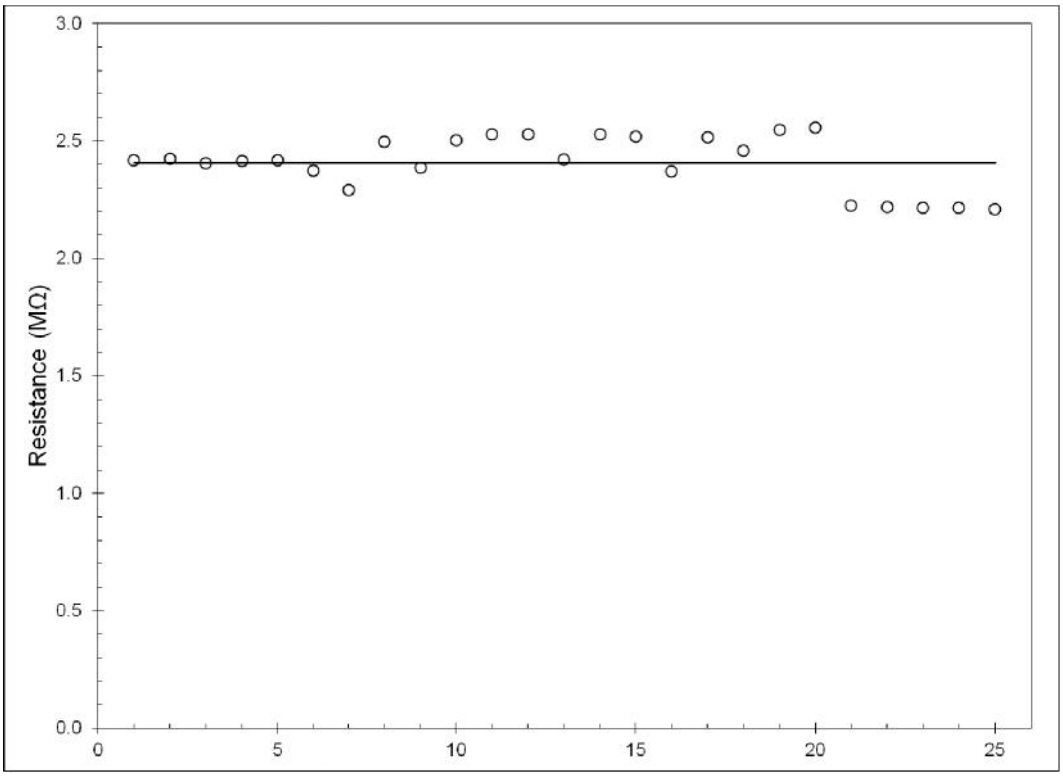

Figure 4-7. Experimental microchannel reference resistance calculated for different square pulses applied. The average is 2.408MΩ (Setup 15)

CHAPTER 5

RESULTS: ELECTRICAL DETECTION

When applying a constant magnitude pulse to the system filled with PBS a proportional current response was detected. If a particle flows through the narrow zone, the resistance is significantly increased so a change in this current is expected to occur while a pulse is being applied. Current response was studied first while flowing polystyrene microparticles ("microbeads") and then with HeLa cells.

5.1 Polystyrene microparticles ("microbeads")

Spherical polystyrene microbeads of 15µm diameter (Polysciences) were used to study the general behavior of a particle flowing through the target zone. Microbeads are more rigid than cells, so when they pass through a narrow zone they do not get deformed. If the width of the channel is larger than the bead diameter, it will flow through it; if the width is smaller, it will get stuck and not cross the channel.

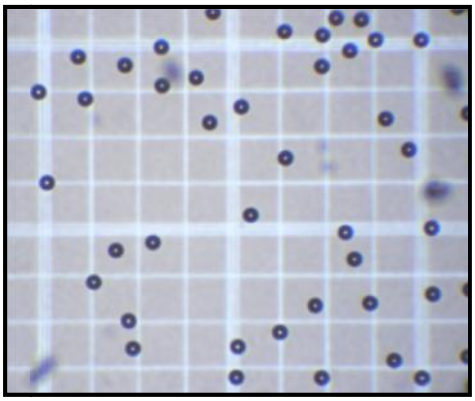

Figure 5-1. Sample of polystyrene beads suspended in PBS. Image of sample was taken at hemocytometer to show scale.

One characteristic of PDMS is that it is flexible, and gets damaged with time. The typical PDMS replica has a narrow zone width of 10-12µm. This difference in the features size gets transferred from the mask to the silicon wafer master in the photolithography process and from the master to the PDMS replica. However, usage with time causes this change as shown in Figure 5-2.

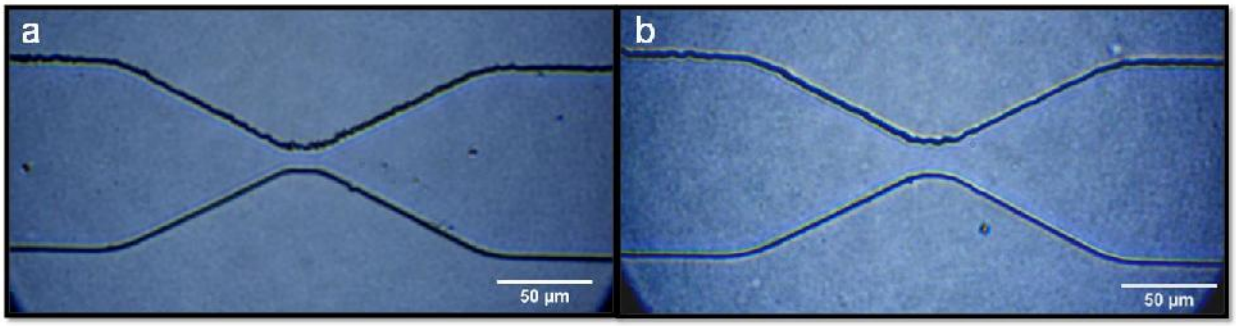

Figure 5-2. Micrograph of narrow section in (a) a typical microdevice used for experimentation and (b) a wider channel used for experimentation with 15µm microbeads.

The narrowest part of the device (shown in Figure 5-2b) measures approximately 16.5µm, so 15µm beads were indeed able to pass through this zone. This enabled us to study the electrical behavior. Although the beads did not deform, they flowed very close to the channel walls in the narrow section, and hence the conductivity area was significantly reduced and the resistance thus increased. When applying a constant magnitude pulse with chronoamperometry, the signal current was proportional, but suddenly changed when a bead passed through the narrow section. A noticeable current drop was observed in real time for each passing bead.

Figure **5-3** shows the data plot obtained with Gamry software for one of the experiments where a 500mV pulse was applied during 3 minutes.

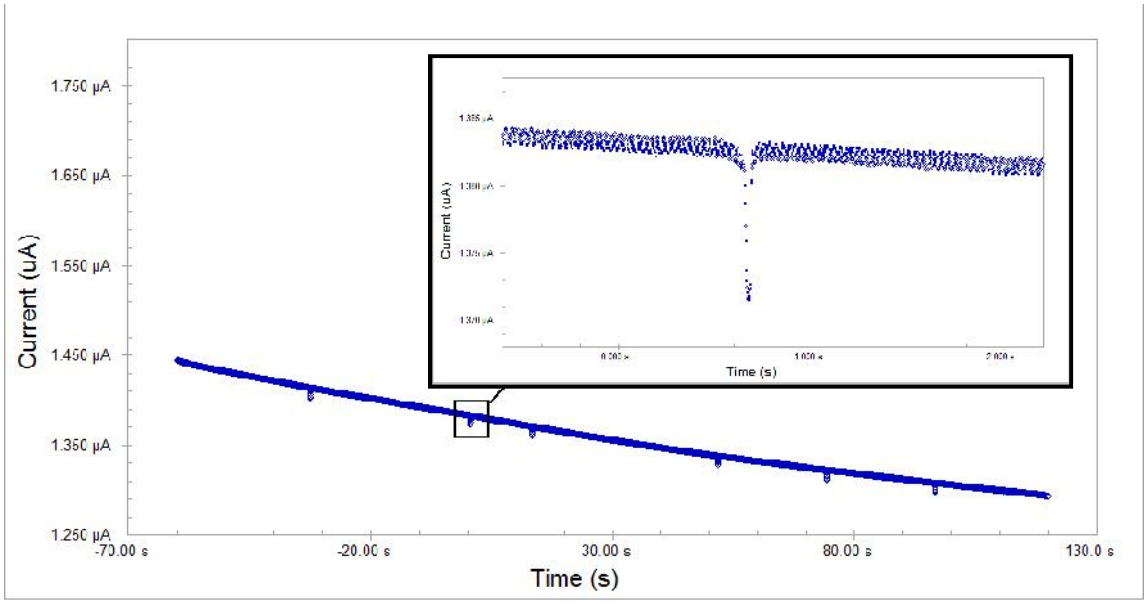

Figure 5-3. Chronoamperometry run for a device filled with PBS and 15µm beads flowing. The inset shows a magnified view of the current drop that occurs when a bead is passing through the narrow zone. Pulse applied = 500mV

It is important to observe that the overall current is not constant along the pulse; it is slowly dropping from 1.44µA to 1.29µA. This 152nA decay represents a voltage drop of ~55.8mV.

This is due to the degradation of the electrodes because the test was run for 3 minutes so the electrochemical effects become significant.

From simple observation, the current drop seems like a vertical line of same magnitude for all the beads. The current drop was measured for each bead passing and it was found to be the approximately the same for all the beads. This makes sense since the beads are approximately the same size and they do not deform at the narrow zone. (Information from the manufacturer indicates a standard deviation of ±1.43µm in bead diameter). Figure 5-4 shows the values for different beads passing through the zone. This corresponds to a mean of ~11.75nA, presenting a voltage drop of approximately 4.3mV.

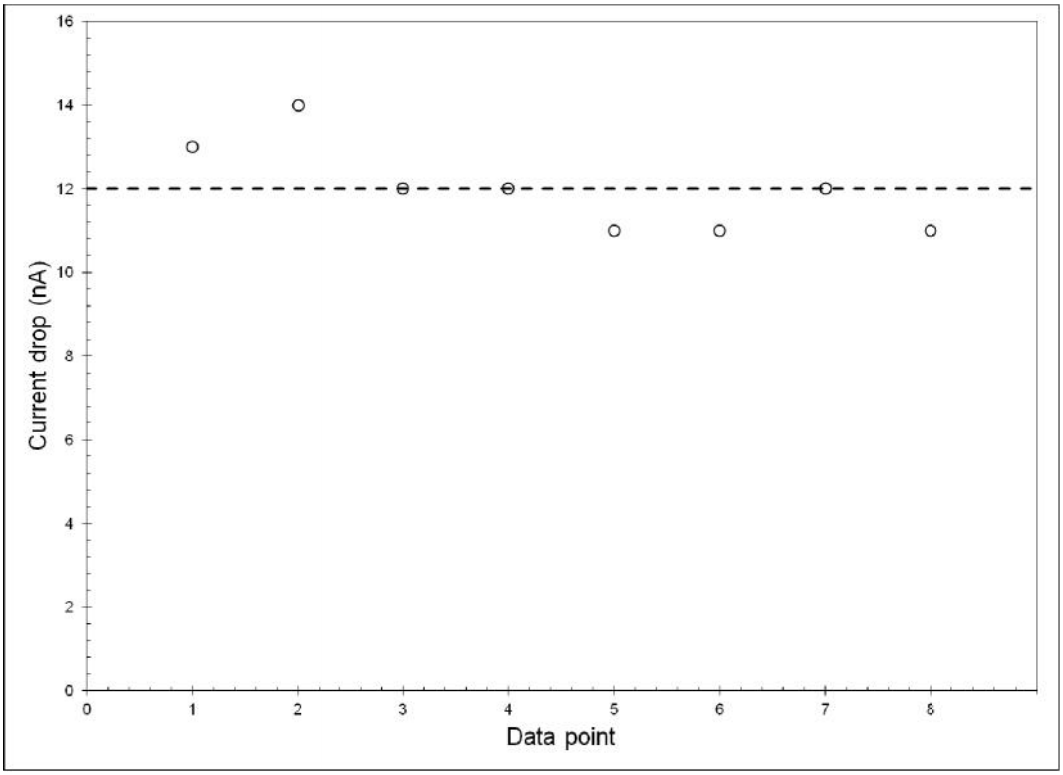

Figure 5-4. Current drop values for beads passing through the narrow zone.

5.2 HeLa cells

Even though the behavior of the device filled with PBS was characterized for the devices as explained in Chapter 4, a slight difference in the resistance values might occur due to different experimental conditions. Thus, the electrical tests were performed previous to each experiment to get a reference value of the average current that passes when no cells are flowing. Figure 5-5 shows the average current flowing for a range of pulses applied when the device was filled with PBS only.

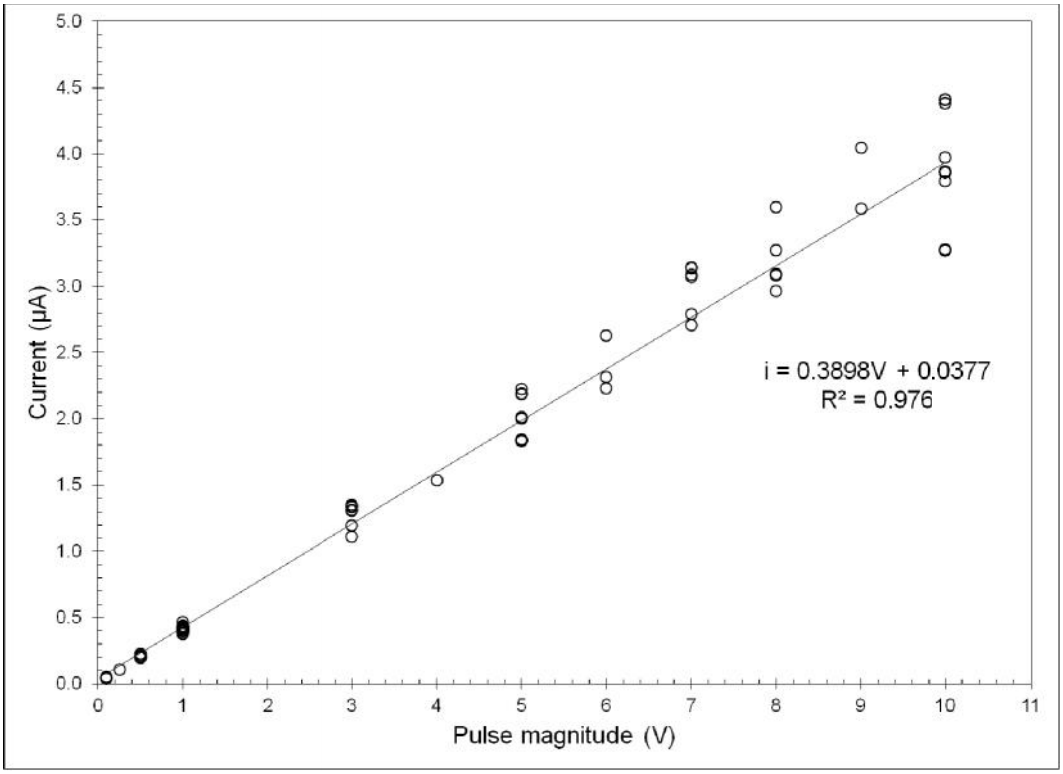

Figure 5-5. Average current for different experiments with different pulses applied to the device with PBS only.

The electrical behavior was found to be resistive, with a resistance of ~2.476MΩ as shown in Figure 5-6.

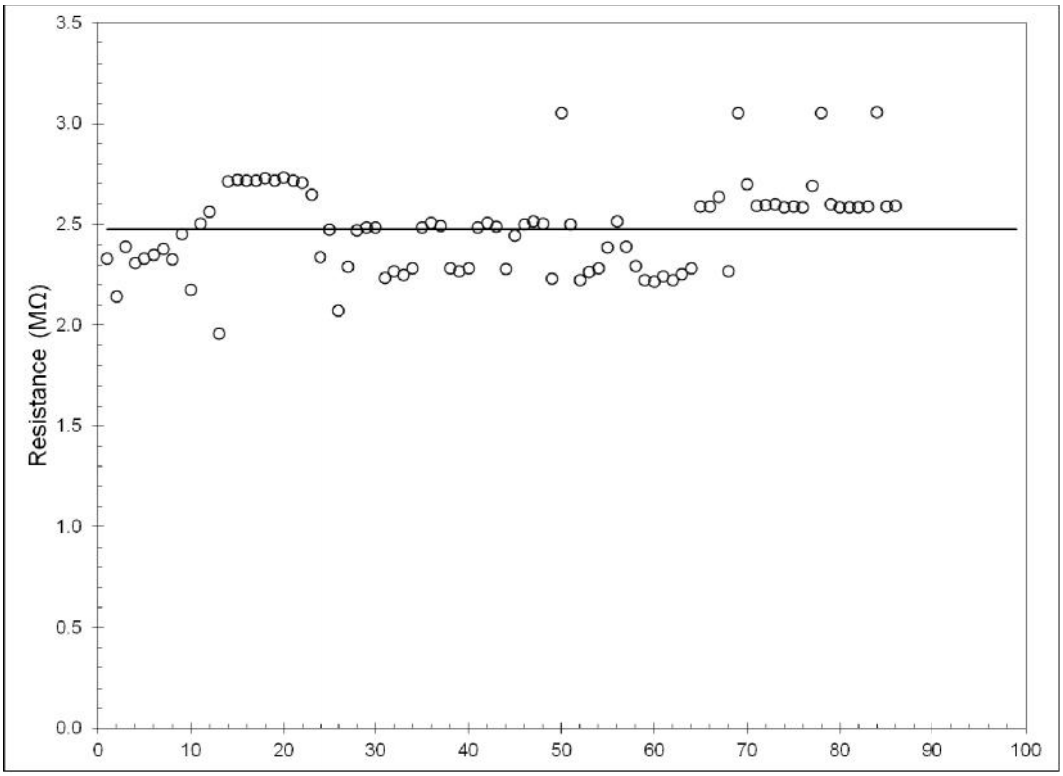

Figure 5-6. Electrical resistance of the device filled with PBS at different voltage pulses.

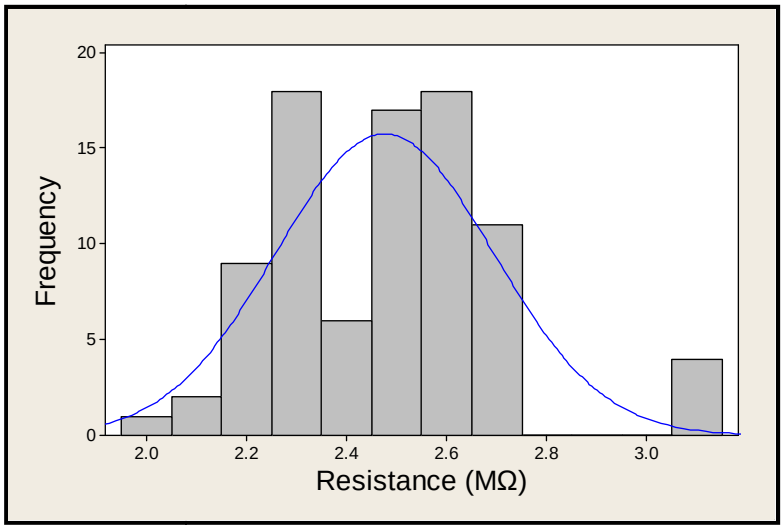

Figure 5-7. Frequency histogram of microchannel resistances calculated by Ohm's law with the average current and applied pulse for different experiments.

After having this set, the cells in culture are suspended in PBS as explained in Section 3.2. The cell suspension is injected into the inlet fitting (port A) using a syringe and cells started

to flow through the main channel in the direction toward the exit (port F). Image frames of the video are shown in Figure 5-8.

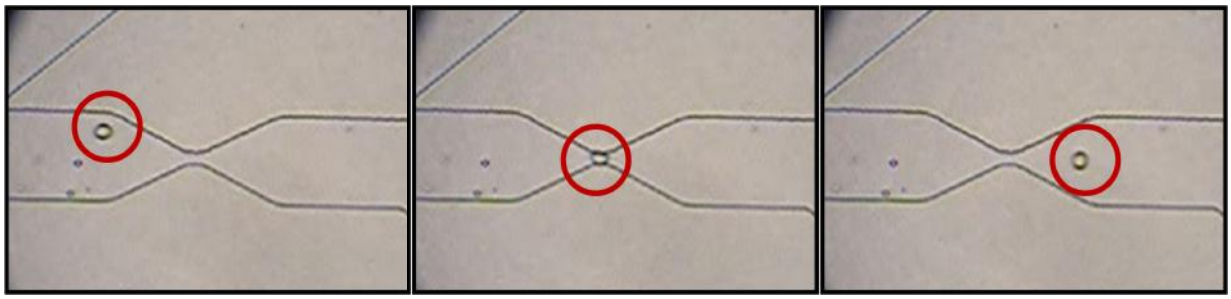

Figure 5-8. Image sequence of a regular sized HeLa cell flowing through the narrow zone of the device. It can be seen how the cell deforms when passing through the narrowest part.

The electroanalytical method that gives information about a sudden change in the current is chronoamperometry, where a constant pulse was applied and the current response was recorded simultaneously. Each time a cell passed through the narrow zone, a sudden current drop was detected as was seen with the microbeads. This can be seen in a screen capture from the Gamry Framework software, shown in Figure 5-9, where a constant pulse of 3V was applied during 6 seconds.

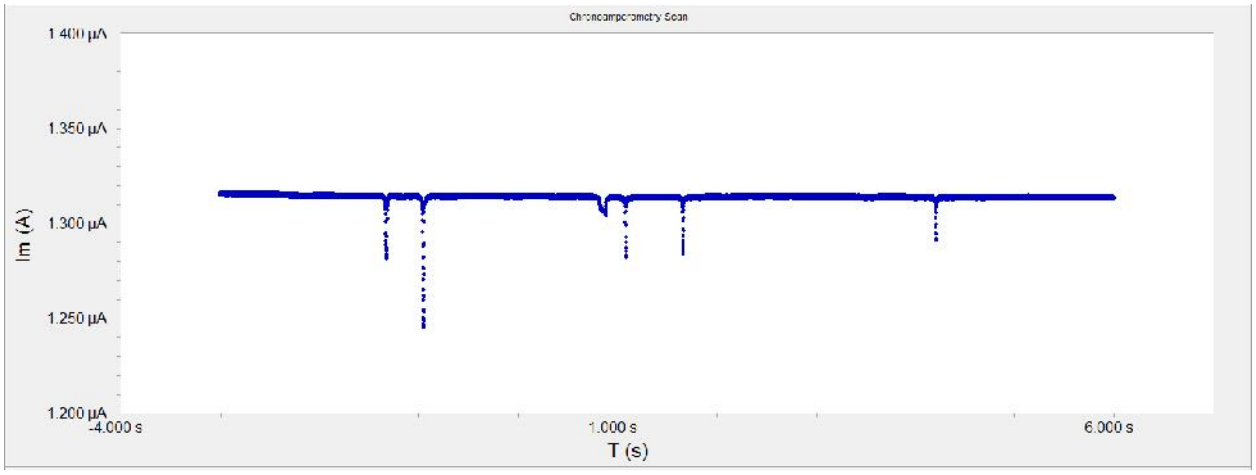

Figure 5-9. Chronoamperometry run for a device filled with PBS and HeLa cells flowing. Pulse applied = 3V

The current drops and rapidly goes back to its constant value in the same manner as with the beads, but the magnitude of this current drop was not the same for all the cells. In this case, the cell deforms when passing through the narrow zone and so the cell is closer to the channel

walls. The time it takes for this current drop to occur can be interpreted as the time the cell is in contact with the channel walls in the narrow zone.

As mentioned before, the larger the cell, the closer it will be to the channel walls and the larger the drop in current. This was in fact observed through the microscope. The larger the cell, the larger the current drop. The relationship between approximate cell size and the current drop was analyzed and is presented in Figure 5-10. Cell diameter was calculated using ImageJ and the current drop was approximated with the data obtained from the electrochemical analysis software.

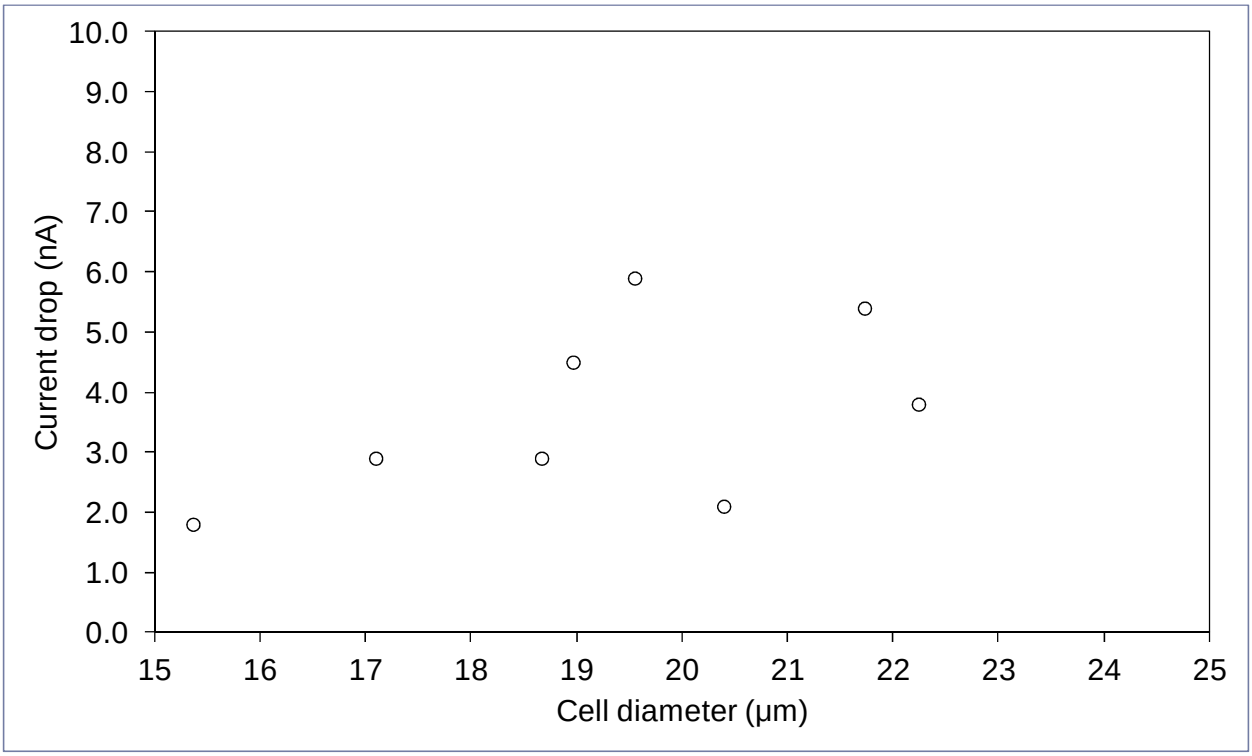

Figure 5-10. Relationship between cell size and electrical current drop.

There are two types of current drops occurring and a zoomed view is shown in Figure 5-11. The current drop at the right shows the same profile as the one seen when microbeads were flowing through the narrow zone. The duration of this drop (~50ms) is very small and the magnitude large in comparison to the other type of current drop. This indicates that a cell flowed very fast through the target zone, inducing a sudden restriction for the current to pass. However, the current drop at the left side has a duration of ~100ms and decreases at a lower rate.

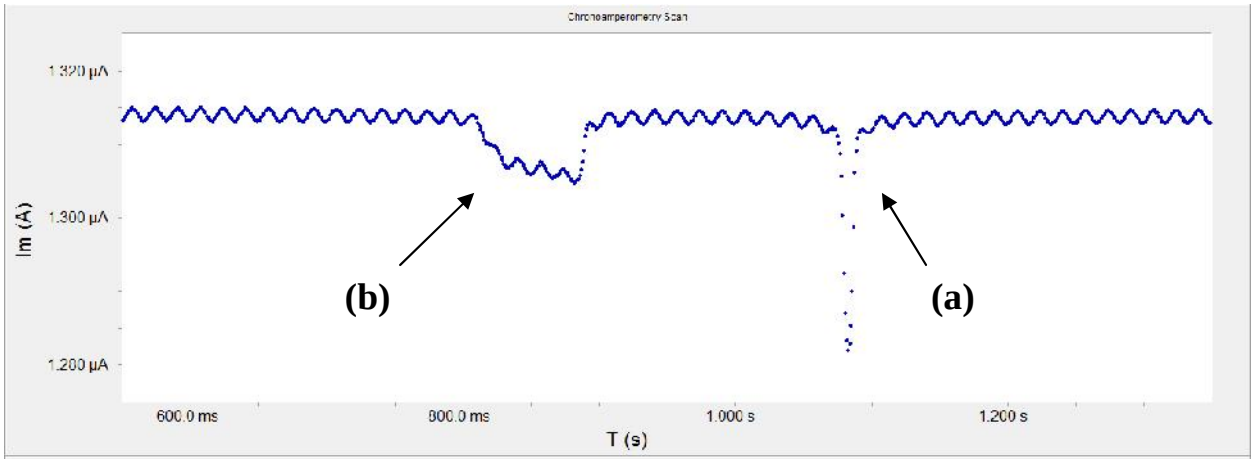

Figure 5-11. Current drop profiles for cells passing through the narrow zone. (a) The current drop, similar to the beads current drop, indicates that a cell is passing through the narrow zone. (b) Current drop is less steep and has longer duration, which might be indicative that permeabilization occurred. The image is a zoomed view of a selected area in Figure 5-9.

Since the duration is larger, it means that the cell took more time to pass through the narrow zone because of its size. A larger cell deforms and travels along the narrow zone for a longer period of time. Also, the less pronounced current drop implies that it did not present much restriction for the current to pass. This might be indicative that permeabilization of the membrane occurred. The large cell deformed when passing through the narrow zone, making a tight seal with the channel walls and thus receiving a high intensity electric field around the membrane. This high electric field induced permeabilization by the electroporation phenomenon, so the current had a path in the membrane to pass. This is shown in the less pronounced current drop. However, optical corroboration is needed to confirm that electropermeabilization occurred.

5.3 Conclusions

- The electrical behavior of the system was characterized with microbeads and HeLa cells and both give the same response when a voltage pulse is applied to the system.
- A current drop occurs when a particle passes through the narrow zone, as a result of restricting the volume for the passage of current.
- Since cells are less rigid than beads, they deform when passing through the channel. It was observed that the current drop is proportional to the size of the cell.
- The current drop allows for a real-time cell counting.

- A characteristic profile of current drop was observed for cells passing through the narrow zone. This drop has duration ib the range of milliseconds and a steep change in magnitude, depending on cell size.
- A characteristic profile is suggested for permeabilized cells, with a variation in the current drop magnitude and longer duration.

CHAPTER 6

RESULTS: OPTICAL DETECTION OF ELECTROPERMEABILIZATION

Optical corroboration of electroporation has been the most commonly used method for corroboration of membrane permeabilization. This method was used to confirm that permeabilization has actually occurred, correlating with the electrical results shown previously.

A constant DC pulse was applied while cells were flowing and the current response was recorded simultaneously with the optical video. Different pulse magnitudes were applied and the change in fluorophore uptake was evaluated optically. Two fluorophores were used for assessing membrane permeabilization. Calcein AM was used to detect healthy cells, since this fluorophore is permeable to the cell membrane and fluoresces in green when a live cell is active. Ethidium homodimer (EthD-1) enters into cells that have a broken membrane and emit a red signal, so it is expected to observe a permeabilized cell change from green to red. A Nikon 80i microscope was connected to a digital camera and a filter B-2A which allowed observation of both fluorophores at the same time.

Cells were suspended in PBS as explained in Section 3.2. EthD-1 was added to the cell suspension at a concentration of 10μM and Calcein at 20μM were added to the cell suspension in a centrifuge tube. The suspension was injected into the device as usual and cells started to flow along the main channel. It was observed that cells entered the channels tinted in green. This means that the cells were alive since Calcein emits a green fluorescence when interacting with live cells.

6.1 Release of Calcein

The permeabilization of the membrane was evaluated qualitatively by observing the release of the Calcein. Figure 6-1 shows a sequence of images of a cell flowing and reaching permeabilization with a constant pulse of 10V.

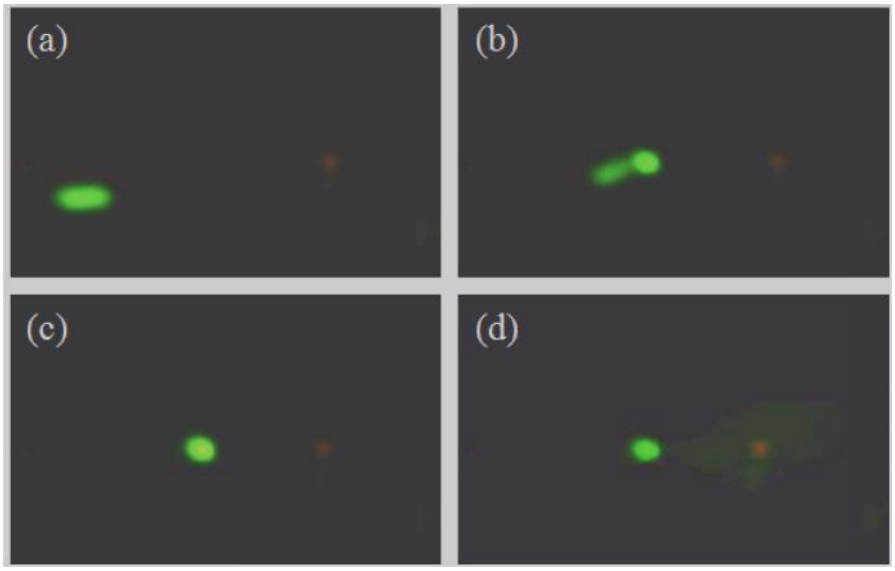

Figure 6-1. Image sequence of fluorescence corroboration of HeLa cell permeabilization at 10V. (a-c) Flow of the cell through the channel into the narrow section. (d) Release of Calcein (green) from the cell.

When a pulse is applied the cell flows through the main channel, reaches the narrow section and stops there, the green dye is released into the channel and the cell continues flowing. This behavior was observed when a pulse was being applied during the trajectory of the cell; but when there was no pulse applied this was not the case. This may be explained by the phenomenon of electrodeformation. Electric fields induce forces at the membrane. It has been showed that DC pulses induced short lived shape deformations in cells and may also lead to fluid flows [43]. Figure 6-2 shows the deformation of the cell that was observed while a pulse of 10V was applied to the device.

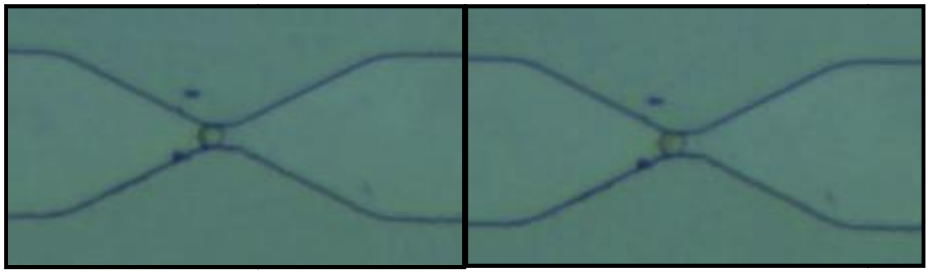

Figure 6-2. HeLa cell expansion of a cell experiencing a 10V pulse.

Ethidium homodimer was observed in some dead cells that were in the suspension and flowed through the channel. However, the intake of this dye was not observed for any pulse applied. Two possible explanations are proposed for this:

- The size of the dye molecule is larger than the pores that formed at the cell membrane.
- The process of diffusion at the membrane was competing and the intake of the dye was not fast enough to express the fluorescence.

However, the release of Calcein is prove that permeabilization of the membrane occurred. It is important to make a relationship between the electrical response, which is obtained in real time, with the electroporation state of the cell. This way the need for optical corroboration can be eliminated.

6.2 Correlation with electrical current drop

Permeabilization was proved for pulses of 10V, 9V and 8V by fluorophore release and was related to the resulting current drop profile for some cells. Not all cells reached permeabilization as it was found to be dependent on size. Many cells flowed through the narrow zone giving a signal of the typical current drop peak explained before. The larger ones that released Calcein showed a current drop of longer duration. Figure 6-3 shows the behavior observed in a cell that was exposed to a pulse of 10V.

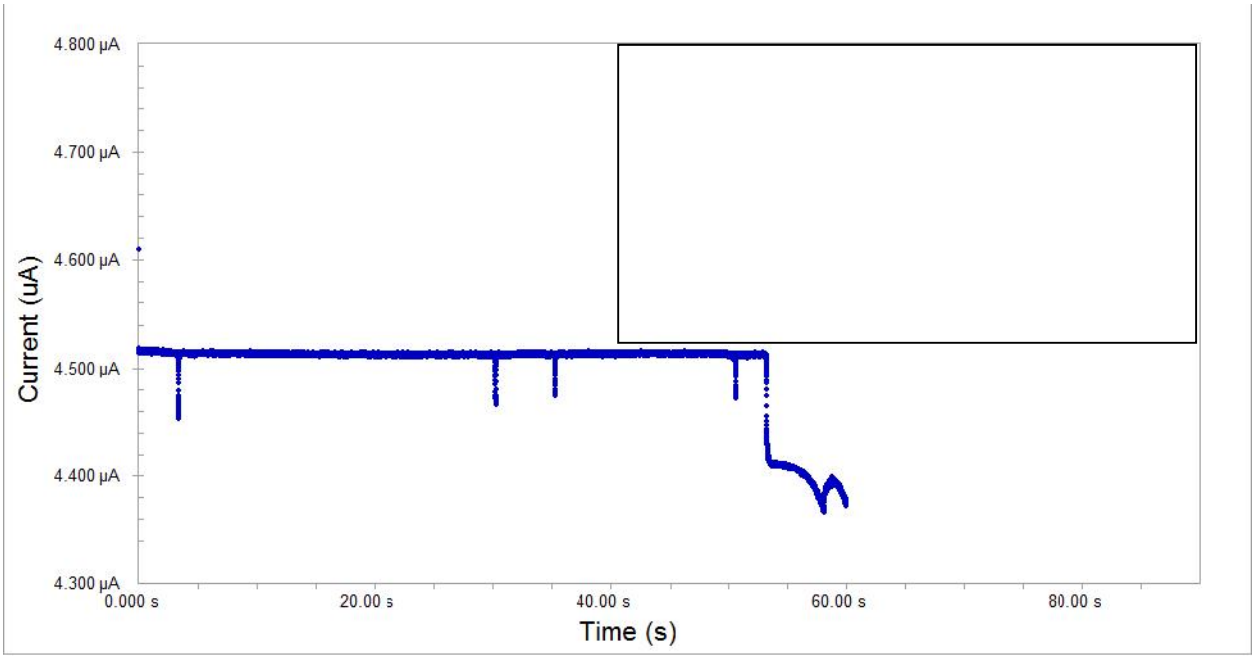

Figure 6-3. Chronoamperometry for permeabilized HeLa cell. Pulse = 10V

It can be seen that the current drop is longer and does not have a constant value but is changing. This may be due to the fact that the cell is changing its shape and moving, so the current goes up and down. However, the previous figure shows the results of a test that finished before the cell exited the narrow zone. The profile of a cell that gets electroporated and continues flowing shows that the current returns to its initial value. This can be observed in Figure 6-4 for a pulse of 10V also.

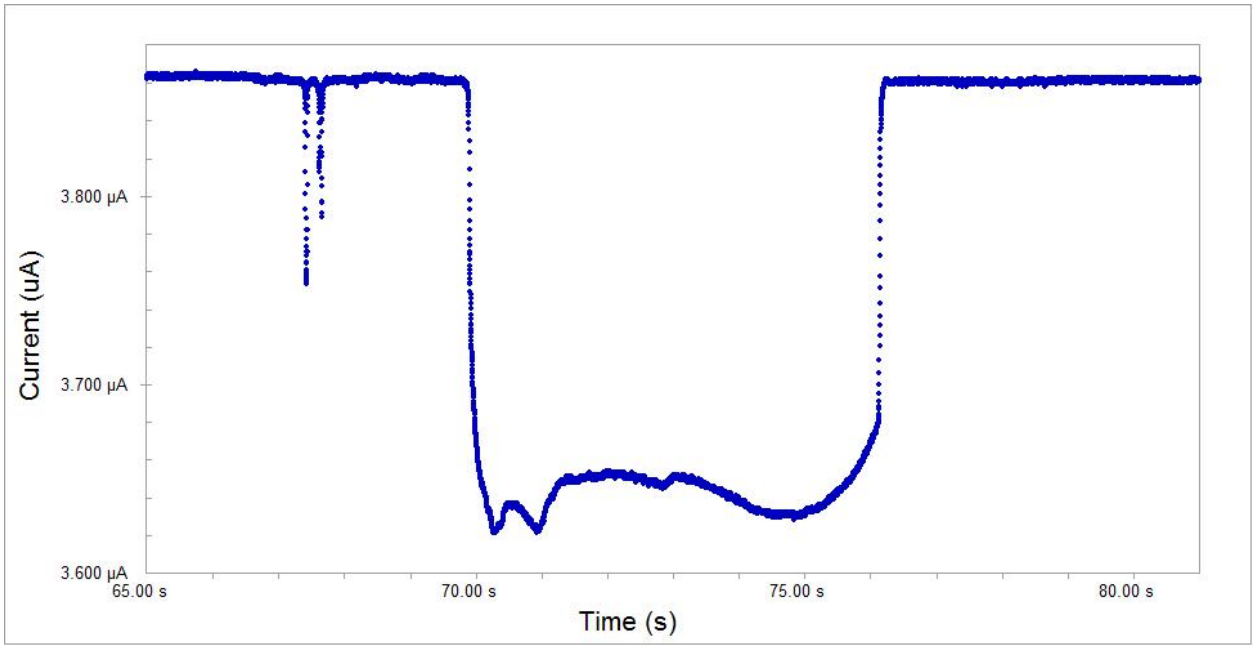

Figure 6-4. Characteristic current drop profile of a HeLa cell that was electroporated and continued flowing. Pulse = 10V

So, there is a characteristic profile for a permeabilized cell that can be distinguishable to the ones of a cell that passes through without being electroporated. Permeabilization was observed only for larger cells, which suggests that the dimensions of the narrow zone need to be changed in order to treat a higher range of cell sizes.

6.3 Stem cells

Experiments were repeated using stem cells to study if behavior was similar. Stem cells were suspended in PBS using the same protocol explained in Section 3.2. Constant pulses were varied from 100mV to 6V while monitoring the release of Calcein. Release of Calcein was seen at voltages of 600mV, 2V, 4V, 5V and 6V.

An image sequence of this at a pulse of 2V is shown in Figure 6-5, the resulting current profile is shown at Figure 6-6. The rest of the current profiles at other pulses are included in Appendix B.3.

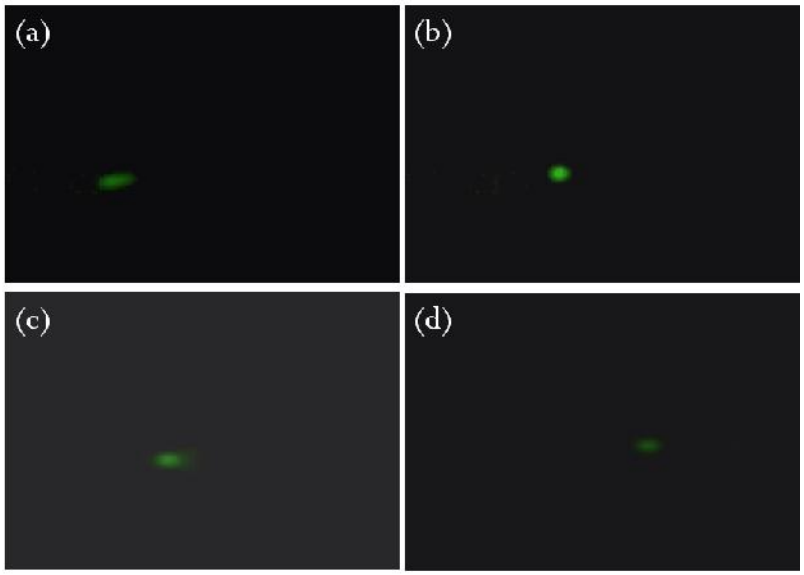

Figure 6-5. Image sequence of fluorescence corroboration of stem cell permeabilization at 2V. (a-c) Flow of the cell through the channel into the narrow section. (d) Release of Calcein (green) from the cell.

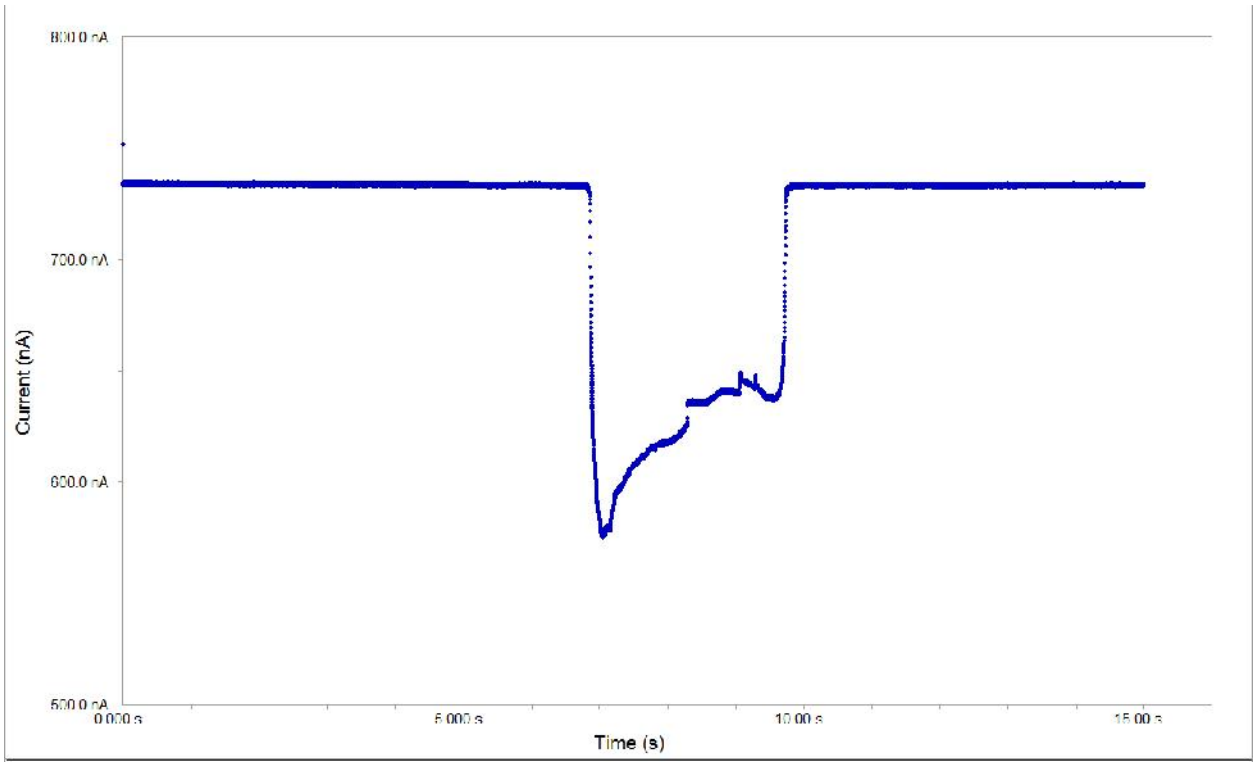

Figure 6-6. Current drop profile for a Stem cell with applied pulse of 2V. The characteristic drop represents permeabilization of the cell passing through the narrow zone.

The behavior is similar to that shown with HeLa cells; the characteristic profile for cell detection was a sudden drop of short duration. Permeabilization profile is longer and with different profile.

These results confirm the characteristic permeabilization profile. However, a threshold value cannot be stated for stem cells since the release of Calcein was not observed for other cells with higher voltages. This reaffirms that the permeabilization of cells based on this geometry restriction is highly dependent on cell size.

CHAPTER 7

CONCLUSIONS AND FUTURE PERSPECTIVE

7.1 Contribution

- BSA showed to be effective in modifying the PDMS surface from its natural hydrophobic state to hydrophilic. This surface modification of the microchannels contributed in the easier filling of liquid and inhibited cell adhesion.
- A passive pumping mechanism that relies on surface tension and pressure head provided volumetric flow high enough to move cells inside a microchannel and adequate enough to prevent agglomeration.
- Simple geometry restriction and using a constant DC pulse allowed to understand if cell permeabilization occurred by means of:
    - A sudden current drop of short duration that suggests a cell is passing through the narrow zone (“current peaks”).
    - A current drop with longer duration (as shown in Figure 6-6) that is characteristic of cell membrane permeabilization.

7.2 Future work

- It was proved that permeabilization occurred using this device, but the long term viability of cells after the treatment was not evaluated. The proper magnitude and duration pulse parameters need to be studied for effective electroporation and viability need to be determined. In vitro devices such as the one presented make more sense to be used for reversible EP. Irreversible EP method is used for killing malignant cells such as in tumor ablation, which is performed *in vivo*.
- The effect of BSA concentration on cell integrity was not studied. This is important to consider if clinical trial are expected.
- Future improvements that can be done to the design such as multiple narrow zones so that, using a constant DC pulse, the cell experiments a train-like pulses when flowing

through each narrow zone. It has been published that a train of pulses is more effective for electroporation than a single pulse.

- It was observed that permeabilization based on this geometry restriction was dependent of cell size. The dimensions of the narrow zone can be reduced (for example, by reducing channel height) so that the majority of cells passing will get deformed and thus permeabilized. A series of restrictions that get smaller and smaller will ensure that a cell that is too small to get electroporated in one zone, will get electroporated in one of the following zones, thus increasing efficiency.

REFERENCES

[1] A. G. Pakhomov, D. Miklavcic, and M. Markov, *Advanced electroporation techniques in biology and medicine*. Boca Raton: CRC Press, 2010.

[2] H. Bermúdez, H. Aranda-Espinoza, D. A. Hammer, and D. E. Discher, "Pore stability and dynamics in polymer membranes," *Europhysics Letters (EPL)*, vol. 64, no. 4, pp. 550–556, Nov. 2003.

[3] D. C. Chang and T. S. Reese, "Changes in membrane structure induced by electroporation as revealed by rapid-freezing electron microscopy," *Biophysical Journal*, vol. 58, no. 1, pp. 1–12, Jul. 1990.

[4] B. Rubinsky, "Irreversible electroporation in medicine," *Technology in Cancer Research and Treatment*, vol. 6, no. 4, p. 255, 2007.

[5] R. V. Davalos, L. M. Mir, and B. Rubinsky, "Tissue Ablation with Irreversible Electroporation," *Ann Biomed Eng*, vol. 33, no. 2, pp. 223–231, Feb. 2005.

[6] G. Sersa, D. Miklavcic, M. Cemazar, Z. Rudolf, G. Pucihar, and M. Snoj, "Electrochemotherapy in treatment of tumours," *European Journal of Surgical Oncology (EJSO)*, vol. 34, no. 2, pp. 232–240, 2008.

[7] D. J. Wells, "Gene therapy progress and prospects: electroporation and other physical methods," *Gene therapy*, vol. 11, no. 18, pp. 1363–1369, 2004.

[8] T. Niidome and L. Huang, "Gene therapy progress and prospects: nonviral vectors," *Gene Ther*, vol. 9, no. 24, pp. 1647–1652, Dec. 2002.

[9] W. Krassowska and P. D. Filev, "Modeling electroporation in a single cell," *Biophysical journal*, vol. 92, no. 2, pp. 404–417, 2007.

[10] E. Neumann and K. Rosenheck, "Permeability changes induced by electric impulses in vesicular membranes," *Journal of Membrane Biology*, vol. 10, no. 1, pp. 279–290, 1972.

[11] G. Matthews, "Cell biology: Vesicle fiesta at the synapse," *Nature*, vol. 406, no. 6798, pp. 835–836, Aug. 2000.

[12] E. Neumann, M. Schaefer-Ridder, Y. Wang, and P. H. Hofschneider, "Gene transfer into mouse lyoma cells by electroporation in high electric fields.," *EMBO J*, vol. 1, no. 7, pp. 841–845, 1982.

[13] R. Goude and T. Parish, "Electroporation of Mycobacteria," *Journal of Visualized Experiments*, no. 15, May 2008.

[14] J. A. Lundqvist, F. Sahlin, M. A. I. Åberg, A. Strömberg, P. S. Eriksson, and O. Orwar, "Altering the biochemical state of individual cultured cells and organelles with ultramicroelectrodes," *Proceedings of the National Academy of Sciences*, vol. 95, no. 18, pp. 10356 –10360, 1998.

[15] K. Nolkrantz, C. Farre, A. Brederlau, R. I. D. Karlsson, C. Brennan, P. S. Eriksson, S. G. Weber, M. Sandberg, and O. Orwar, "Electroporation of Single Cells and Tissues with an Electrolyte-filled Capillary," *Anal. Chem.*, vol. 73, no. 18, pp. 4469–4477, 2001.

[16] K. Haas, W. C. Sin, A. Javaherian, Z. Li, and H. T. Cline, "Single-cell electroporation for gene transfer in vivo," *Neuron*, vol. 29, no. 3, pp. 583–591, Mar. 2001.

[17] K. G. Klemic, J. F. Klemic, M. A. Reed, and F. J. Sigworth, "Micromolded PDMS planar electrode allows patch clamp electrical recordings from cells," *Biosensors and bioelectronics*, vol. 17, no. 6–7, pp. 597–604, 2002.

[18] A. Stett, V. Bucher, C. Burkhardt, U. Weber, and W. Nisch, "Patch-clamping of primary cardiac cells with micro-openings in polyimide films," *Medical and Biological Engineering and Computing*, vol. 41, no. 2, pp. 233–240, 2003.

[19] Y. Huang and B. Rubinsky, "Flow-through micro-electroporation chip for high efficiency single-cell genetic manipulation," *Sensors and Actuators A: Physical*, vol. 104, no. 3, pp. 205–212, 2003.

[20] C. Wood, C. Williams, and G. J. Waldron, "Patch clamping by numbers," *Drug discovery today*, vol. 9, no. 10, pp. 434–441, 2004.

[21] M. Khine, C. Ionescu-Zanetti, A. Blatz, L.-P. Wang, and L. P. Lee, "Single-cell electroporation arrays with real-time monitoring and feedback control," *Lab Chip*, vol. 7, no. 4, pp. 457–462, Mar. 2007.

[22] M. A. McClain, C. T. Culbertson, S. C. Jacobson, N. L. Allbritton, C. E. Sims, and J. M. Ramsey, "Microfluidic devices for the high-throughput chemical analysis of cells," *Analytical chemistry*, vol. 75, no. 21, pp. 5646–5655, 2003.

[23] M. Khine, C. Ionescu-Zanetti, A. Blatz, L.-P. Wang, and L. P. Lee, "Single-cell electroporation arrays with real-time monitoring and feedback control," *Lab Chip*, vol. 7, no. 4, p. 457, 2007.

[24] G. M. Walker and D. J. Beebe, "A passive pumping method for microfluidic devices," *Lab Chip*, vol. 2, no. 3, pp. 131–134, Aug. 2002.

[25] E. Berthier, J. Warrick, H. Yu, and D. J. Beebe, “Managing evaporation for more robust microscale assays,” *Lab Chip*, vol. 8, no. 6, pp. 860–864, May 2008.

[26] H.-Y. Wang and C. Lu, “Electroporation of Mammalian Cells in a Microfluidic Channel with Geometric Variation,” *Anal. Chem.*, vol. 78, no. 14, pp. 5158–5164, 2006.

[27] Y. Zhan, C. Lu, and N. Bao, “Microfluidic electroporative flow cytometry for studying single-cell biomechanics.,” *Analytical Chemistry*, vol. 80, no. 20, pp. 7714–7719.

[28] “The Molecular Composition of Cells - The Cell - NCBI Bookshelf.” [Online]. Available: http://www.ncbi.nlm.nih.gov/books/NBK9879/. [Accessed: 13-Jun-2012].

[29] Kotnik Tadej and Pucihar Gorazd, “Induced Transmembrane Voltage: Theory, Modeling, and Experiments,” in *Advanced Electroporation Techniques in Biology and Medicine*, CRC Press, 2011, pp. 51–70.

[30] K. A. DeBruin and W. Krassowska, “Modeling electroporation in a single cell. I. Effects of field strength and rest potential,” *Biophysical journal*, vol. 77, no. 3, pp. 1213–1224, 1999.

[31] B. Valič, M. Golzio, M. Pavlin, A. Schatz, C. Faurie, B. Gabriel, J. Teissié, M.-P. Rols, and D. Miklavčič, “Effect of electric field induced transmembrane potential on spheroidal cells: theory and experiment,” *European Biophysics Journal*, vol. 32, no. 6, pp. 519–528, 2003.

[32] J. de Melo and S. Blackshaw, “In vivo Electroporation of Developing Mouse Retina,” *J Vis Exp*, no. 52, p. e2847, Jun. 2011.

[33] M. B. Fox, D. C. Esveld, A. Valero, R. Luttge, H. C. Mastwijk, P. V. Bartels, A. Berg, and R. M. Boom, “Electroporation of cells in microfluidic devices: a review,” *Anal Bioanal Chem*, vol. 385, no. 3, pp. 474–485, Mar. 2006.

[34] Y. Huang and B. Rubinsky, “Microfabricated electroporation chip for single cell membrane permeabilization,” *Sensors and Actuators A: Physical*, vol. 89, no. 3, pp. 242–249, 2001.

[35] M. Khine, A. Lau, C. Ionescu-Zanetti, J. Seo, and L. P. Lee, “A single cell electroporation chip,” *Lab Chip*, vol. 5, no. 1, p. 38, 2005.

[36] S. K. Kim, J. H. Kim, K. P. Kim, and T. D. Chung, “Continuous Low-Voltage dc Electroporation on a Microfluidic Chip with Polyelectrolytic Salt Bridges,” *Anal. Chem.*, vol. 79, no. 20, pp. 7761–7766, Oct. 2007.

[37] A.-M. Spehar, S. Koster, V. Linder, S. Kulmala, N. F. de Rooij, E. Verpoorte, H. Sigrist, and W. Thormann, “Electrokinetic characterization of poly(dimethylsiloxane) microchannels,” *ELECTROPHORESIS*, vol. 24, no. 21, pp. 3674–3678, 2003.

[38] R. Ziv, Y. Steinhardt, G. Pelled, D. Gazit, and B. Rubinsky, “Micro-electroporation of mesenchymal stem cells with alternating electrical current pulses,” *Biomed Microdevices*, vol. 11, no. 1, pp. 95–101, Feb. 2009.

[39] R. Díaz-Rivera, “Micro and Nano Scale Bioelectronics in Cell Micro-Electroporation,” University of California, Berkeley, California, 2005.

[40] T. Pan and W. Wang, “From cleanroom to desktop: emerging micro-nanofabrication technology for biomedical applications,” *Ann Biomed Eng*, vol. 39, no. 2, pp. 600–620, Feb. 2011.

[41] J. M. Gale, C. P. Romero, G. B. Tafoya, and J. Conia, “Application of optical trapping for cells grown on plates: optimization of PCR and fidelity of DNA sequencing of p53 gene from a single cell,” *Clinical chemistry*, vol. 49, no. 3, p. 415, 2003.

[42] “Two-, Three-, and Four-electrode experiments.” 26-Apr-2011.

[43] Dimova Rumiana, “Electrodeformation, Electroporation, and Electrofusion of Cell-Sized Lipid Vesicles,” in *Advanced Electroporation Techniques in Biology and Medicine*, CRC Press, 2011, pp. 97–122.

APPENDIX A:
DERIVATION OF APPROXIMATED THEORETICAL RESISTANCE EQUATION FOR TRAPEZOIDAL AREAS

The electrical resistance for the trapezoidal areas was calculated based on Equation 2-3 which depends on the resistivity f the electrolyte (ρ), the length of the portion considered (L) and the cross- sectional area where current is flowing (A). In this case the cross-sectional area is rectangular, with one side being the height of the channel (h) which is fixed and the other side being the width (w). In the trapezoidal areas this width changes along the length of the channel as shown in Figure A-1. The width starts at w_o and is reduced until reaching its final width w_f.

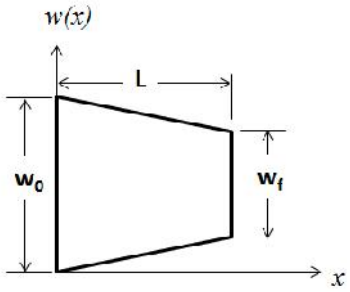

Figure A-1. Schematic of trapezoid area considered for resistance calculation.

Since the width changes along the channel so does the area, which is defined as:

$$A(x) = h \cdot w(x) \qquad \textbf{Equation A-1}$$

Thus, the resistance of the trapezoidal region can be defined by the following integral

$$R^{\text{trapezoid}} = \int_0^L \frac{\rho}{h w(x)}\, dx \qquad \textbf{Equation A-2}$$

Taking the constant terms out of the integral:

$$\frac{\rho}{h}\int_0^L \frac{1}{w(x)}\, dx \qquad \textbf{Equation A-3}$$

The width of the channel can be defined using the equation of a line:

$$w(x) = \frac{w_f - w_0}{L} x + w_0 \qquad \textbf{Equation A-4}$$

Inserting Equation A-4 into Equation A-3:

$$\frac{\rho}{h}\int_0^L \left[\frac{w_f - w_0}{L} x + w_0\right]^{-1} dx \qquad \textbf{Equation A-4}$$

And integrating from $x=0$ to $x=L$ results in:

$$\frac{°L}{h}\left(\frac{w_f + w_0}{2}\right) \qquad \textbf{Equation A-5}$$

APPENDIX B:
CHRONOAMPEROMETRY RESULTS WITH PARTICLES FLOWING THROUGH THE NARROW ZONE OF THE CHANNNEL

B.1 Polystyrene beads

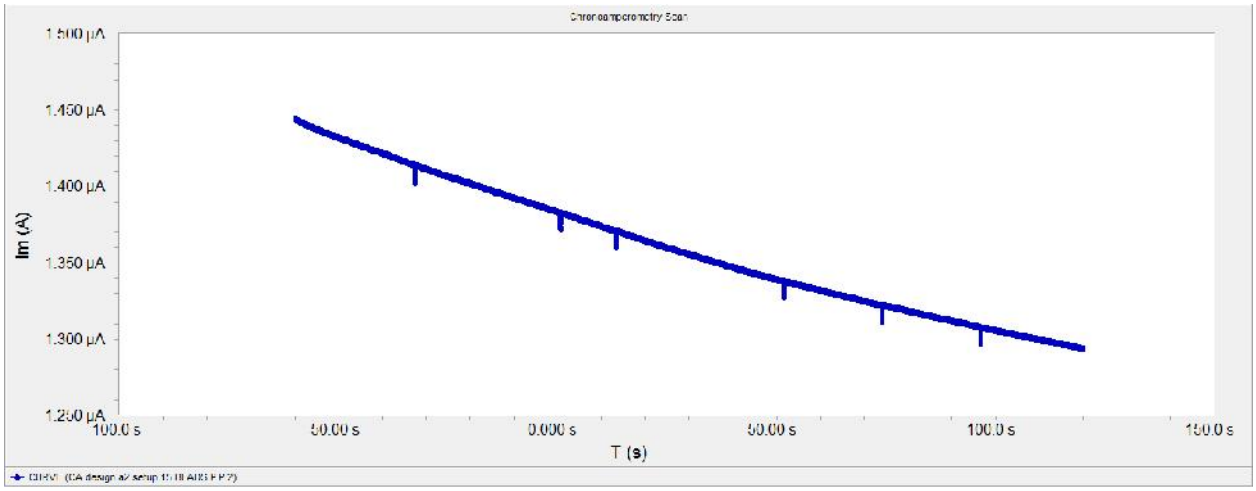

Figure B-7-1. Chronoamperometry for beads. Pulse = 500mV

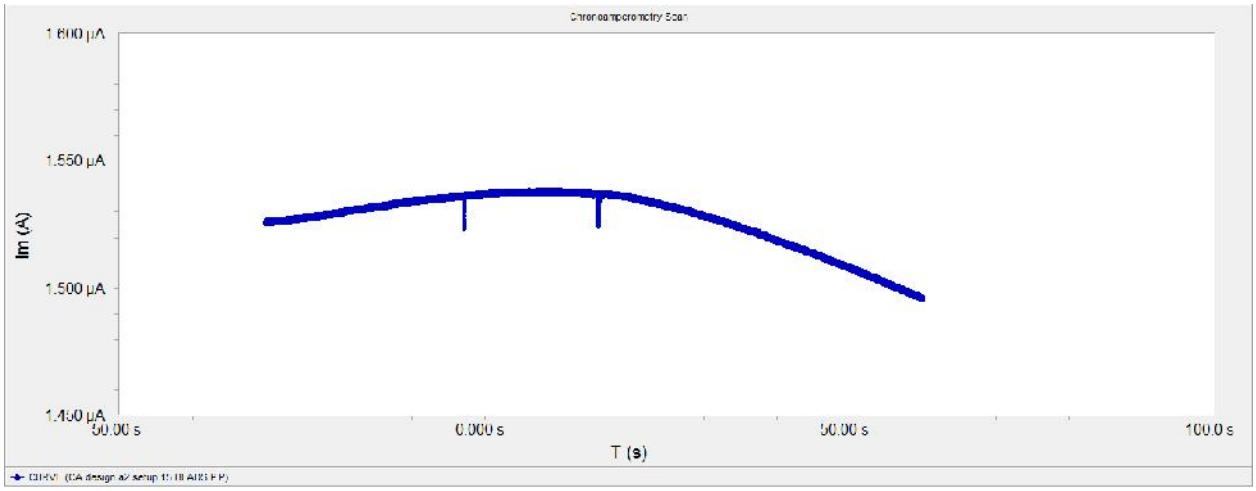

Figure B-7-2. Chronoamperometry for beads. Pulse= 500mV

B.2 HeLa cells

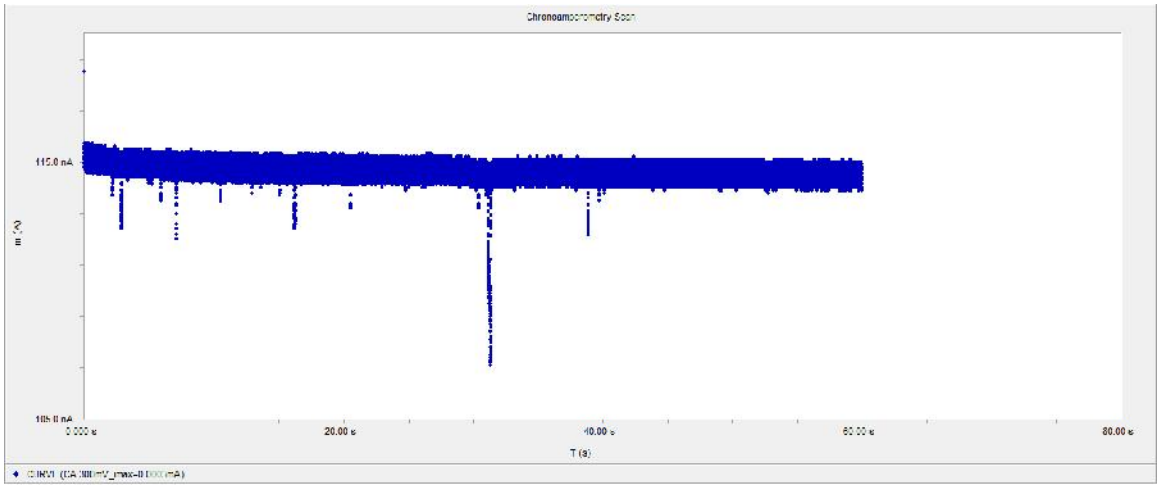

Figure B-7-3. Chronoamperometry for HeLa cells. Pulse = 300mV

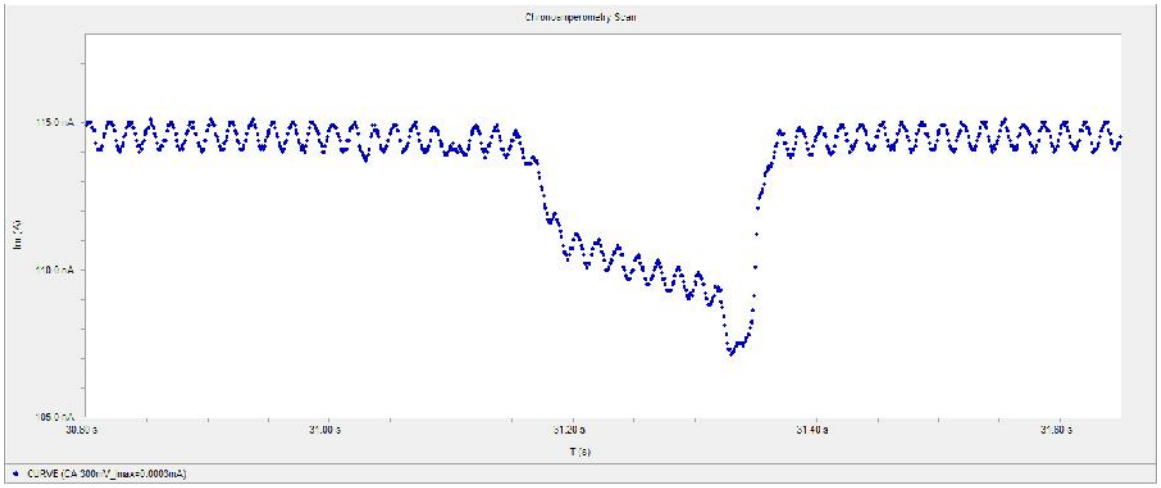

Figure B-7-4. Zoomed view of current drop of Figure B-7-3.

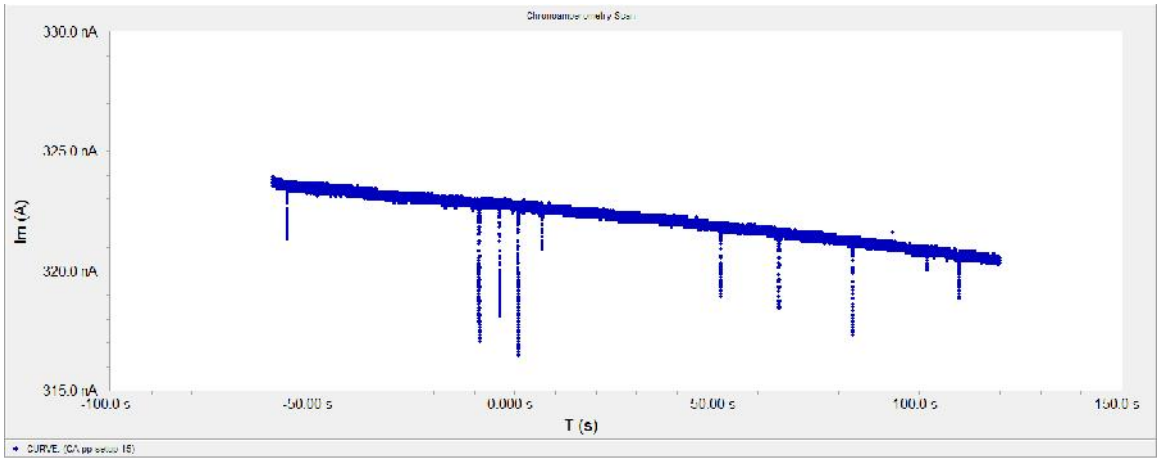

Figure B-7-5. Chronoamperometry for HeLa cells. Pulse = 500mV

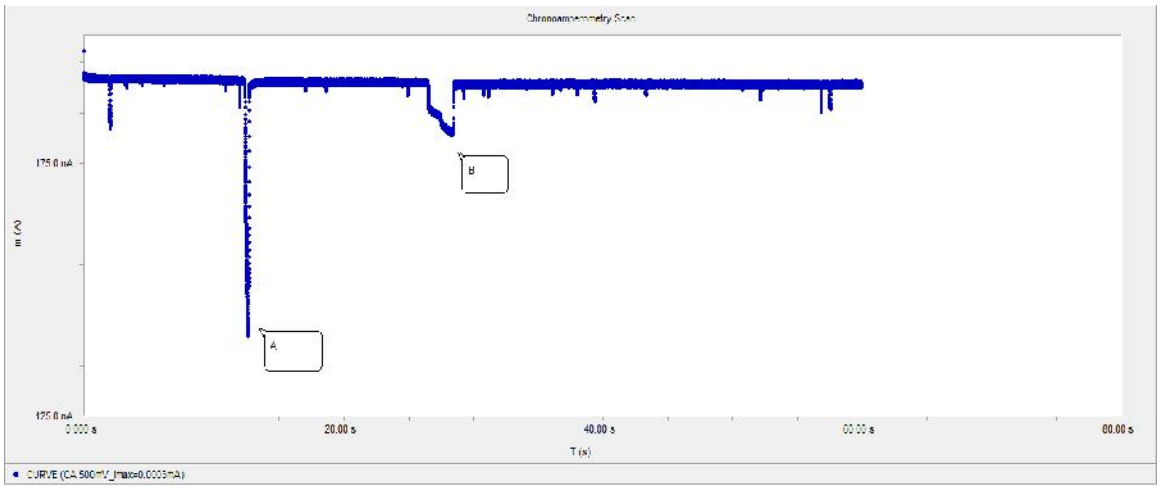

Figure B-7-6. Chronoamperometry for HeLa cells. Pulse = 500mV

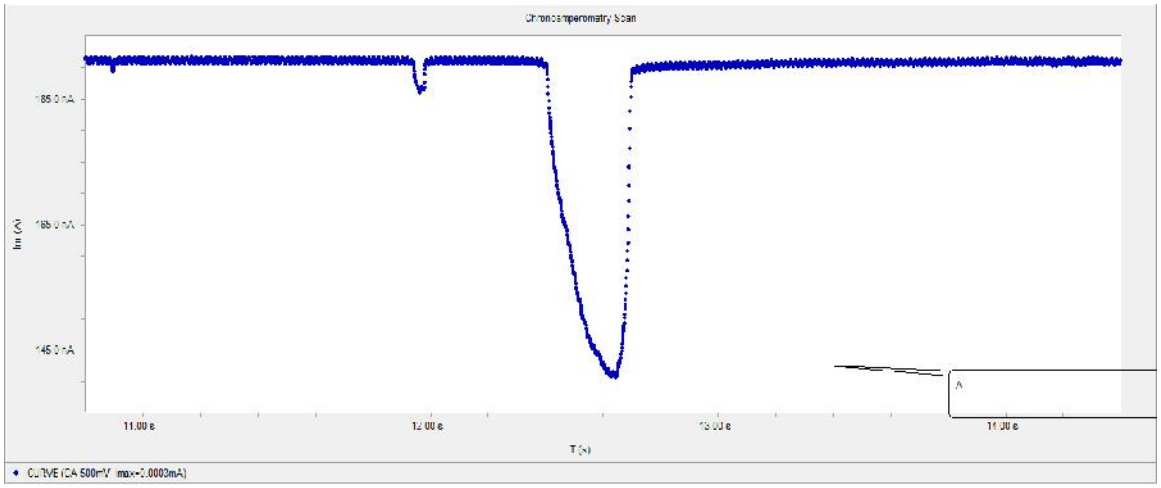

Figure B-7-7. Zoomed view of current drop of Figure B-7-6.

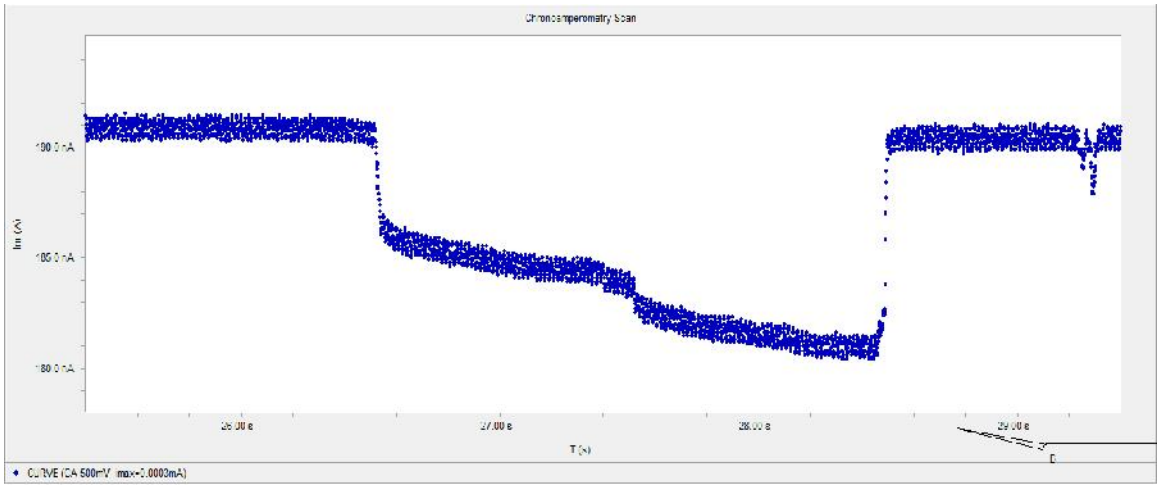

Figure B-7-8. Zoomed view of current drop of Figure B-7-6.

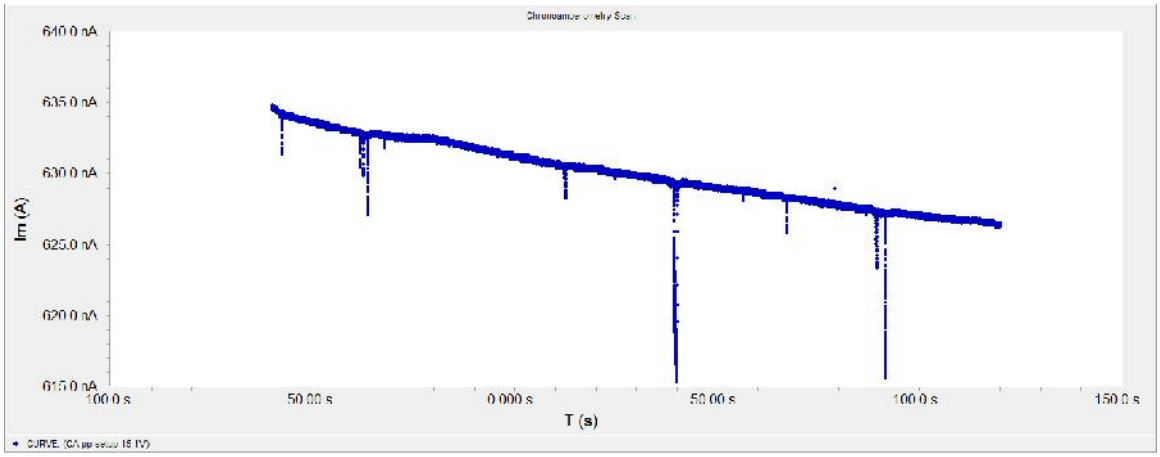

Figure B-7-9. Chronoamperometry for HeLa cells. Pulse=1V

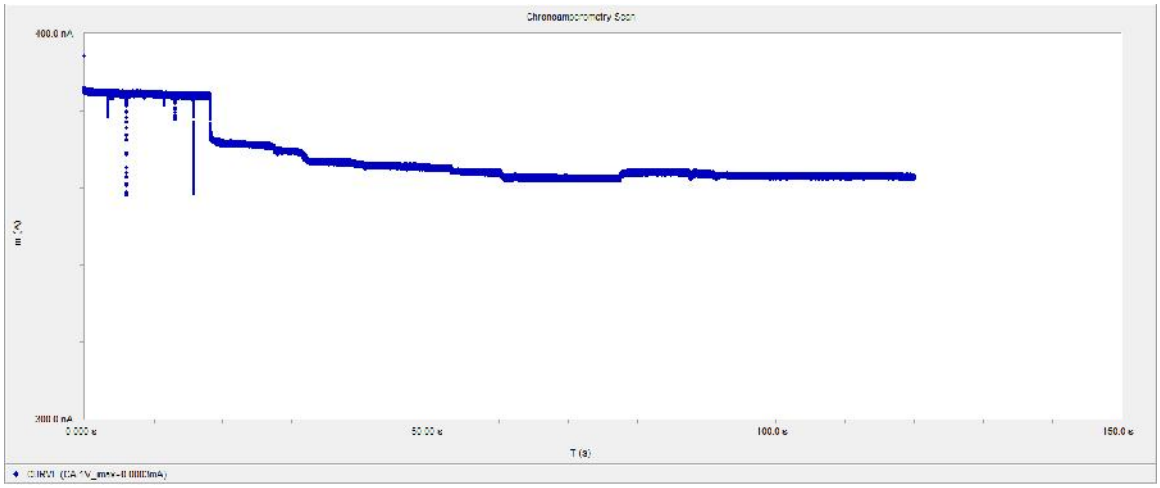

Figure B-7-10. Chronoamperometry for HeLa cells. Pulse = 1V

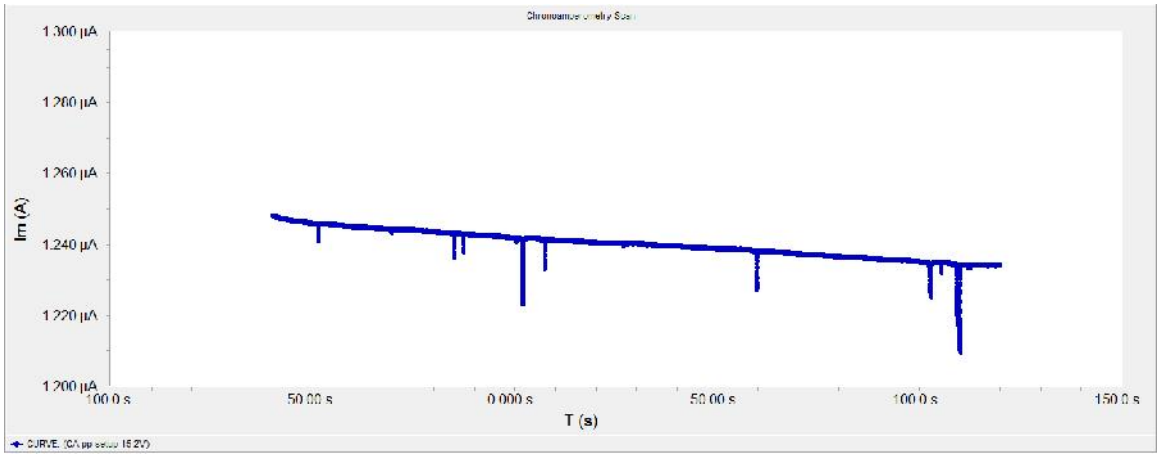

Figure B-7-11. Chronoamperometry for HeLa cells. Pulse = 2V

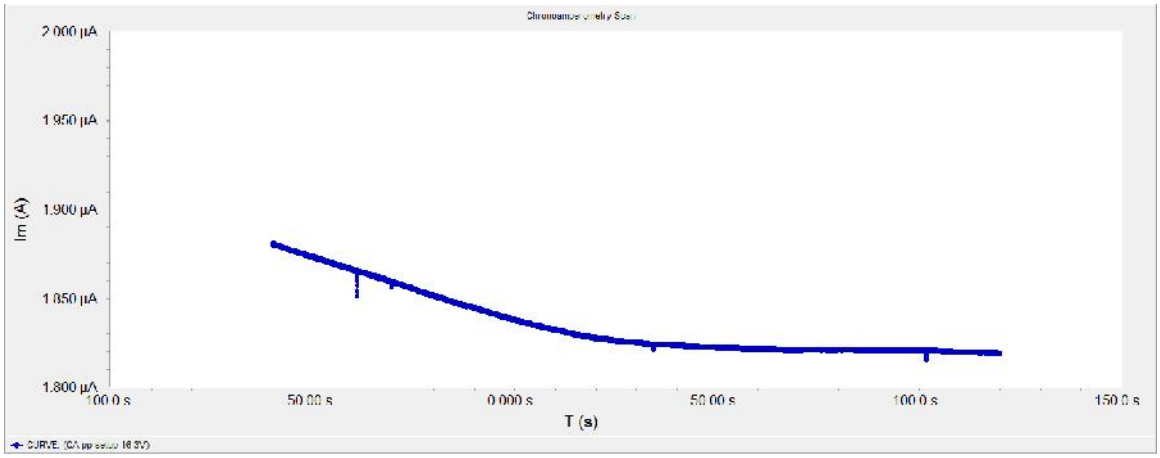

Figure B-7-12. Chronoamperometry for HeLa cells. Pulse = 3V

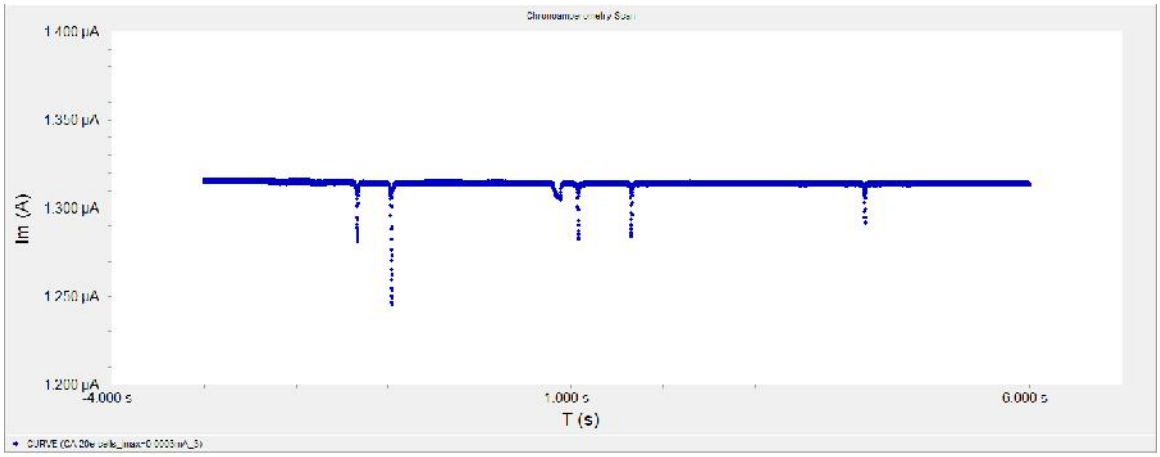

Figure B-7-13. Chronoamperometry for HeLa cells. Pulse 3V

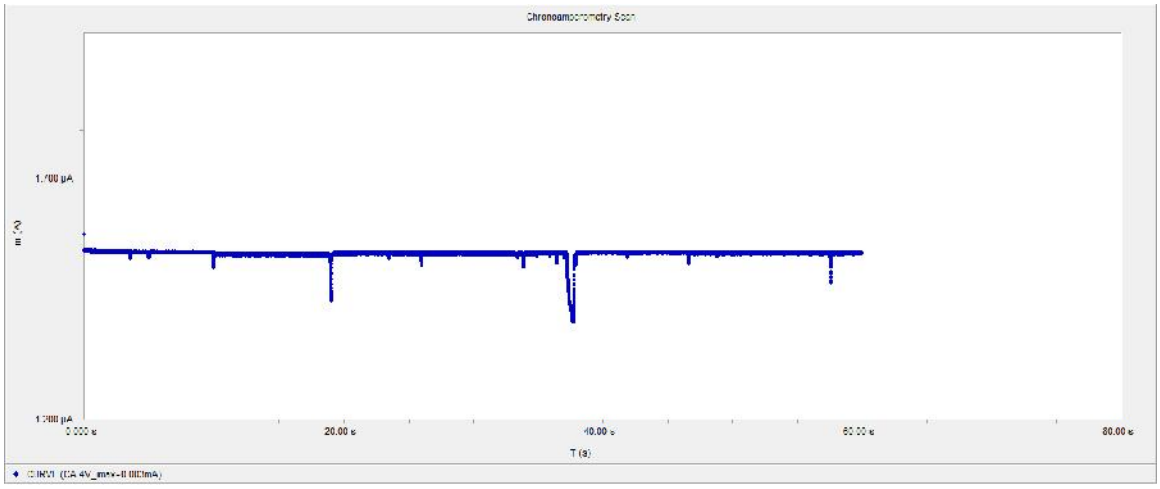

Figure B-7-14. Chronoamperometry for HeLa cells. Pulse = 4V

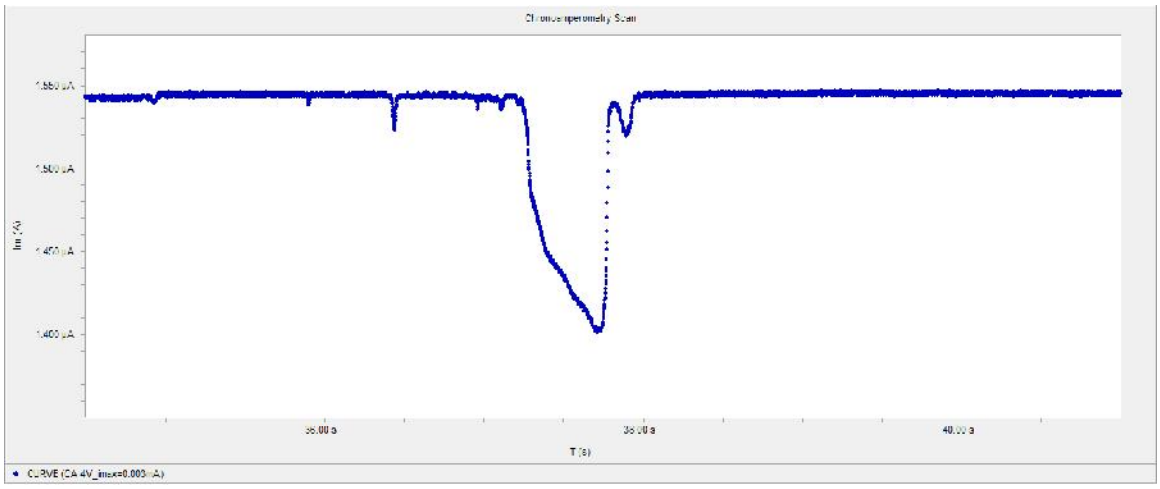

Figure B-7-15. Zoomed view of current drop of Figure B-7-14

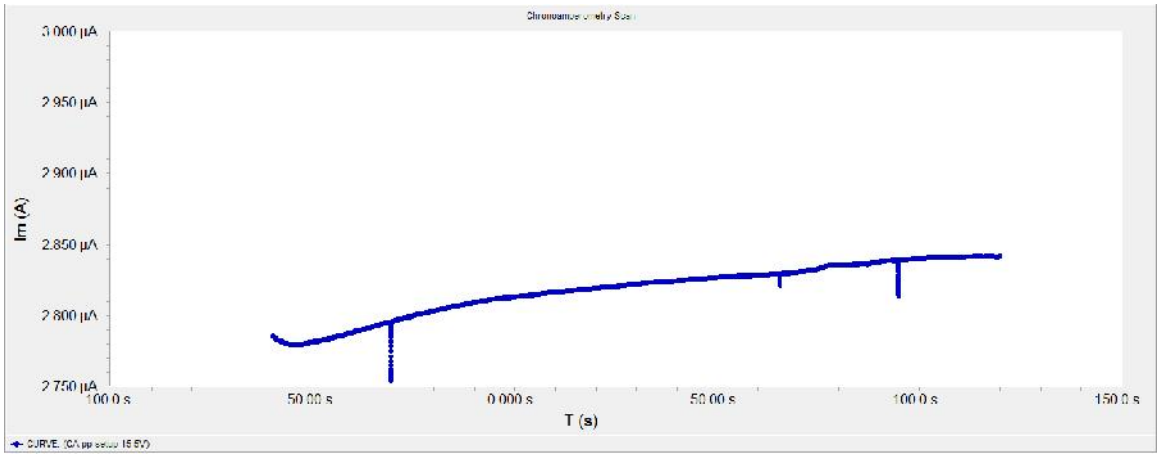

Figure B-7-16. Chronoamperometry for HeLa cells. Pulse = 5V

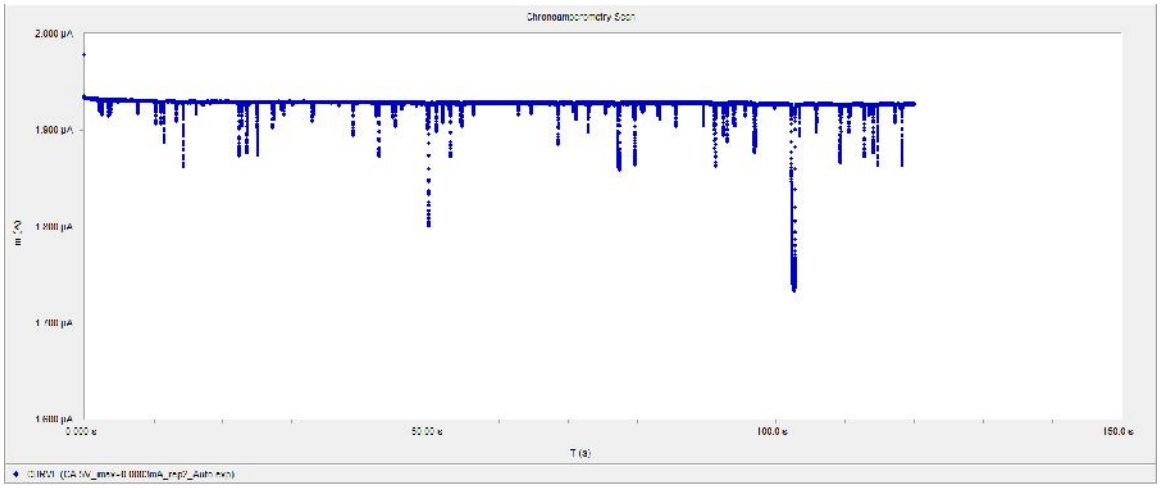

Figure B-7-17. Chronoamperometry for HeLa cells. Pulse = 5V

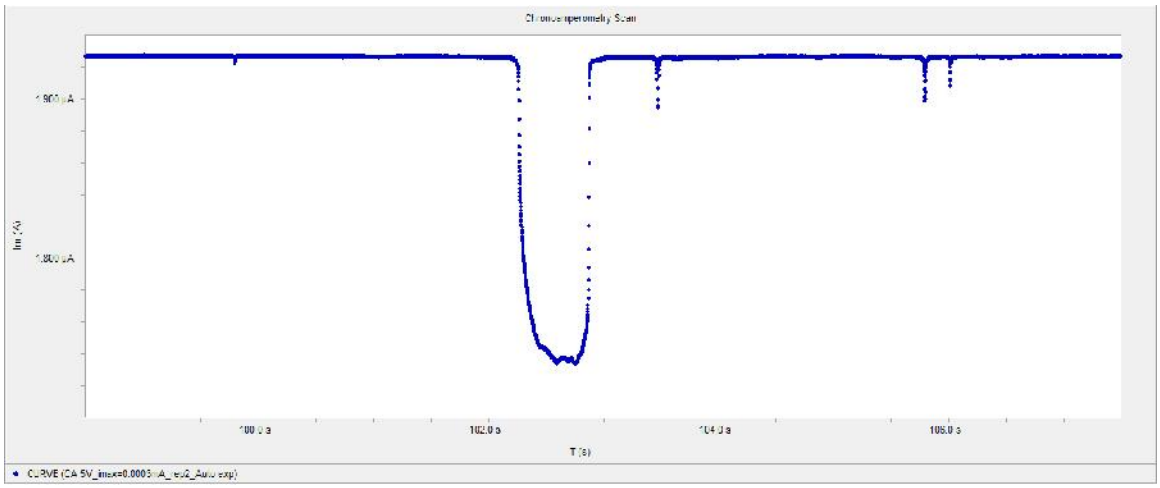

Figure B-7-18. Zoomed view of current drop of Figure B-7-17

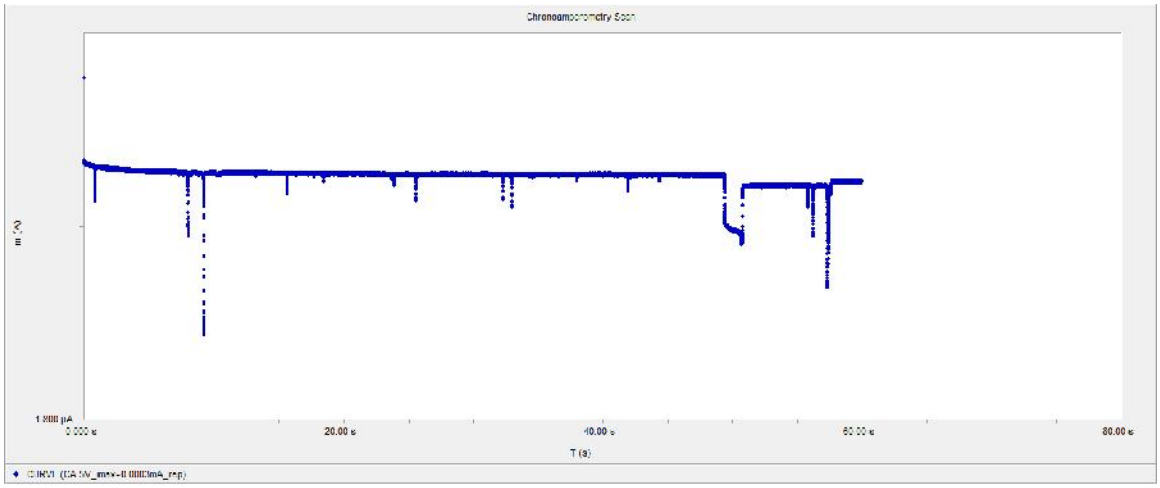

Figure B-7-19. Chronoamperometry for HeLa cells. Pulse = 5V

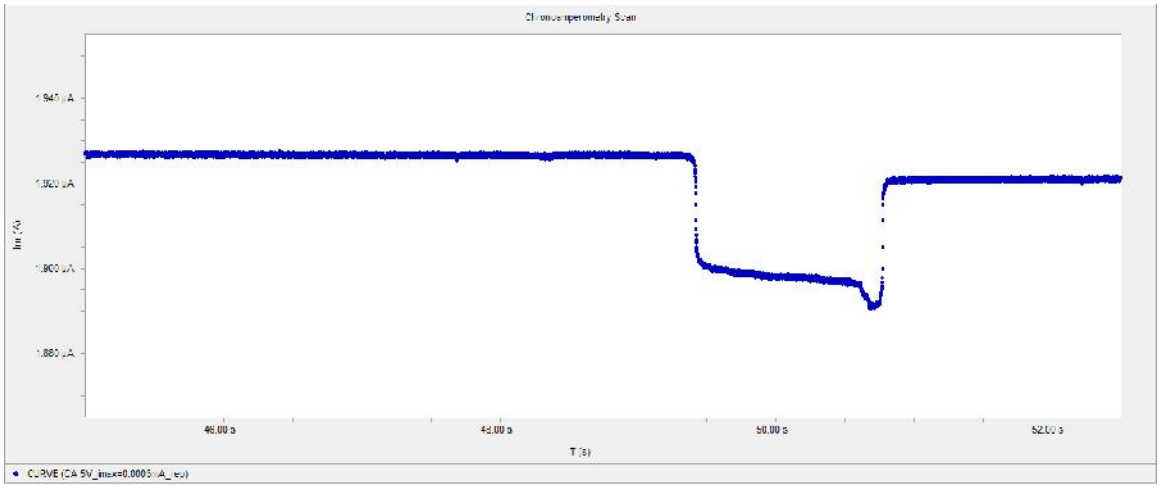

Figure B-7-20. Zoomed view of current drop of Figure B-7-19

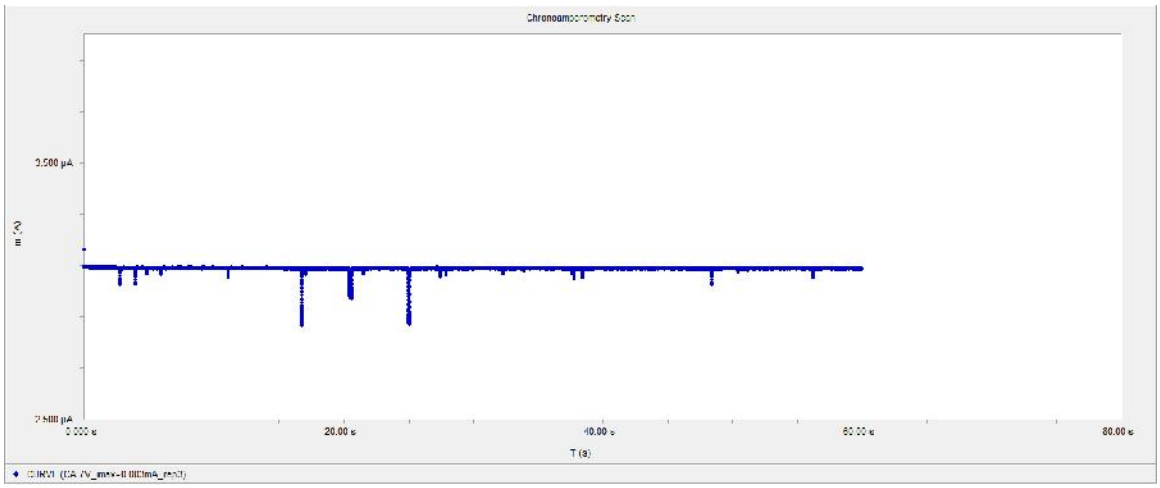

Figure B-7-21. Chronoamperometry for HeLa cells. Pulse = 7V

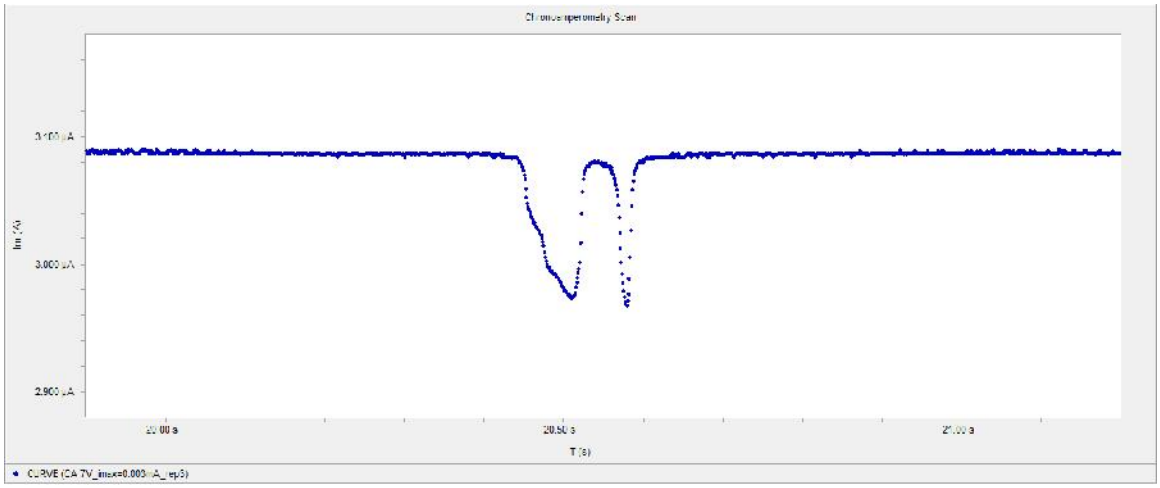

Figure B-7-22. Zoomed view of current drop of Figure B-7-21

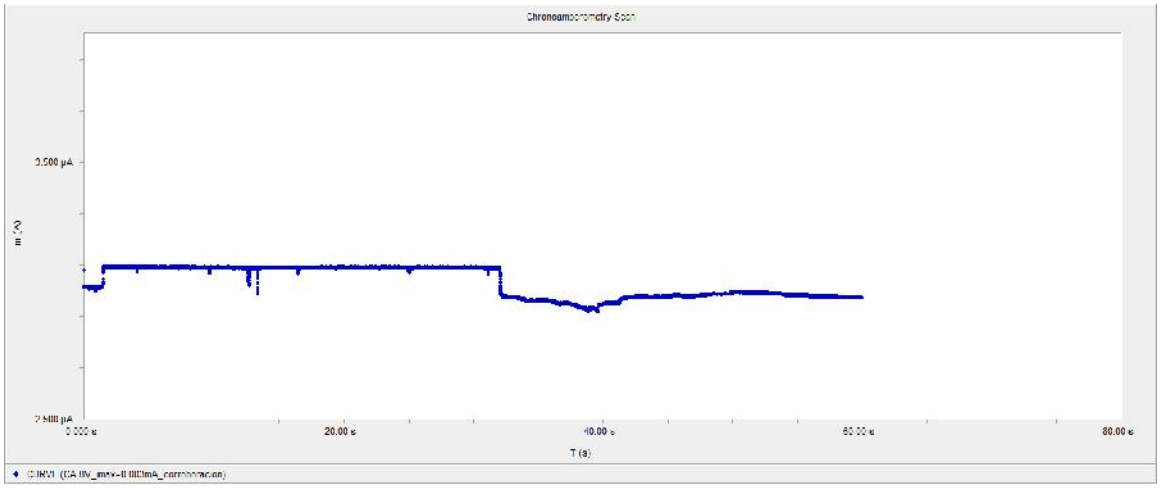

Figure B-7-23. Chronoamperometry for HeLa cells. Pulse =8V

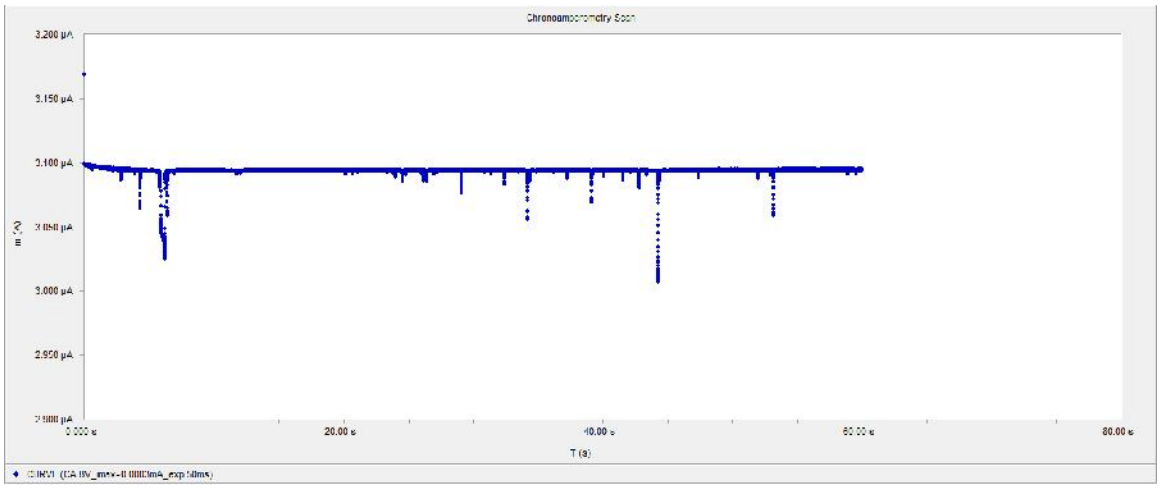

Figure B-7-24. Chronoamperometry for HeLa cells. Pulse = 8V

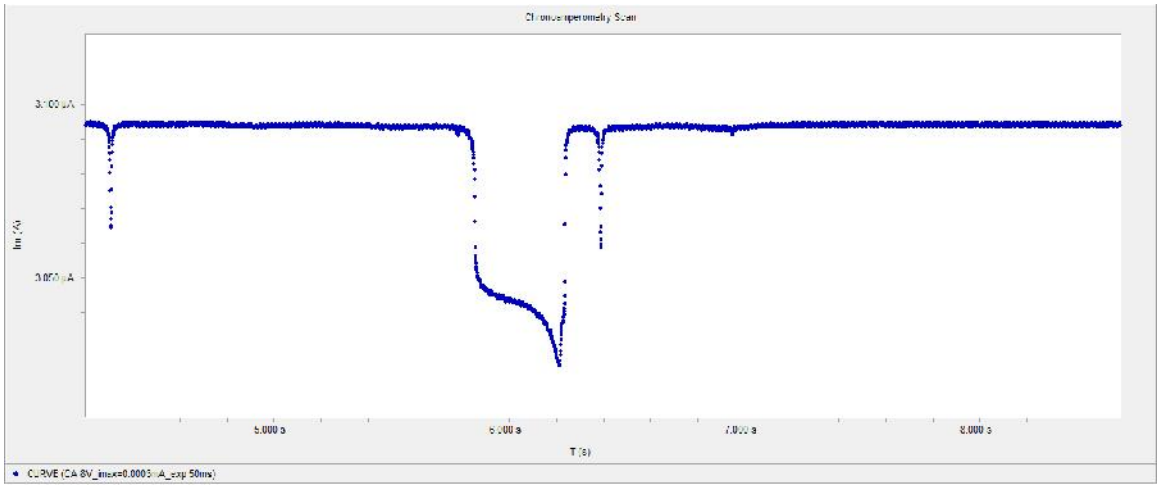

Figure B-7-25. Zoomed view of current drop of Figure B-7-24

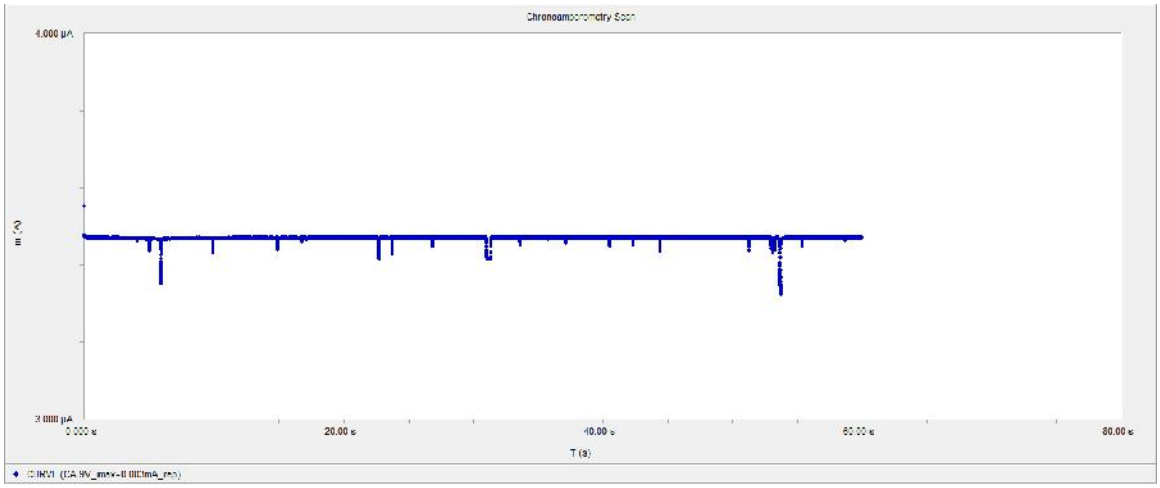

Figure B-7-26. Chronoamperometry for HeLa cells. Pulse = 9V

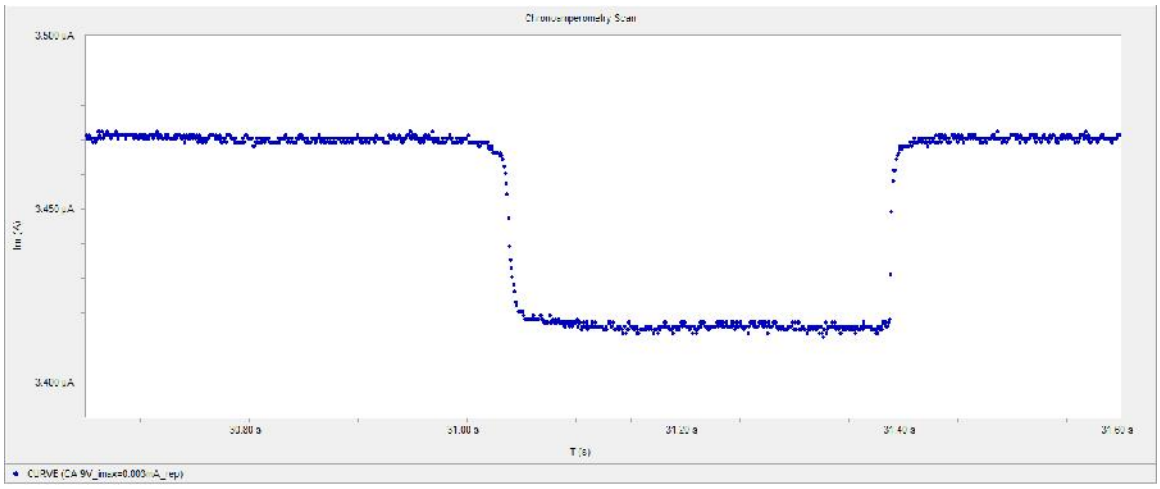

Figure B-7-27. Zoomed view of current drop of Figure B-7-26

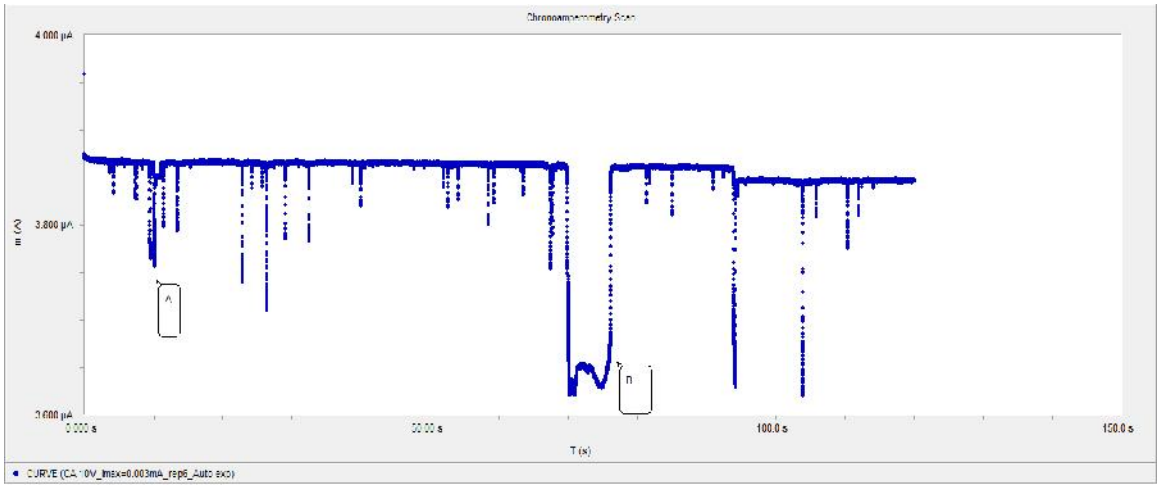

Figure B-7-28. Chronoamperometry for HeLa cells. Pulse =10V

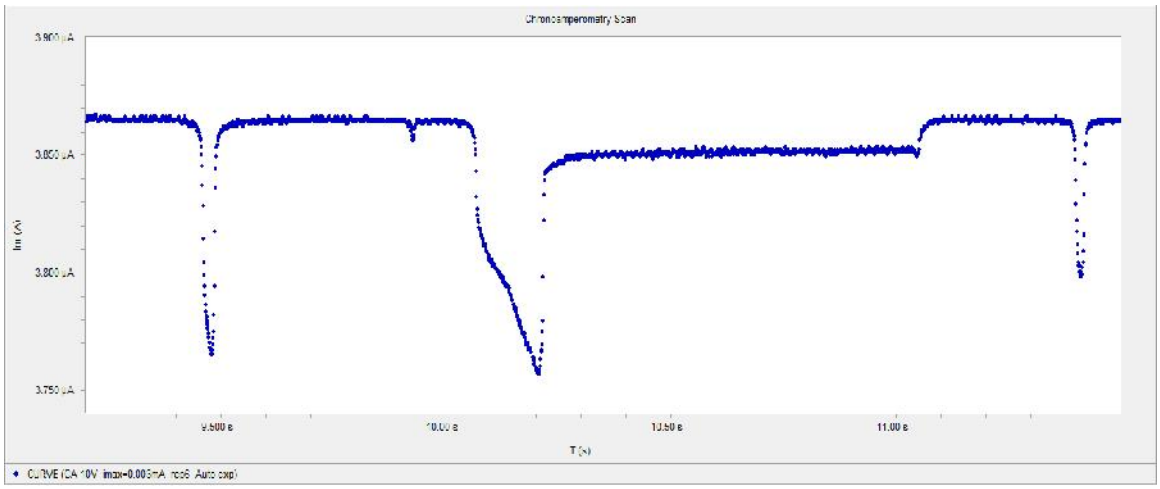

Figure B-7-29. Zoomed view of current drop of Figure B-7-28

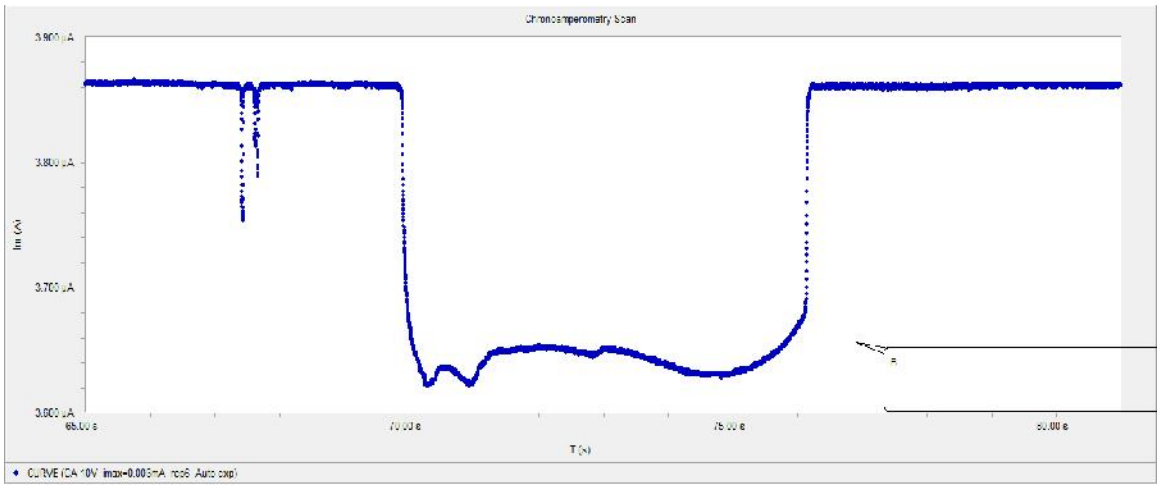

Figure B-7-30. Zoomed view of current drop of Figure B-7-28

B.3 Stem cells

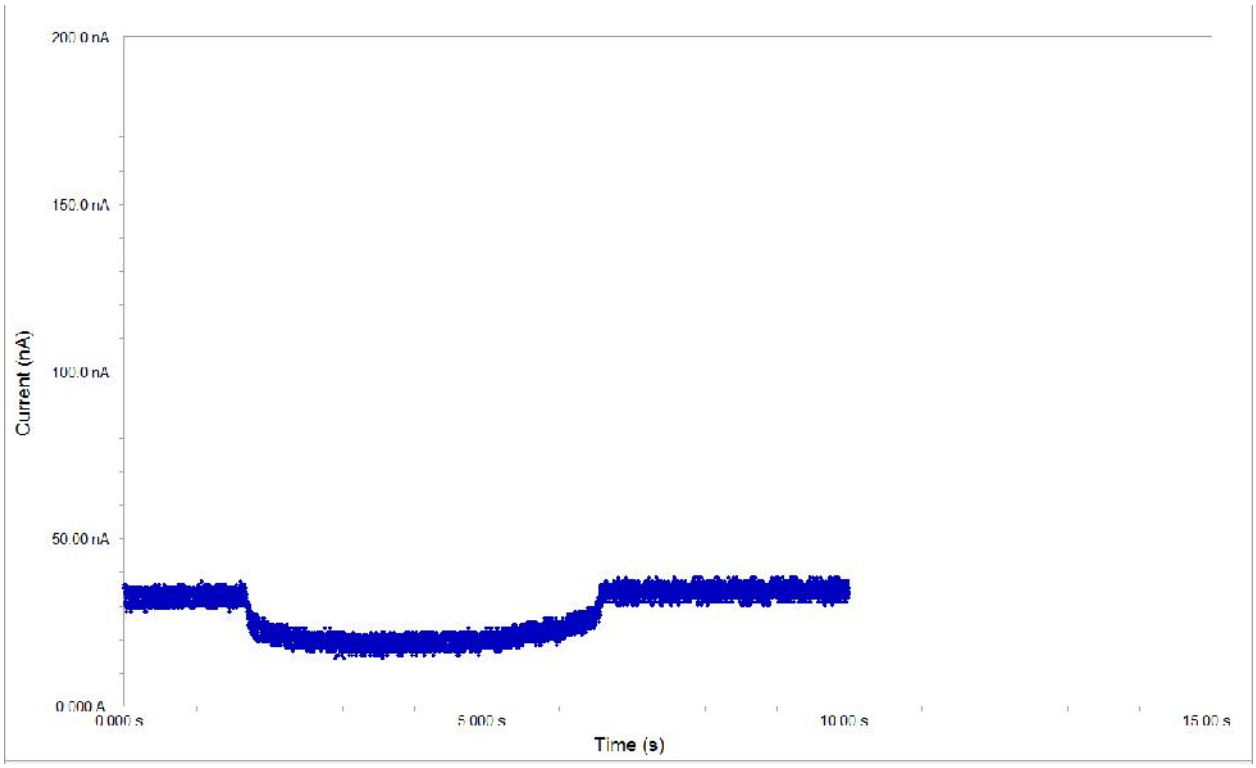

Figure B-7-31. Stem cells 100mV

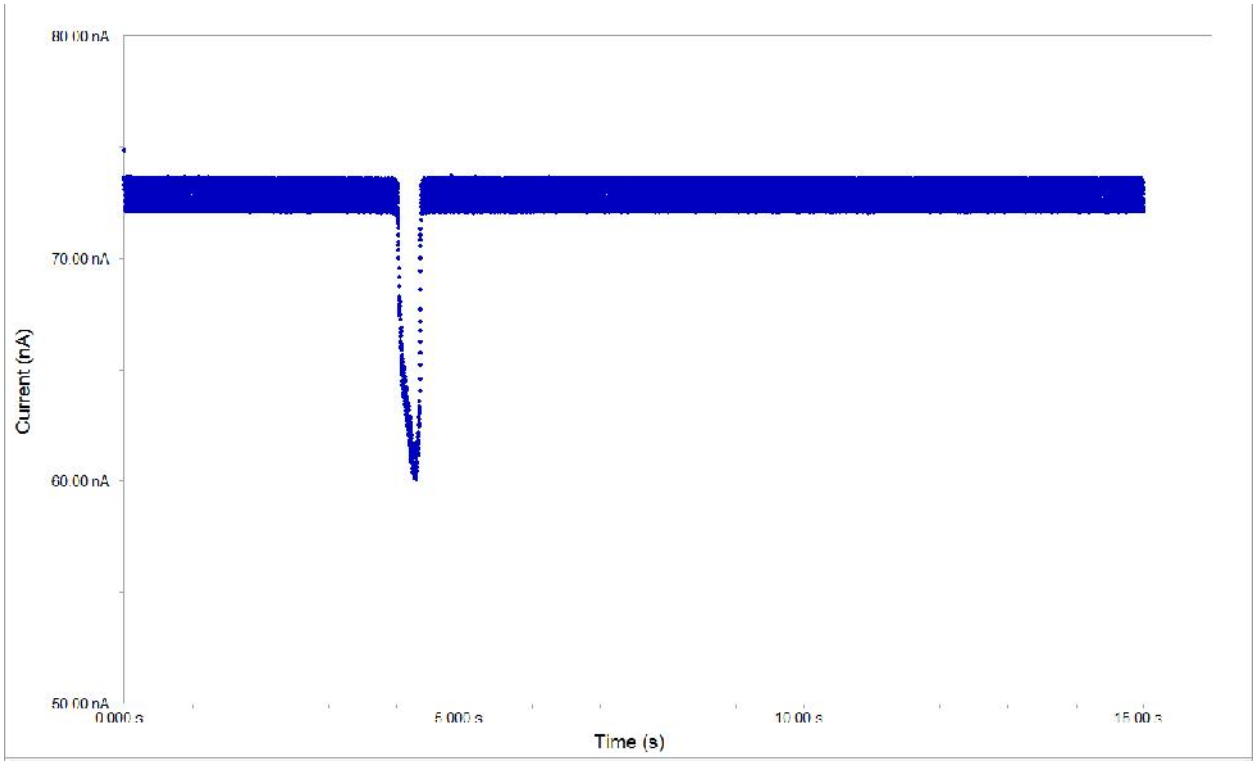

Figure B-7-32. Stem cells 200mV

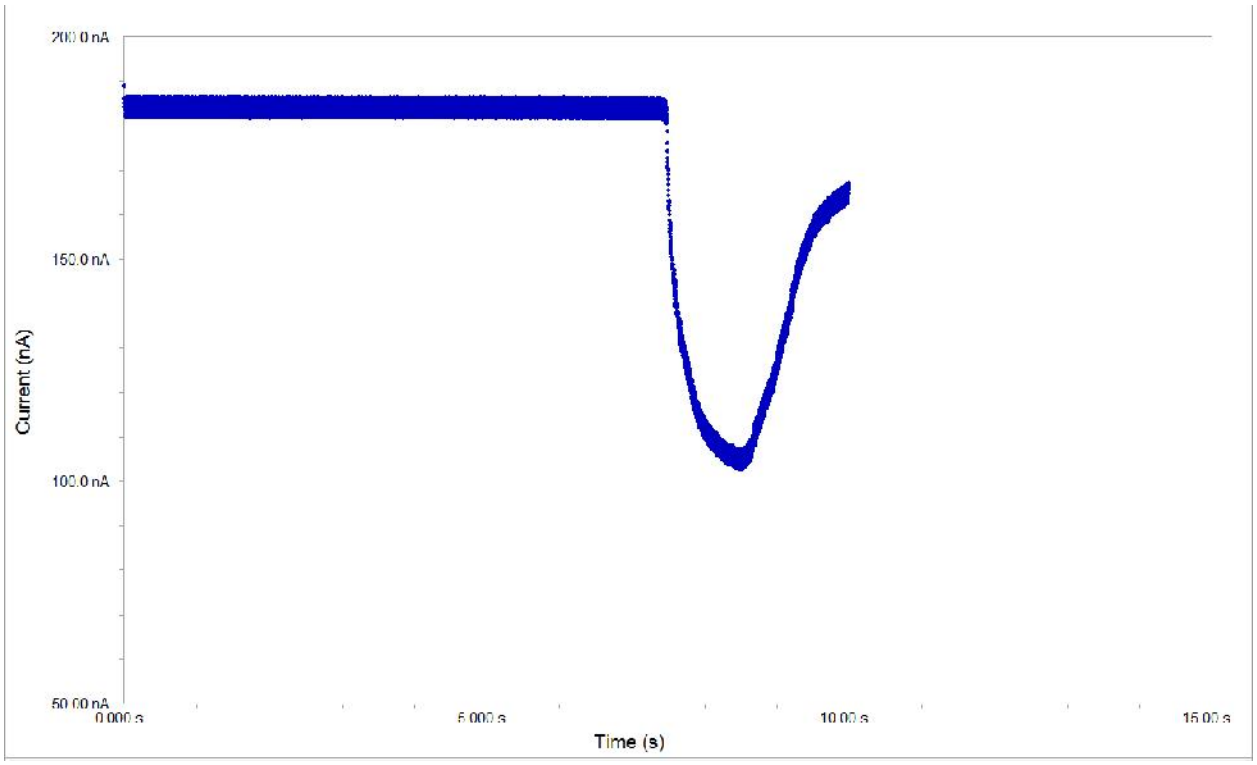

Figure B-7-33. Stem cells 500mV

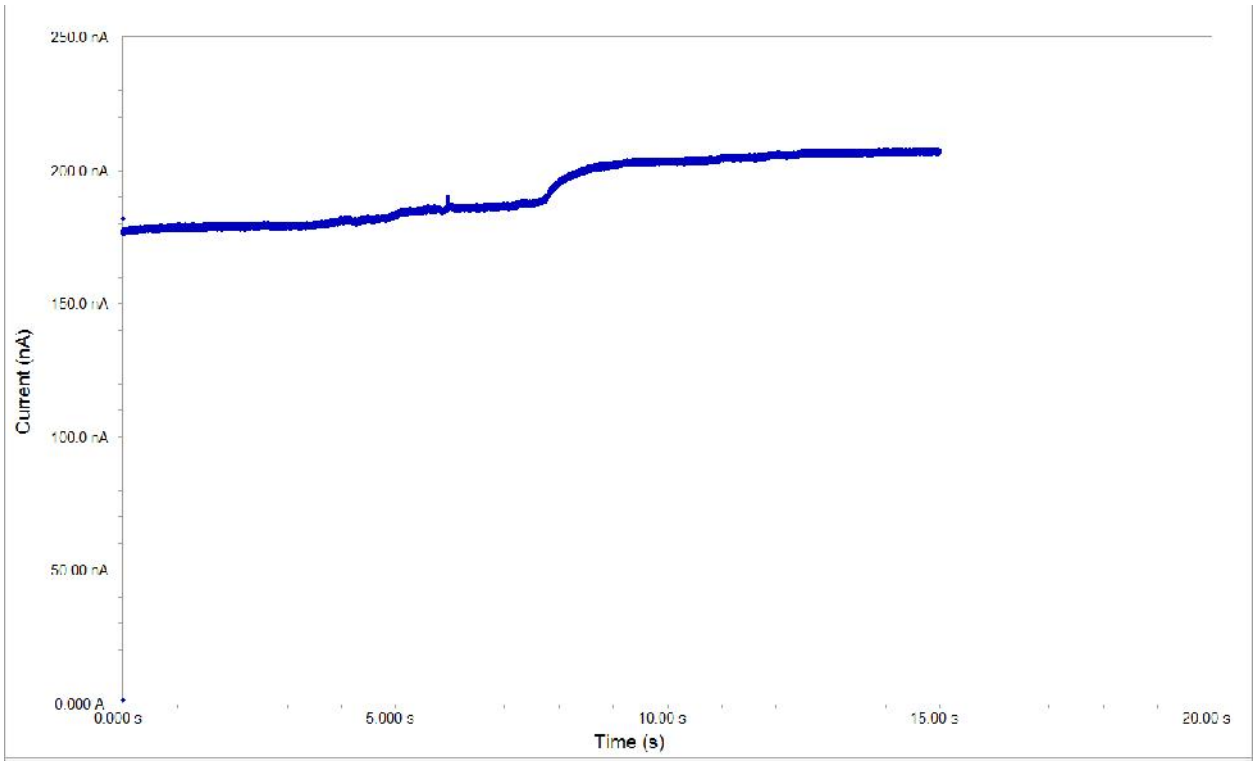

Figure B-7-34. Stem cell trapped 600mV

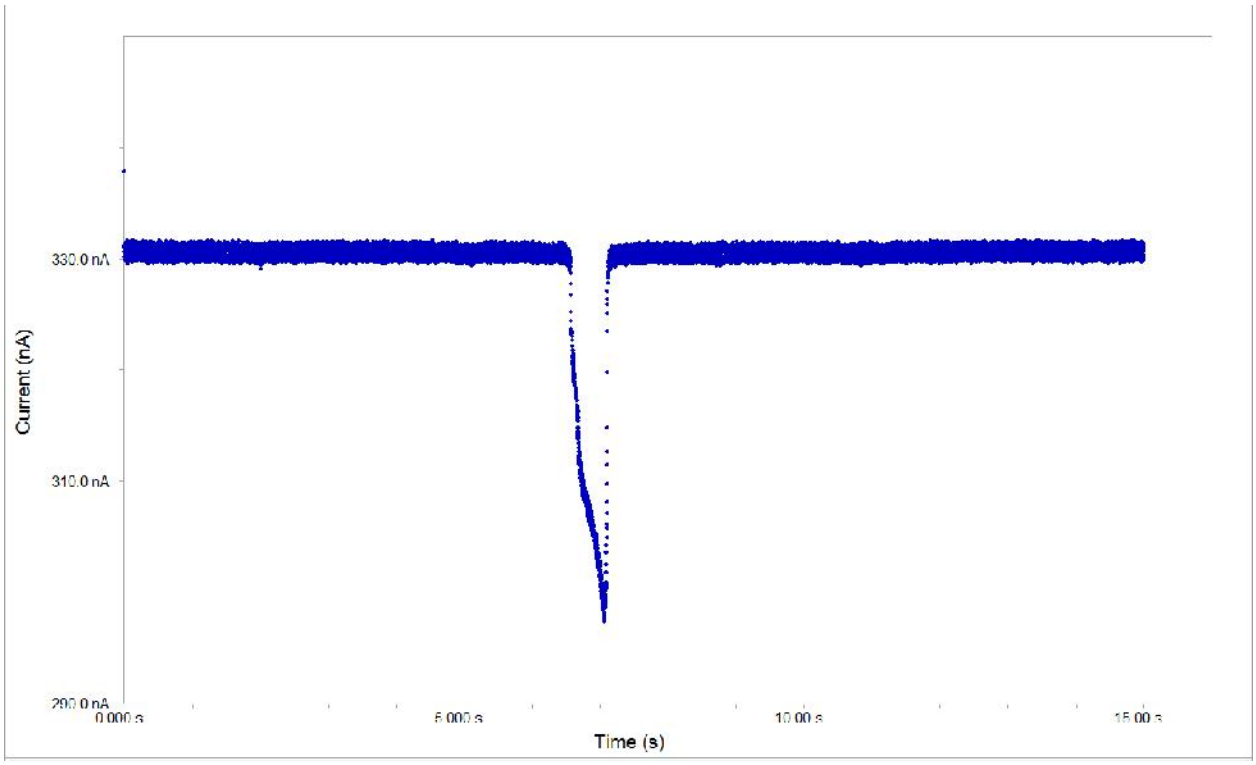

Figure B-7-35. Stem cells 900mV

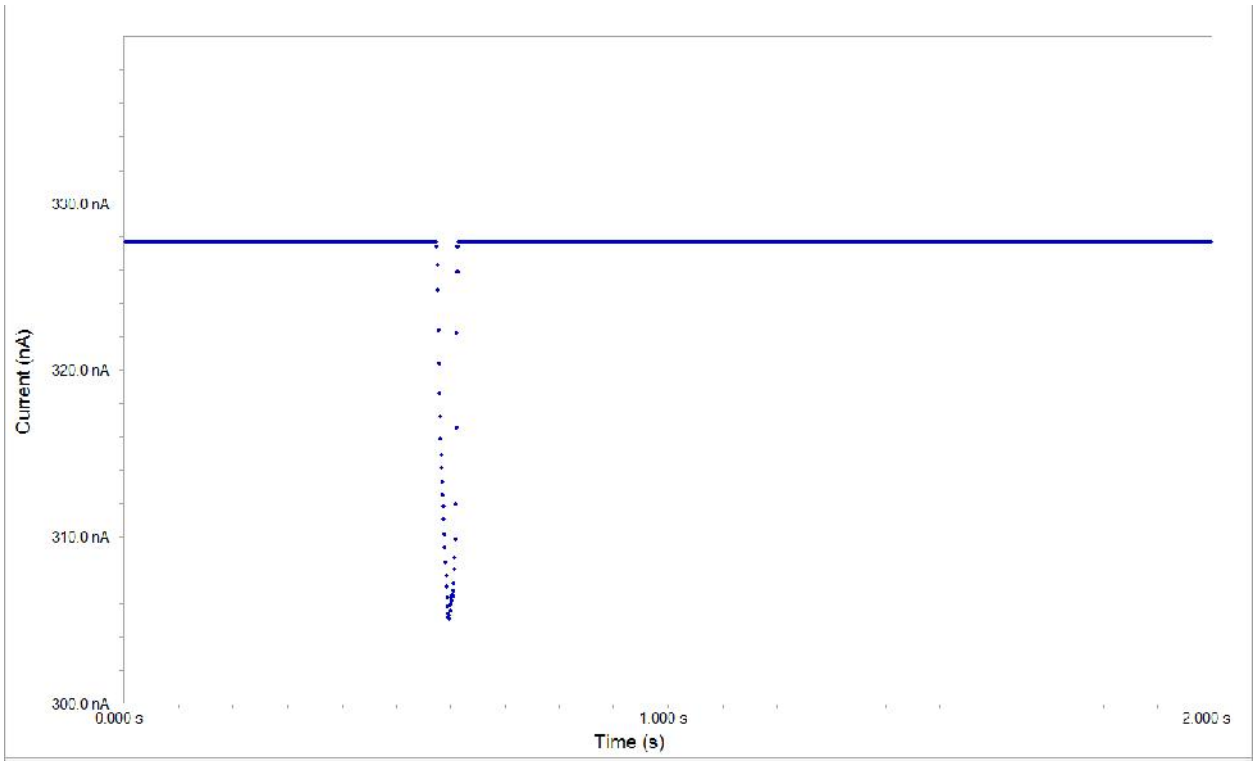

Figure B-7-36. Stem cells 900mV

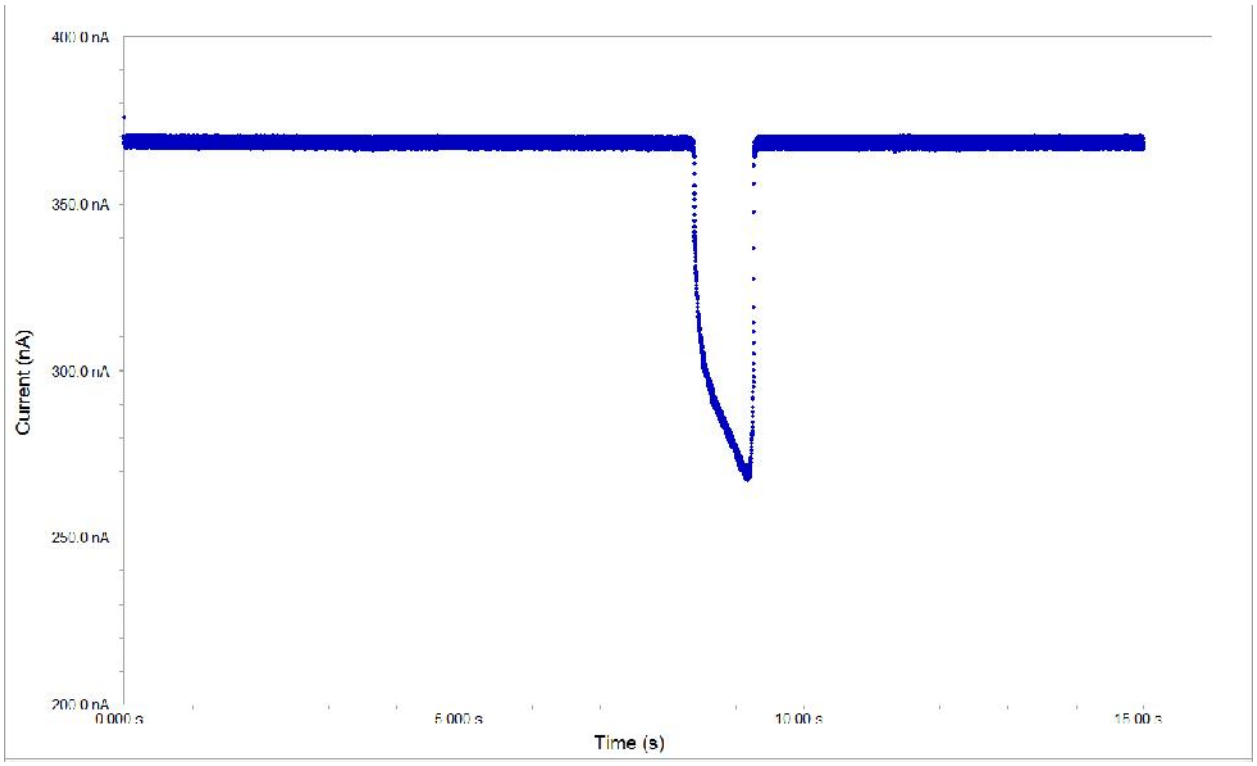

Figure B-7-37. Stem cells 1V

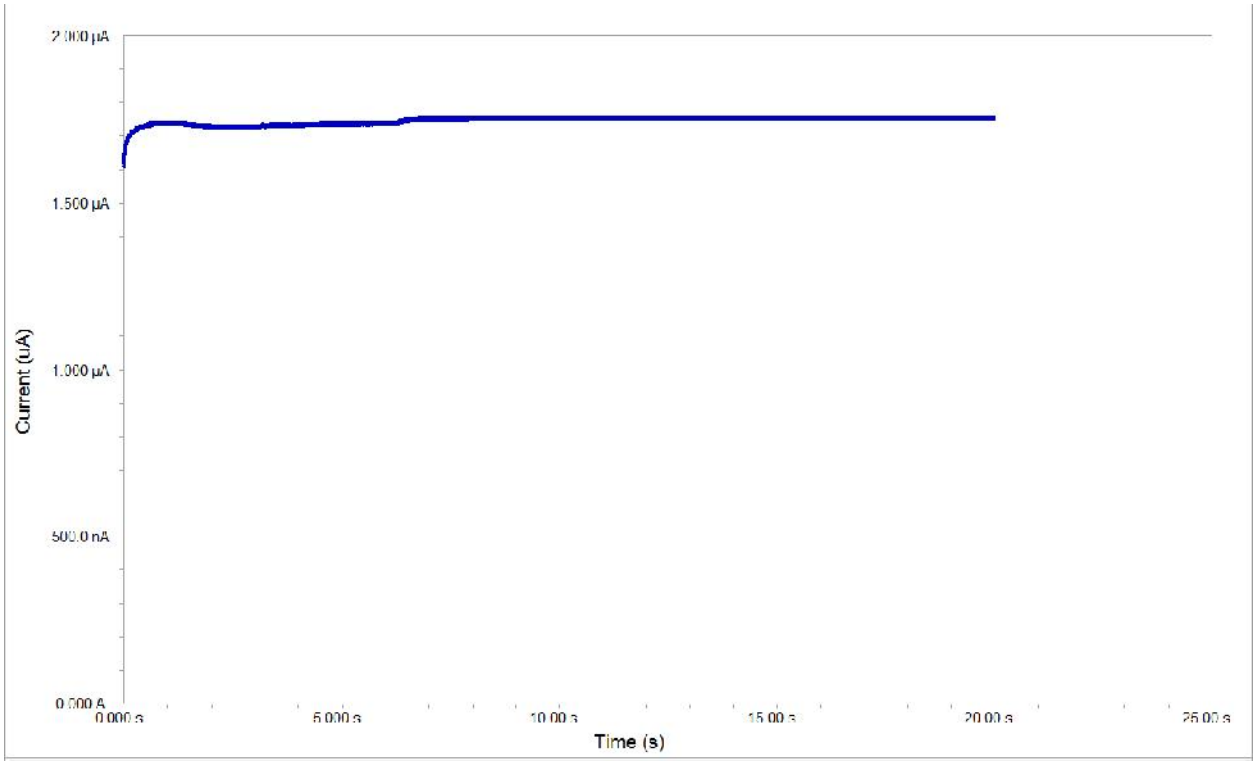

Figure B-7-38. Stem cell trapped 5V